POLITECNICO
MILANO 1863

Effect of passive vehicle design in semi-active primary suspension control

---

MSc Mechanical Engineerig - Mechatronics and Robotics
15 December, 2020

STUDENT: *Di Stefano Flaviano*
SUPERVISOR: *Bruni Stefano*
CO-SUPERVISOR: *Di Gialleonardo Egidio*

Contents

List of Figures

List of Tables

Abstract

In the vehicle engineering, the passengers comfort has always represented a critical feature because of the intrinsic conflicting behaviour of the suspensions: from one side, it would be preferred a soft suspension in order to isolate the car body from the external disturbances; on the other side, a stiff suspension is required in order to sustain the vehicle weight. In the last years, thanks to the growth of the Mechatronic Engineering, the introduction of control devices has been proposed in order to improve the dynamic behaviour of the mechanical systems and to solve this duality. In particular, several researches have demonstrated that it's possible to isolate the vehicle from the external disturbances by controlling the secondary suspension, which is directly connected to the car body itself.

In this work, an advanced semi active primary suspension control strategy for the improvement of the passenger comfort in a railway vehicle is investigated, together with the issues related to the dynamic property of the passive system. In fact as long as the control force is no longer acting directly on the car body, the dynamics properties of the passive system play a central role. For the numerical simulations, it has been developed a mathematical model describing the vehicle vertical dynamics, with the advanced introduction of the car body bending modes and the air spring modelling. For what concerns the controller, the classical two state SkyHook and ADD - Acceleration Driven Damper logic have been employed. Furthermore, the critical evaluation of the results allowed to understand how the coupling of the mechanical and control system may enhance the positive features of the passive system rather than compensate its gaps.

Very interesting results have been pointed out and they may represent a starting point for a new challenging development in control engineering, compliant with greater design flexibility, more demanding requests and ambitious goals.

Abstract

Nell'ingegneria del veicolo, il comfort del passeggero ha sempre rappresentato un aspetto critico a causa dell'intrinseco comportamento conflittuale delle sospensioni: da un lato, è preferibile una sospensione morbida al fine di isolare la carrozzeria dai disturbi esterni; dall'altro, è richiesta una sospensione rigida per sostenere il peso del veicolo. Negli ultimi anni, grazie alla crescita dell'Ingegneria Meccatronica, è stata proposta l'introduzione di dispositivi di controllo in modo tale da migliorare il comportamento dinamico dei sistemi meccanici e risolvere questa dualità. In particolare, diverse ricerche hanno dimostrato la possibilità di isolare il veicolo dai disturbi esterni attraverso il controllo della sospensione secondaria, in quanto direttamente connessa alla carrozzeria.

In questo studio viene investigata un'innovativa strategia di controllo semiattivo della sospensione primaria, al fine di migliorare il comfort del passeggero nei veicoli ferroviari, in parallelo ai problemi relati alle proprietà dinamiche del sistema passivo. Infatti, dal momento in cui la forza di controllo non agisce più direttamente sulla cassa, le proprietà dinamiche del sistema passivo giocano un ruolo centrale. Per le simulazioni numeriche, è stato sviluppato un modello matematico che descrive la dinamica verticale del veicolo, con l'innovativa introduzione dei modi flessionali della cassa e della modellazione della molla ad aria. Per quanto riguarda il controllore, sono state impiegate le classiche logiche ADD - Acceleration Driven Damper e SkyHook a due stati. In aggiunta, la valutazione critica dei risultati ha permesso di valutare come l'accoppiamento del sistema di controllo a quello meccanico possa valorizzare le caratteristiche positive del sistema passivo piuttosto che compensare i suoi limiti.

I risultati osservati sono molto interessanti e potrebbero rappresentare la base di partenza per uno stimolante sviluppo nell'ingegneria del controllo, in linea con l'esigenza di una maggiore flessibilità di progettazione, le sempre più stringenti richieste e i nuovi ambiziosi obiettivi.

Introduction

In recent years, it has been observed a strong and rapid development of ground vehicle engineering, driven by more demanding requirements in terms of stability, comfort and safety. For what concerns the railway engineering, the global trend has furthermore enhanced the research toward the development of faster vehicles; but in order to avoid detrimental effect on the other features, the traditional design approach has to be revolutionized.

In particular, the recent forward-thinking researches have been highlighting the central role of the suspension design for the achievement of improved performances, compliant to the new challenging goals. The suspension, which has to bear the vehicle weight, furthermore represents the element establishing the connection with the railway and has the role to transmit and filter its irregularities.

The classical design approach, based on the employment of traditional passive spring and damper, is limited by an unsolvable duality: from one side, a *soft* suspension would be preferred in order to isolate the car body from the external disturbances; on the other side, a *stiff* suspension is required to reduce changes in car body level caused by charge of the payload.

The introduction of new mechatronic technologies has made possible to solve this intrinsic suspension duality: the integrated design of mechanical and electronic control system ensures more flexibility and allows to achieve different goals that have been traditionally considered contradictory. In fact it has been demonstrated that by replacing or complementing the passive suspension with an active or semi active element, it is possible to improve the dynamic response of the system and to reduce the vibrations of the car body.

The use of active elements, like hydraulic or electromechanic actuators, ensures from a theoretical point of view the best results since it can be used both for dissipating or introducing power in the system. Anyway, from a practical point of view, their implementation results very complex and expensive: additional elements are required, like the measurement and monitoring equipment, but particularly outstanding is the need of an external power source. Moreover, the overall complexity affects the system reliability.

An attractive alternative is represented by semi active devices: they combine a good performances improvement, typical of the full active system, with the simplicity of the

traditional passive elements. The main feature of the semi active dampers is the characteristic parameter adjustability, which ensures a certain flexibility in the response, while their main constraint is the possibility to work only by dissipating energy. Anyway, the latter aspect results in the stability warranty: whatever the value of the damping coefficient, this element is never able to provide energy to the system and hence to produce an unstable behaviour .

For this reason, recent researches have been investigating the possibility to introduce semi active control strategies, generally applied on the secondary suspension: in this way the semi active element would be acting directly on the car body, ensuring a straight forward benefit in the vibration reduction and passenger comfort.

In this work, an alternative control system layout for the improvement of the passenger comfort is proposed, consisting in a semi active primary suspension control strategy. This solution is based on replacing of the primary suspension passive damper by a semi active element and is aimed to the reduction of car body vibrations transmitted through the bogie frame by controlling the response of the latter.

The strengths of this alternative layout consist in reaching good improvements with few changes respect to the passive configuration and in enabling a wider vehicle design flexibility. Anyway from the other side, the effectiveness of this primary suspension control strategy is very tricky since it is not dependent on the characteristic of the implemented semi active element and on the control logic only.

In fact a strong coupling between the car body vibration reduction and the dynamic properties of the passive vehicle has been detected: as long as the control force is acting on the bogie frame, the interaction between the bogie frame itself and the car body, in terms of transmissibility and mode shapes, rules the vibrations experienced by the passenger.

For this reason, in this work, a comparison between two vehicles with different data set and passive dynamic property has been proposed with the aim to highlight and characterize this aspects, which have never been described in the previous literature.

In order to evaluate this concept, a mathematical model accounting for the vertical dynamics of the railway vehicle has been developed in *MATLAB*. The strength of this model consists in coupling the modelling of the rigid degrees of freedom of the system with the flexible property of the car body. In fact, for the evaluation of the passenger comfort, it is very important to account for the coach bending deformation, whose natural frequencies stand in a frequency range of interest. Furthermore, in order to represent a study case as close as possible to reality, the dynamics properties of the air spring have been included by referring to the *Nishimura* model.

For what concerns the control strategy, two classical algorithms have been tested: the two state *Sky Hook* and the *ADD - Acceleration Driven Damper* logic. This choice reflects the challenging purpose to look for a control system smart and simple at the same time, without involving predictive tools or complex measurement and monitoring equipment.

Despite the simple control algorithms, the control system layout modelling has been developed with high accuracy, introducing both the saturation of the required force, depending on the semi active damper performance curve, and the effect of the signal delay between the command and the actuation, consistency with the latest literature.

The introduction of the saturation allows to keep a direct control on the generated force: this on one hand is fundamental to enable consistent comparison between the different systems and control strategies, leading to the detection of relevant considerations; on the other side it gives the opportunity to evaluate the effect of the use of devices with different properties on the system response.

In order to account for the signal delay, an advanced solution has been proposed, consisting of the introduction of an intermediate variable. As it happens in reality, the intermediate variable signal carries the information about the value of the semi active damper characteristic parameter or, in other words, the magnitude of the required force. By undergoing a first order system, the signal is filtered and the actuation is smoothed, with positive effects in the overall response.

In this thesis, the stream of contents is organized and discussed according to the work flow and the steps just presented:

- in chapter 2, the *State of Art* regarding the development and applications of control strategies for ground vehicles aimed to the passenger comfort improvement is outlined;
- in chapter 3, the vehicle mathematical model is described with special attention to the modelling of the air spring and to the characterization of the coach bending modes;
- chapter 4 is concerned with the control strategy and of the control system architecture, with the analysis of the advantages carried by the introduction of the intermediate variable and the damper performance curve;
- in chapter 5 the results are shown and, going though their comment, the considerations on the passive system properties effect on the control strategy are discussed;
- finally, some conclusive remarks are provided in chapter 6.

State of the art

In the last years the desire to reach higher velocities, better ride quality, comfort and safety has been strongly pushing the development in ground vehicle engineering.

Several researches have demonstrated that all of this objectives are strictly correlated one another and strongly depend on the suspension performances.

In fact the suspension is the single element of a vehicle which mostly affects its entire dynamic behaviour: it has the role to sustain the charge of the payload and, as long as it establishes the connection between the track and the vehicle itself, it has furthermore the role to filter the track irregularities, which cause the car body vibration and affect the safety and comfort level [1].

In order to achieve those challenging goals, the traditional suspension layout, consisting on simple passive spring and damper elements, has to be reworked. In fact it carries an intrinsic duality in vertical direction: for sustaining the weight a *stiff* suspension is required, while for isolating the external disturbances a *soft* one would be preferred [2].

From the second half of the 1980s, the advanced purpose to solve this duality found a solution in the new mechatronic technologies: the integrated design of mechanical and electronic control system ensures more flexibility and furthermore allows to achieve simultaneously different goals that have been traditionally considered contradictory.

For what concerns the railway vehicles, this innovation has lead to a fundamental change: for 150 years the train design has been a pure mechanical engineering discipline, but it is becoming a more complex control engineering problem [3].

Nowadays some state of the art reviews are available keeping updated the applications of the control system in railway vehicles [3] [4] [5] [6] [7]. Going through this documentation, the main aim of the employment of control systems can be summarized as follow:

- dynamically keep the proper vehicle posture when subjected to various inertial and external force, caused by braking, turning, wind gust and other events;
- provide a good ride comfort in presence of railway irregularities, which acts as a major disturbance to the vehicle;
- ensure good handling and an overall vehicle agility, providing a safe dynamical behaviour in different running conditions;

- avoid excessive suspension deflection or related hard stop/impacts;
- improve the stability, by controlling the modes of the bogie;
- perform special functions in addition to the passive suspension, for example tilting the car body.

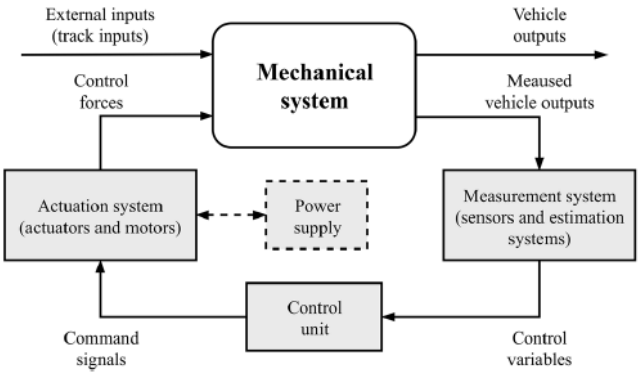

Figure 2.1: Control system layout [3]

The layout of the control system, described in figure 2.1, generally consists of:

- measurement equipment for the estimation of the mechanical system state;
- control unit, that evaluates the system state and depending on a control algorithm compute the control force;
- actuation system, which apply the required force;
- eventually, power supply unit.

As shown in figure 2.2, the control systems can be grouped in two families depending on the degrees of actuation: the *semi active* and *full active* control system.

In the first group, semi active elements able to work only dissipating power are used; in the latter, actuators able to both dissipate and introduce power to the mechanical system are employed. Thus in the second layout, in order to introduce power to the system, the additional power supply unit is required.

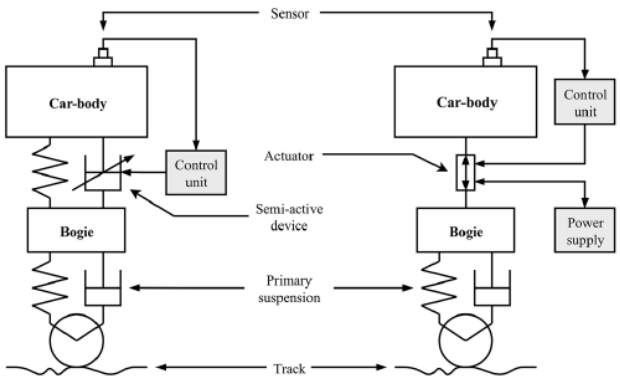

Figure 2.2: *Semi active* and *full active* control system comparison [3]

The *full active* suspension golden age is probably located in the second half of the 1980s: analog electronics were already well developed, the era of embedded digital micro controllers was starting and the magic of full active suspensions attracted the car manufacturers. During these years, the exceptional potential of replacing a traditional spring-damper system with a full active suspension was demonstrated; but the high costs, significant power absorption, system unreliability and safety issues made the attraction last only few years without leaving a significant impact on the mass market [1].

In fact, the active suspension layout already introduced consists on complex and expensive devices [2], in particular the actuator itself, usually hydraulic, electromechanic, pneumatic or magnetic, as force or torque generator, the measurement and sensing devices, like accelerometers, potentiometers or transducers and the external power source.

Depending on the actuation bandwidth [8] [1], the active suspension can be grouped in three families, as shown in figure 2.4:

- *load leveling* suspensions, generating a quasi static adjustment of the vertical displacement, whose bandwidth is below the suspension dynamics;
- *slow-active* suspensions, whose bandwidth is in between body and wheel dynamics;
- *fully active* suspensions, with full bandwidth active suspension.

For what concerns the *active* control, both primary and secondary suspension application have been explored: the primary suspension approaches are mainly aimed to the improvement of the guidance, steering capability and stability; the secondary suspension solutions aim at enhancing the passenger comfort.

Remaining focused on the researches for railway vehicles dealing with the improvement of passenger comfort, it is possible to cite three important representative studies:

- in Sweden, *KTH* and *Bombadier Transportation* have developed an active lateral and vertical secondary suspension in the program *Green Train* [9], their tests performed from 2007 to 2013 showed a good comfort improvement and the possibility to reduce the lateral displacements by the 50 %;
- in Korea, *Railroad Research Institute* has performed some tests with lateral electromagnetic actuators in the secondary suspension controlled with *SkyHook* strategy [10], their tests demonstrated a reduction of the later accelerations of $7dB$;
- in Japan, the *Japanese National Railway* tested lateral pneumatic actuators in the secondary suspension for high speed railway vehicles [11], even at 425 km/h the vibration can be reduced by the 50 %.

Despite the complexity and the cost of the *full active* control system, the improvements are not limited only to the vehicle dynamics itself.

For example, focusing on the primary suspension applications, apart from the guidance, steering capability and stability improvement, additional benefits can be exploited thanks to the control of the contact force [5]:

- noise abatement, fundamental in urban vehicles;
- reduction of wear and of maintenance costs, which can balance the total life costs;
- to apply on-demand maintenance plan, based on the condition monitoring;
- to provide a positive impact on the infrastructure due to a more friendly track vehicle interaction.

In the second half of 1990s a new trend emerged: it became clear that the best compromise between costs, weight, power consumption, encumbrance and performances, comfort, safety may lay in *semi active* suspension solutions [1].

The *semi active* elements are able to work only by dissipating energy and can drive the system response through simple regulations of their characteristic parameter. The fact that they can not introduce power to the system is surely a limitation; but on the other hand it ensures appealing features:

- the power demand is negligible and there is a limited power supply requirement;
- as a stability warranty, without the introduction of additional power they can not determine an unstable behaviour of the mechanical system;
- the fail safe condition is guaranteed;
- lower weight, cost and encumbrance.

In other words, the *semi active* elements achieve some of the *active* system performances with components close to the passive in terms of cost and complexity [12].

For what concerns the *semi active* damper, it is possible to distinguish two main technologies depending on the system used for adjusting the characteristic parameter [8]: the *electro hydraulic* and the *magneto rheological* dampers.

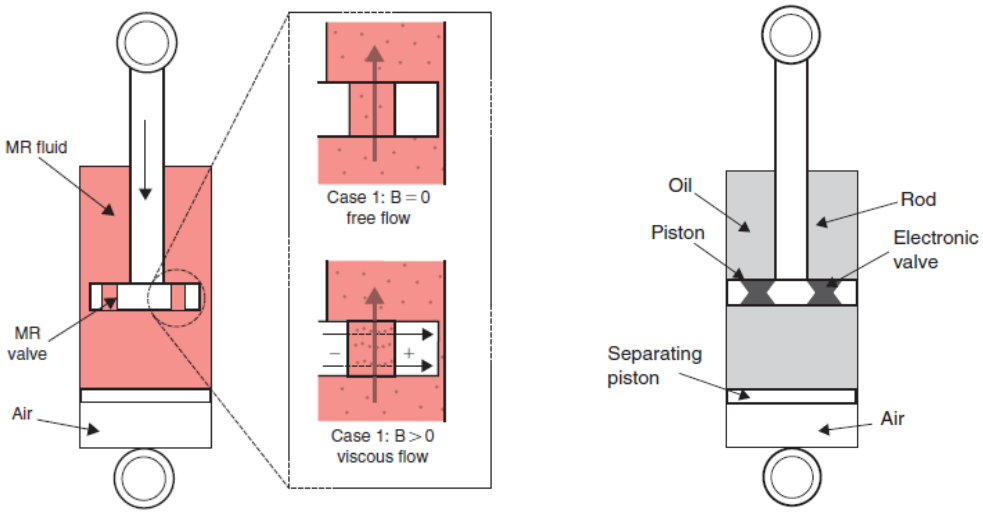

(a) *Magneto rheoloical* (b) *Electro hydraulic*

Figure 2.3: Semi active damper [1]

In the *magneto rheological* elements, the fluid viscosity varies. The working fluid is a mineral or silicone oil carrying magnetic particles that, thanks to the addition of proper additives, remain suspended in the fluid [13]. When an external magnetic or electric field is imposed, the magnetic align, limiting the fluid movement and giving the same result of an increased viscosity. They are cheap and ensure good performances.

In the *electro hydraulic* elements, the geometrical feature of the orifice varies. A valve regulates the fluid flow, generally air or oil, thus the chamber pressure and the generated thrust. In particular, it is generally possible to find two kinds of valves [14]:

- the *servo valves*: ensure quick response, a linear behaviour and a great accuracy in fluid flow control but are more expensive and complex;
- the *solenoid valves*: they are the most widely used since they are simple devices, whose design can be optimized for every specific application.

Depending on the actuation bandwidth, the *semi active* elements as well can be grouped into two families [8] [1], as shown in figure 2.4:

- *adaptive suspension*, with slowly modified damping ratio;
- *semi active* suspension, whose parameter can be modified over a large bandwidth.

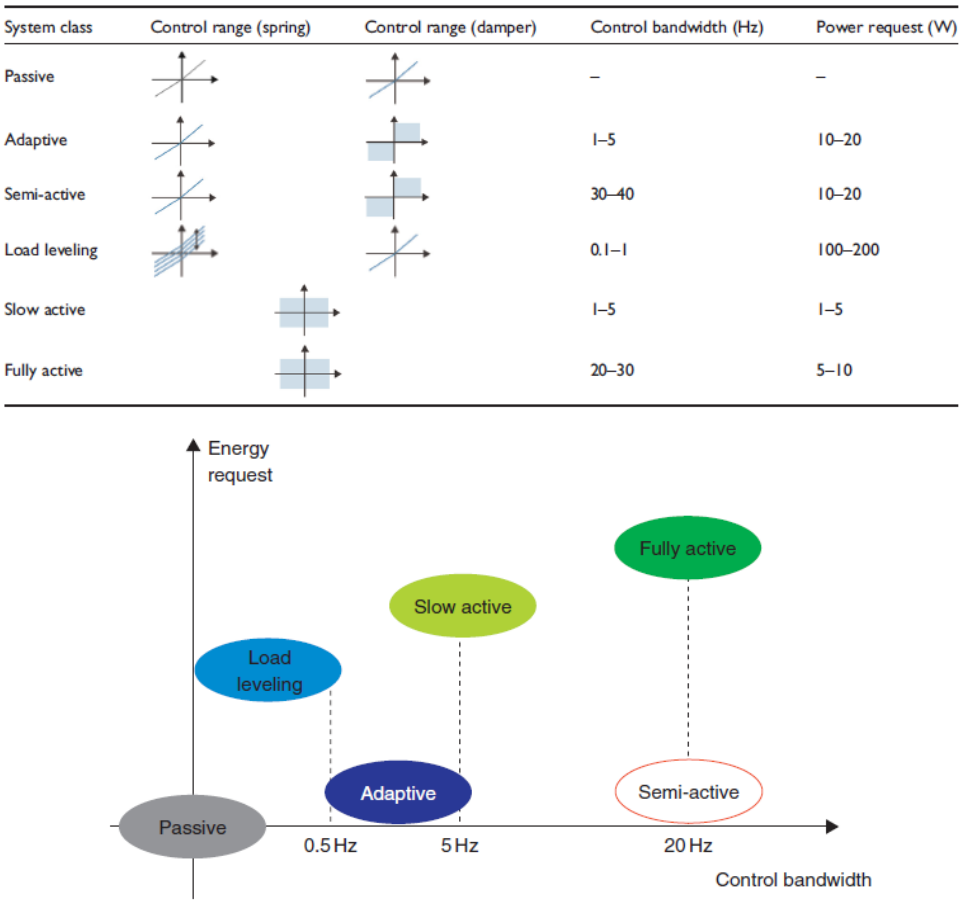

Figure 2.4: Control strategy classification [1]

For what concerns the practical implementation of the *semi active* suspension control strategy aimed to the improvement of the passenger comfort, both primary and secondary suspension approaches have been investigated.

About the semi active control strategies on the secondary suspension, a wide literature is available both regarding the road [15] [16] [17] and the railway vehicles. Remaining focused in the railway engineering field, it is possible to cite three representative researches:

- in Japan, the *Railway Technical Research Institute* has developed a semi active air spring control system [18] by placing an orifice control valve in between the rubber bellow and the auxiliary chamber and has performed a test supposing to simulate a vehicle running on vertical curves at $300\,km/h$; the results showed the effectiveness of the control system about the natural frequency of the air spring system $1.05\,Hz$ with large benefits of the car body rigid modes;

- in China, the *Jilin University Changechun* has developed a semi active air spring control system [19] by placing a throttle valve in between the rubber bellow and the auxiliary chamber, able to work both in low and high frequency range and to change the opening area from $615\,mm^2$ to $15\,mm^2$; the results demonstrated the possibility to reduce the noise in the car body acceleration;

- in United Kingdom, the *Land Rover* has developed a semi active control of the air spring [20] by placing a butterfly valve in between the rubber bellow and the auxiliary chamber; the experiments on a quarter vehicle test rig demonstrated the possibility achieve an acceleration reduction up to 29 % while from the numerical simulation of the whole vehicle up to 20 %.

For what concerns the semi active control strategies for the primary suspension aimed to the carbody vibration reduction for the passenger comfort, as long as it is an emerging technology, the only study case available is a Japanese research, at the *Railway technical research institute*, of the senior researcher Sugahara. This control system has been defined in 2007 [21] and it has been tested in the following years [22] [23] [24] [25].

Noticing the closeness of the natural frequency of the primary suspension system to that of the first bending mode of the carbody, the possibility to suppress the elastic vibration of the carbody by controlling and reducing the vibration of the primary suspension has been theorised [21]. In order to control the vibrations of the primary suspension, the introduction of a semi active variable axle damper has been proposed.

The first step has been a numerical simulation [21] on a vehicle model with 16 degrees of freedom, accounting for vertical and longitudinal displacements in addition to the pitch rotations: the results showed a reduction of the power spectra density of the bending mode of 60 %, but just in the range $[5 \div 15]\,Hz$.

The same observations have been carried out by the running tests with the semi active control system on the primary suspension, both at high [24] and low running velocities [25]. Furthermore by coupling the semi active primary and secondary control [22] [23], the improvement in the vibration reduction can be extended in the low frequency range, below $2\,Hz$, about the natural frequency of the rigid modes of the carbody.

The control strategies commonly used in the semi active control strategies, both for primary and secondary suspension, and found in the discussed literature are:

- *two state SkyHook* [1] [15] [21] [22] [23] [24] [25] [26], consisting in changing the characteristic parameter c of the *semi active* damper according to the chassis velocity $\dot{z}$ and the suspension deflection velocity $\dot{z}_{def}$ by using a logical law;

$$c = \begin{cases} c_{min} & if\ \dot{z}\dot{z}_{def} < 0 \\ c_{max} & if\ \dot{z}\dot{z}_{def} \geqslant 0 \end{cases}$$

- *linear SkyHook* [1], an improvement of the *two state* used to handle a continuously variable characteristic parameter; its value varies in a range $c \in [c_{min};\, c_{max}]$ depending on a tuning parameter $\alpha \in [0;\, 1]$ that modifies the closed loop performances;

$$c \begin{cases} c_{min} & if\ \dot{z}\dot{z}_{def} < 0 \\ \frac{\alpha c_{max}\dot{z}_{def} + (1-\alpha)c_{cax}\dot{z}}{\dot{z}_{def}} & if\ \dot{z}\dot{z}_{def} \geqslant 0 \end{cases}$$

- *ADD - Acceleration Driven Damper control* [1] [27] [28], an optimal control law that minimizes the vertical body accelerations $\ddot{z}$ when no track information is available;

$$c = \begin{cases} c_{min} & if\ \ddot{z}\dot{z}_{def} < 0 \\ c_{max} & if\ \dot{z}\ddot{z}_{def} \geqslant 0 \end{cases}$$

- *PDD - Power Driven Damper Control* [1], obtained from the port Hamiltonian techniques; the strengths of this control strategy consists in avoiding the chattering phenomena; given the suspension stiffness k, the logic condition is

$$c = \begin{cases} c_{min} & if\ k\, z_{def}\, \dot{z}_{def} + c_{min}\, \dot{z}_{def} \geqslant 0 \\ c_{max} & if\ k\, z_{def}\, \dot{z}_{def} + c_{min}\, \dot{z}_{def} < 0 \\ 0.5(c_{min} + c_{max}) & if\ z_{def} \neq 0\ and\ \dot{z}_{def} = 0 \\ -\frac{k\, z_{def}}{\dot{z}_{def}} & otherwise \end{cases}$$

- adaptive *LQG - Linear Quadratic Gaussian* [17] [22] [24] [25], which based on the extracted least squares estimation algorithm or on a *Kalman* filter, evaluates the running condition and adapts the gain of the controller in order to selectively achieve dual objectives, for example the ride quality and handling performances.

Mathematical model of the railway vehicle

The implementation of the primary suspension control system is aimed to the reduction of the vibration of the car body flexible modes, which are strongly coupled to the longitudinal dynamic of the vehicle.

For this reason, it has been developed a two dimensional model in the vertical plane accounting for the bounce displacements z and the pitch rotations θ of both the carbody and the bogie frames.

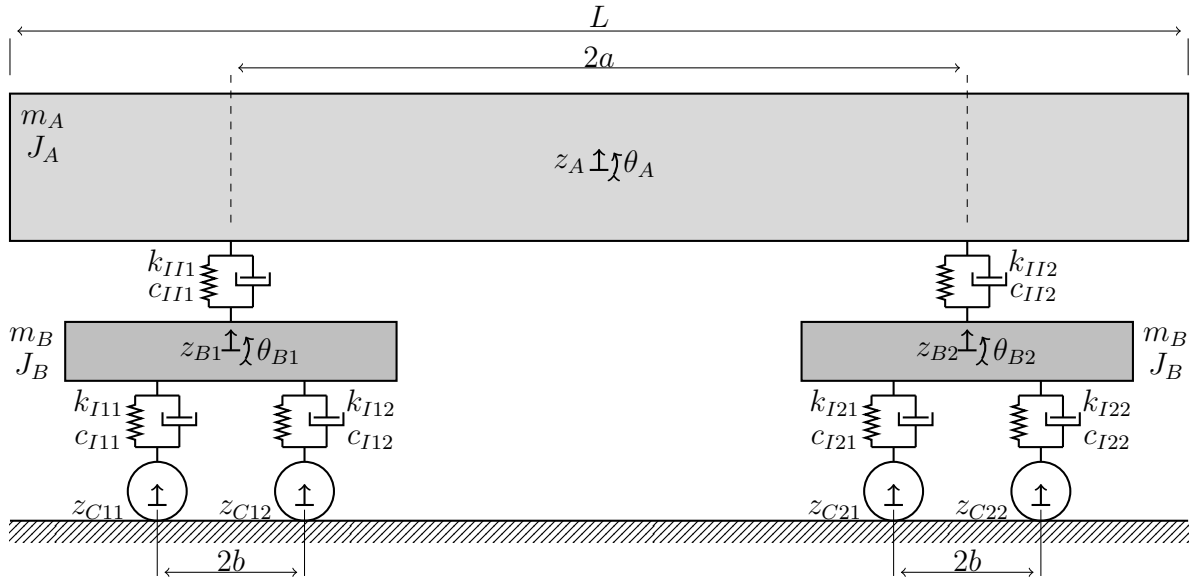

Figure 3.1: Model of vertical dynamics of the railway vehicle

All of the bodies are homogeneous: the centre of gravity is located in their point of symmetry. Moreover the independent variables are defined as displacements and rotations of the centre of mass itself in order to lead to an easier kinetic energy formulation.

The system is characterized by six degrees of freedom associated to the rigid body motions: the bounce and the pitch of the rear bogie frame (z_{B1}, θ_{B1}); the bounce and the pitch of the front bogie frame (z_{B2}, θ_{B2}); the bounce and the pitch of the carbody (z_A, θ_A).

The resulting free independent variable vector is:

$$\underline{x}_F = \{z_{B1};\ \theta_{B1};\ z_{B2};\ \theta_{B2};\ z_A;\ \theta_A\}$$

Furthermore there are four additional components of constraint motion z_{Cij}, that account for the track irregularity and are responsible for the system excitement. They can be collected in the constrained independent variable vector:

$$\underline{x}_C = \{z_{C11};\ z_{C12};\ z_{C21};\ z_{C22}\} \tag{3.0.1}$$

The contact between the wheel and the railway is modeled as completely rigid: the vertical displacement that characterizes the track irregularity is directly experienced by the wheelset. This assumption is consistent as long as the contact bodies are made of cast iron and their deformation is negligible in the frequency range of interest $[0 \div 25\ Hz]$.

The wheelsets are equally spaced respect to the bogie centre, with a wheelbase $2b$. The connecting element between the bogie frame and the wheelset is the primary suspension. The suspension is modelled as a linear spring and damper in parallel, with constant characteristic parameter $(k_{Iij},\ c_{Iij})$.

The bogie frames as well are equally spaced respect to the carbody centre and their distance is $2a$. The carbody is connected to the bogie frame though the secondary suspension. The suspension is modelled as a linear spring and damper in parallel as well, with a constant characteristic parameter $(k_{IIi},\ c_{IIi})$.

Since the secondary suspension is connected to the central point of the bogie frame, its pitch rotation won't affect the carbody excitement and is decoupled from the other the degrees of freedom. Thus the $(\theta_{B1};\ \theta_{B2})$ independent variables may appear useless for the bending mode vibration reduction, but on the contrary they are needed for the computation of the primary suspension elongation and elongation velocity, thus for the definition of the force generated by the control system.

Moreover it is important to specify that all the primary suspensions share the same parameter $k_{Iij} = k_I$ and $c_{Iij} = c_I$ just like the secondary suspensions, with $k_{IIij} = k_{II}$ and $c_{IIij} = c_{II}$. This detail coupled together with the geometrical features of the system leads to the system symmetry.

3.1 Characterization of the bending vibrations of the carbody

In order to evaluate the passenger comfort, it is necessary to account for all of the vibrating modes standing in the frequency range of interest, including the carbody bending mode satisfying this condition.

The challenging aim of this numerical model is to properly represent the deformable property of the carbody, in particular its transverse bending deformation, and to correctly describe the interaction between the rigid body discrete degrees of freedom and the independent variable characterizing the flexible body vibration.

For the description of the carbody transverse vibration, it is possible to refer to a uniform beam study case [29].

For the modal mass, stiffness and damping contribution in the equation of motion there is the need to introduce the modal matrices in addition to the rigid system matrices.

For the definition of the kinematic relationship it is important to notice that the secondary suspension elongation is affected by the transverse displacement of the carbody in the connecting point, which has to be consequently defined.

3.1.1 Modal analysis of the carbody

Assuming that the carbody is slender enough to be considered as a uniform beam, its transverse vibration $w(x,t)$ is ruled by the *Euler - Bernoulli* partial differential equation:

$$EJ\,\frac{\partial^4 w}{\partial x^4} = -\lambda\,\frac{\partial^2 w}{\partial t^2} \tag{3.1.1}$$

In order to have the derivative of the function $w(x,t)$ respect to the space always equal to the derivative respect to the time, it is possible to impose that the transverse vibration function $w(x,t) = \Phi(x)G(t)$ is the product of a function depending on the only space variable $\Phi(x)$ and another function depending on the only time variable $G(t)$.

In particular the function space dependent $\Phi(x)$ defines the mode shapes, so the beam intrinsic and fixed way of vibrating: just like it happens in the discrete system, the beam motion can be described as a linear combination of its natural mode shapes.

On the contrary the function time dependent $G(t)$ has the role to modulate the mode shape amplitude in time domain and to assign a specific weight to each mode shape, thus to characterize the response to an excitement.

After mathematical manipulation discussed in the appendix, it is possible to obtain the general standing wave solution of the partial differential equation 3.1.1:

$$w(x,t) = [A\sin(\gamma x) + B\cos(\gamma x) + C\sinh(\gamma x) + D\cosh(\gamma x)]\cos(\omega t + \psi) \tag{3.1.2}$$

By imposing the proper boundary and initial conditions it is always possible to adapt the general equation 3.1.2 to every specific study case, defining (A, B, C, D, γ, ω, ψ).

In case of free response, the set of the time dependent function $G_i(t) = \cos(\omega_i t + \psi_i)$ of equation 3.1.2, one for each mode shape, can be computed imposing the initial conditions.

Anyway since the carbody receives a random excitation from the track irregularities, their value has to be integrated together with the equation of motion by introducing a new set of independent variables $\underline{G}$ in addition to the discrete free degrees of freedom (z_{B1}; θ_{B1}; z_{B2}; θ_{B2}; z_A; θ_A) of the rigid system.

This leads to a new definition of the free independent variables vector:

$$\underline{x}_F = \{z_{B1};\ \theta_{B1};\ z_{B2};\ \theta_{B2};\ z_A;\ \theta_A;\ G_1;\ ...G_n\} \tag{3.1.3}$$

Instead the set of the space dependent functions of equation 3.1.2, one for each bending mode, $\Phi_I(x) = A_I \sin(\gamma_I x) + B_I \cos(\gamma_I x) + C_I \sinh(\gamma_I x) + D_I \cosh(\gamma_I x)$ can be computed by imposing the boundary conditions.

In particular the carbody can be schematized as a beam with free-free boundary conditions, excited by the forces transmitted through the secondary suspensions in correspondence of the connection points.

Since the ends are free to translate and rotate, there are no information about $w(0,t)$ or $w(L,t)$ and $\frac{\partial w}{\partial x}|_{x=0}$ or $\frac{\partial w}{\partial x}|_{x=L}$; so the proper boundary conditions consist in null shear force and bending moment at the beam ends: $T(0,t) = T(L,t) = M(0,t) = M(L,t) = 0$.

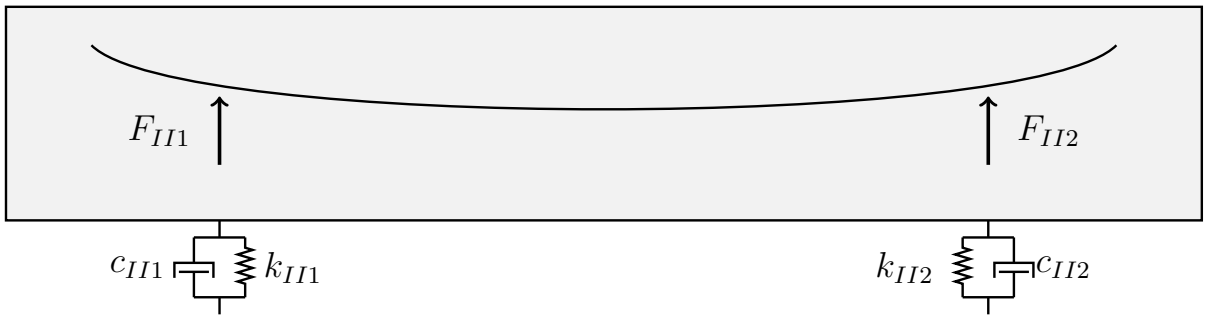

Figure 3.2: Modelling of the carbody with a *free-free* beam

After some computations summarized in the appendix, through the boundary conditions application it is possible to obtain the equation defining the carbody mode shapes:

$$\Phi_i(x) = [\cos(\gamma_i x) + \cosh(\gamma_i x)] + K_i [\sin(\gamma_i x) + \sinh(\gamma_i x)] \tag{3.1.4}$$

Where the constant γ results from the characteristic equation:

$$\cosh(\gamma_i L)\cos(\gamma_i L) = 1 \tag{3.1.5}$$

And the variable K is defined as:

$$K_i = \frac{\sin(\gamma_i L) + \sinh(\gamma_i L)}{\cos(\gamma_i L) - \cosh(\gamma_i L)}$$

Since the characteristic equation 3.1.5 is a non homogeneous second order trigonometrical function, it has infinite number of solution corresponding to infinite number of mode

shapes, as requested for the continuous systems, and it has to be solved numerically: the MatLab tool *fsolve* implementing a minimization algorithm has been used.

Moreover, thanks to the relationship $\omega^2 = \frac{EJ}{\lambda}\,\gamma^4$ coming from the *Euler - Bernoulli* equation 3.1.1, it is possible to compute the flexible bending natural frequencies ω.

By referring to the data set reported in [29] with carbody length $L = 20\,m$, linear density $\lambda = \frac{m}{L} = 600\,kg/m$ and bending rigidity $EJ = 2e8\,Nm^2$, it is possible to compute the following representative natural frequencies:

Flexible bending mode	First	Second	Third	Fourth	Fifth	Sixth
$\gamma_i L$	4.730	7.853	10.996	14.437	17.279	20.420
$\omega_i\,[rad/s]$	32.293	89.017	174.509	288.472	430.928	601.874
$f_i\,[Hz]$	5.140	14.168	27.774	45.912	68.584	95.791

Table 3.1: Representative natural frequencies of bending modes of the carbody

And after the substitution of γ_i in the mode shape equation 3.1.4 it is moreover possible to represent the intrinsic bending modes of the car body:

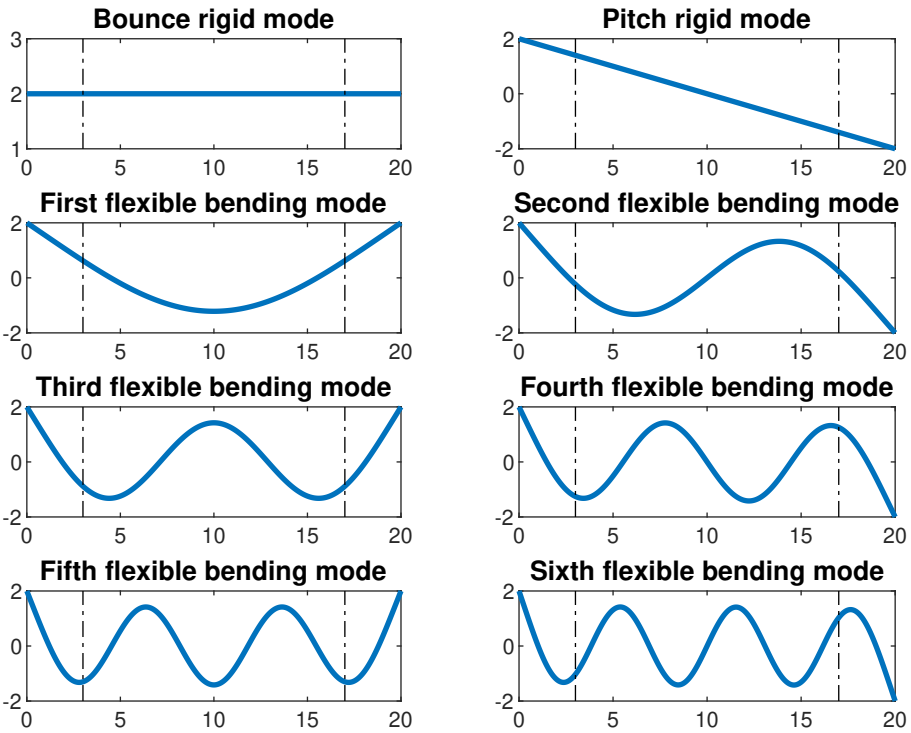

Figure 3.3: Representative mode shapes of the transverse vibration of the carbody

Where on the abscissa axis there is the coach length $[0 \div L = 20m]$ and on the ordinate axis the transverse displacement. In addition the black dotted vertical lines represent the secondary suspension position, defining the support position: the left at $L_1 = 3\,m$ and the right one at $L_2 = 17\,m$.

3.1.2 Definition of the modal matrices of the carbody

Once the mode shapes have been defined, it is possible to compute the modal mass matrix, accounting for the inertia related to the transverse displacement of the carbody, and the modal damping and stiffness matrices, due to the bending rigidity of the carbody.

The modal mass definition can be obtained from the kinetic energy formulation:

$$\left[M_m^1\right] = \begin{bmatrix} \int_0^L \lambda\Phi_1(x)\,\Phi_1(x)\,dx & \dots & \int_0^L \lambda\Phi_1(x)\,\Phi_n(x)\,dx \\ \dots & & \dots \\ \int_0^L \lambda\Phi_n(x)\,\Phi_1(x)\,dx & \dots & \int_0^L \lambda\Phi_n(x)\,\Phi_n(x)\,dx \end{bmatrix} \tag{3.1.6}$$

It is important to specify that, thanks to the orthogonality property of the shape function $\Phi_i(x)$, the modal mass matrix will always be diagonal: the integral of the product of two different mode shape $\Phi_i(x)\Phi_j(x)$ will always be null.

In order to be able to sum up the modal contribution to the mass matrix of the overall rigid system, there is the need to make the modal matrix consistent respect to the other matrices, which are referred to both the constrained (z_{C11}; z_{C12}; z_{C21}; z_{C22}) and the free *dof* vectors (z_{B1}; θ_{B1}; z_{B2}; θ_{B2}; z_A; θ_A; G_1; ...; G_n). This is possible by hemming the modal matrix of zeros in correspondence of the discrete system rigid independent variables:

$$\left[M_m\right] = \begin{bmatrix} [0] & [0] \\ [0] & [M_m^1] \end{bmatrix} \tag{3.1.7}$$

The integral $\lambda \int_0^L \Phi_i(x)\Phi_j(x)\,dx$ has been computed numerically by applying the trapezoidal method with a discretization of $L/1000$, since the analytical solution is not trivial.

The modal stiffness as well can be obtained from the potential energy formulation:

$$\left[K_m^1\right] = \begin{bmatrix} EJ\int_0^L \Phi_1'(x)\,\Phi_1'(x)\,dx & \dots & EJ\int_0^L \Phi_1'(x)\,\Phi_n'(x)\,dx \\ \dots & & \dots \\ EJ\int_0^L \Phi_1'(x)\,\Phi_n'(x)\,dx & \dots & EJ\int_0^L \Phi_n'(x)\,\Phi_n'(x)\,dx \end{bmatrix} \tag{3.1.8}$$

Just like the modal mass matrix, the modal stiffness matrix will always be diagonal and the same hamming procedure has to be performed.

An alternative way for computing the main diagonal terms of the modal stiffness matrix $k_{M\,ii}$, is by means of the corresponding modal mass $m_{M\,ii}$ and natural undamped frequency $\omega_{0\,i}$, avoiding the integral expression:

$$k_{M\,ii} = m_{M\,ii}\,\omega_{0\,i}^2$$

For what concerns the damping matrix, supposing the availability of experimental data for the damping ratio ξ_i estimation, the modal contribution can be computed by reversing the relationship $\xi_i = c_{M\,ii} \,/\, (2\, m_{M\,ii}\, \omega_{0\,i})$:

$$\left[R_m^1\right] = \begin{bmatrix} 2\xi_1 m_{M_{11}}\omega_{0_1} & \dots & 0 \\ \dots & & \dots \\ 0 & \dots & 2\xi_n m_{M_{nn}}\omega_{0_n} \end{bmatrix} \tag{3.1.9}$$

The modal damping matrix $[R_m]$ has to undergo the hamming procedure as well.

3.1.3 Displacement of the point on the carbody connected to the secondary suspension

For the computation of the secondary suspension elongation, there is the need to briefly focus on the displacement of the upper ends, connected to the carbody.

In fact, while for the suspension ends connected to the bogie frame only the rigid degrees of freedom are involved, for the point on the carbody the contribution of the flexible transverse vibration has to be taken into account as well.

The general rule of the *superimposition principle* still holds in case of a flexible body: the bounce z_A and pitch $\pm\, b\, \theta_A$ contributions have to be summed up to the transverse displacement of the rear w_R or front w_F connecting point, due to the flexible modes.

By definition, the transverse displacement $w_R(t)$ of a point belonging to a flexible body can be approximated by summing all of the contribution of the first N mode shapes evaluated in its corresponding position along the beam curvilinear abscissa x_R:

$$w_R(t) = w(x_R, t) \approx \sum_{i=1}^{N} w_i(x_R, t) = \sum_{i=1}^{N} \Phi_i(x_R)\, G_i(t) = \sum_{i=1}^{N} \Phi_{iR}\, G_i(t)$$

Thus there is just the need to define respectively $(\Phi_{iR};\, \Phi_{iF})$ since the time variable G_i modulating the vibration amplitudes under the external excitement is integrated with the other rigid independent variables, as already explained. By referring again to the data set of [29] already introduced and given the bogie wheelbase $b = 14\, m$, is possible to get the following transverse displacement contribution of the connection points:

Flexible mode	First	Second	Third	Fourth	Fifth	Sixth
$x_R = \frac{L}{2} - b$	$\Phi_{1R} = 0.624$	$\Phi_{2R} = -0.235$	$\Phi_{3R} = -0.883$	$\Phi_{4R} = -1.255$	$\Phi_{5R} = -1.300$	$\Phi_{6R} = -1.029$
$x_F = \frac{L}{2} + b$	$\Phi_{1F} = 0.624$	$\Phi_{2F} = 0.235$	$\Phi_{3F} = -0.883$	$\Phi_{4F} = 1.255$	$\Phi_{5F} = -1.300$	$\Phi_{6F} = 1.029$

Table 3.2: Contributions of the bending modes in the secondary suspension elongation

It is worth noticing that in the odd modes the deflection has the same direction and value, while in the even modes the deflection has still the same value but opposite sign: this is thanks to the symmetry of both boundary condition and evaluated point. Furthermore this is consistent with the already discussed mode shapes shown in figure 3.3.

At this point it is moreover possible to introduce the topic of the *virtual work* generation. In fact, if the secondary suspension force F_k is applied on a node of the *i-th* bending mode so that $\Phi_i(x_k) = 0$, that mode will not be excited as long as there is no *virtual displacement* δs_k and no resulting *virtual work* $\delta L_k = \overrightarrow{F}_k \times \overrightarrow{\delta s}_k$.

This means that, because of the carbody support position, it will be generally easier for the forces transmitted by the secondary suspension to excite the fourth and the fifth bending mode, which undergoes to a large transverse displacement in correspondence of the connection points, rather than the first and the second, which are closer to the nodes.

Anyway, only by looking at table 3.2, it is impossible to state which will be the more excited mode: additional information about the magnitude, frequency and phase of the applied force are fundamental as well in order to exploit the response of a mode.

3.2 Kinematics

The convention chosen for the spring elongation is positive during tensile deformation. Thus for the computation of the reaction forces it is possible to refer to the general rule:

$$\Delta L = x_U - x_D$$

$$F_k = -k\,\Delta L$$

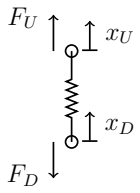

Figure 3.4: Kinematic convention

The same consideration can be extended to damper elongation velocity $\dot{\Delta L}$ in order to compute the dissipative damping force $F_c = -c\,\dot{\Delta L}$ generated.

The last thing to refresh before going through this section, is the definition of the independent variables: the constraint motions are collected in the vector $\underline{x}_C$ defined in equation 3.0.1; the vehicle degrees of freedom in the vector $\underline{x}_F$ defined in equation 3.1.3:

$$\underline{x} = \{\underline{x}_C;\ \underline{x}_F\} \qquad where \quad \begin{cases} \underline{x}_C = \{z_{C11};\ z_{C12};\ z_{C21};\ z_{C22}\} \\ \underline{x}_F = \{z_{B1};\ \theta_{B1};\ z_{B2};\ \theta_{B2};\ z_A;\ \theta_A;\ G_1;\ ...G_n\} \end{cases} \tag{3.2.1}$$

3.2.1 Primary suspension

The lower end of the primary suspension is connected to the wheelset, thus is straight forward to define the displacement as $x_D = z_{Cij}$. On the contrary the upper end in connected to the bogie frame, which undergoes to a bounce z_{Bi} and pitch θ_{Bi} movement.

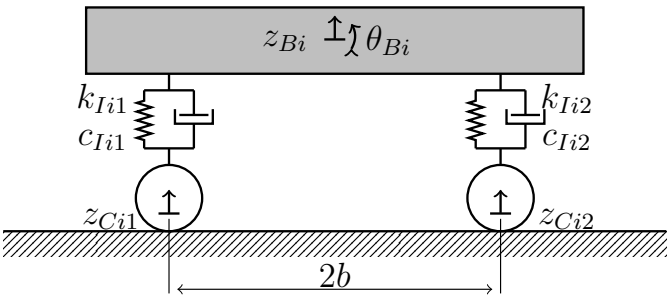

Figure 3.5: Primary suspension in passive vehicle

In order to combine the displacement and rotation contribute, the *superimposition principle* can be used: the upper end displacement results in $x_U = z_{Bi} \pm b\theta_{Bi}$. Thus at the end the overall primary suspension elongation will be:

$$\Delta L_{Iij} = x_U - x_D = (z_{Bi} \pm b\theta_{Bi}) - z_{Cij} \tag{3.2.2}$$

With + for the front suspension, with $j = 2$, and − for the rear suspension, with $j = 1$ while $i = [1,\ 2]$ refers to the front or rear bogie frame

The general rule of equation 3.2.2, can be used for the computation of all of the elongations $\Delta L_{I_{ij}}$ of the primary suspension, leading the following *jacobian* matrix definition:

$[\Lambda_{\Delta L_I}]$	z_{C11}	z_{C12}	z_{C21}	z_{C22}	z_{B1}	θ_{B1}	z_{B2}	θ_{B2}	z_A	θ_A	G_1	G_n
ΔL_{I11}	-1				1	-b						
ΔL_{I12}		-1			1	b						
ΔL_{I21}			-1				1	-b				
ΔL_{I22}				-1			1	b				

Table 3.3: *Jacobian* of the elongations of the primary suspension

Where the empty cells means null value.

At this point, the contribution of the primary suspension to the *stiffness* matrix $[K_I]$ can be computed: from the *potential energy* formulation it is possible to state that:

$$[K_I] = [\Lambda_{\Delta L_I}]^T [k_I] [\Lambda_{\Delta L_I}] \tag{3.2.3}$$

Where $[k_I]$ is a matrix collecting on its main diagonal the value of the stiffness of the springs: $diag\{k_I; k_I; k_I; k_I\}$. The same computation can be adapted for the contribution of the primary suspension to the damping matrix $[R_I]$ once is given $[c_I] = diag\{c_I; c_I; c_I; c_I\}$:

$$[R_I] = [\Lambda_{\Delta L_I}]^T [c_I] [\Lambda_{\Delta L_I}] \tag{3.2.4}$$

3.2.2 Secondary suspension

The lower end of the secondary suspension is connected to the middle of the bogie frame, thus the pitch rotation θ_{Bi} does provide no contribution and it is straight forward to define the displacement as $x_D = z_{Bi}$, with only the bogie bounce. The upper end is connected to the carbody and it is affected by its bounce z_A, pitch θ_A and bending vibration $\underline{G}$.

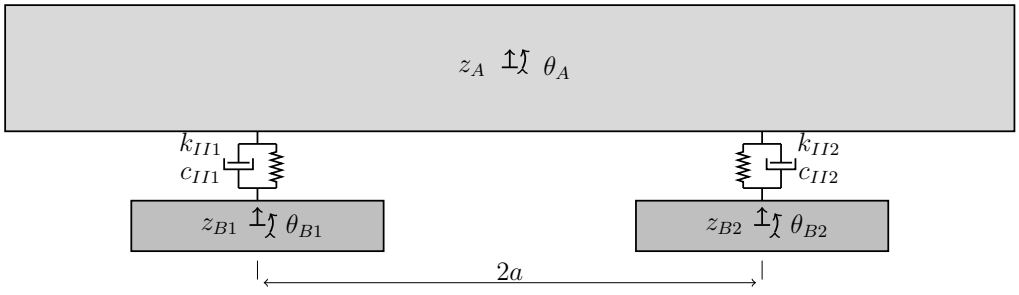

Figure 3.6: Linear secondary suspension

The *superimposition principle* allows to state that $x_U = z_A \pm a\theta_A + \Phi_{1i}G_1 + ...\Phi_{ni}G_n$ leading to the following definition of the overall elongation:

$$\Delta L_{IIi} = x_U - x_D = (z_A \pm a\theta_A + \Phi_{1i}G_1 + ...\Phi_{ni}G_n) - z_{Bi} \tag{3.2.5}$$

Where $i = 1$ refers to the rear suspension (Φ_{jR}) and requires the sign $-$, while $i = 2$ refers to the front suspension (Φ_{jF}) and requires the sign $+$.

In order to compute the contribution of the secondary suspension to the stiffness $[K_{II}]$ and damping $[R_{II}]$ matrices, the *jacobian* matrix of the elongations of the secondary suspension $[\Lambda_{\Delta L_{II}}]$ has to be defined by referring to the equation 3.2.5:

$[\Lambda_{\Delta L_{II}}]$	z_{C1}	z_{C2}	z_{C3}	z_{C4}	z_{B1}	θ_{B1}	z_{B2}	θ_{B2}	z_A	θ_A	G_1	G_n
ΔL_{II1}					-1				1	-a	Φ_{1R}	Φ_{nR}
ΔL_{II2}							-1		1	a	Φ_{1F}	Φ_{nF}

Table 3.4: *Jacobian* of the elongations of the secondary suspension

Again from the *potential energy* formulation it is possible to state that:

$$[K_{II}] = [\Lambda_{\Delta L_{II}}]^T [k_{II}] [\Lambda_{\Delta L_{II}}] \tag{3.2.6}$$

Where $[k_{II}] = diag\{k_{II};\ k_{II}\}$ is a matrix collecting on its diagonal the values of the stiffness of the secondary suspension. The same computation can be extended to the contribution of the secondary suspension to the damping matrix $[R_{II}]$ once is given $[c_{II}] = diag\{c_{II};\ c_{II}\}$:

$$[R_{II}] = [\Lambda_{\Delta L_{II}}]^T [c_{II}] [\Lambda_{\Delta L_{II}}] \tag{3.2.7}$$

3.3 Equations of the first configuration

Once all of the contributions of the matrices have been computed, it is possible to assemble and define the terms required for the equations of motion of the passive system.

Knowing that the human perception is sensible up to $25Hz$, by looking at the reference table 3.1 it is possible to state that both the first and the second bending mode belong to the frequency range of interest for the passengers comfort, thus have been introduced in the study. By recalling the generic formulation of the vector $\underline{x}$ collecting the independent variables in equation 3.2.1, its final expression can be defined as follow:

$$\underline{x} = \{z_{C11};\ z_{C12};\ z_{C21};\ z_{C22};\ z_{B1};\ \theta_{B1};\ z_{B2};\ \theta_{B2};\ z_A;\ \theta_A;\ G_1;\ G_2\} \tag{3.3.1}$$

3.3.1 Equations of motion for the passive system

For what concern the *stiffness* matrix $[K]$, there are three contributions.

The contribution of the primary suspension $[K_I]$, defined in equation 3.2.3, shows non zero values in the columns and rows referred to both constrained $\underline{x}_C$ and free $\underline{x}_F$ variables: it provides the system excitement and ensures the coupling between the constraint motion and the response of the free degrees of freedom.

The contribution of the secondary suspension $[K_{II}]$, defined in equation 3.2.6, has non zero values only in the south east submatrix, in correspondence of the free variables $\underline{x}_F$: it relates the bogie displacement to the response of the carbody and has to role to couple the rigid and the flexible independent variables.

The contribution of the modal stiffness $[K_m]$, defined in equation 3.1.8, has the only values on the main diagonal, in correspondence of the flexible variables: it accounts for the bending stiffness of the car body.

$$[K] = [K_I] + [K_{II}] + [K_m] \tag{3.3.2}$$

The same considerations hold for the *damping* matrix: the contributions of the primary suspension $[R_I]$ is defined in equation 3.2.4; the contribution of the secondary suspension $[R_{II}]$ in equation 3.2.7; the modal contribution $[R_m]$ in equation 3.1.9.

$$[R] = [R_I] + [R_{II}] + [R_m] \tag{3.3.3}$$

For what concerns the *mass* matrix, there are two contribution: one accounting for the rigid *dofs* $[M_d]$ and the other shown in equation 3.1.6 for the modal mass $[M_m]$.

In order to compute the matrix of the rigid *dofs* $[M_d]$, it is important to highlight that: the inertia associated to the constrained variables $\underline{x}_C$ is neglected since there is no interest in the computation of the contact forces; the rigid *dofs* correspond to the rotations and displacements of the centre of mass of the bodies, thus to allocate the proper inertia in the relative position on the main diagonal of $[M_d]$ is straight forward.

The resulting matrix will be $[M_d] = diag\{0; 0; 0; 0; m_B; J_B; m_B; J_B; m_A; J_A; 0; 0\}$.

At the end, the overall *mass matrix* will result from the following expression:

$$[M] = [M_d] + [M_m] \tag{3.3.4}$$

Once all of matrices have been computed, the equations of motion of the passive configuration referred to the independent variable $\underline{x}$ of equation 3.3.1 can be defined:

$$[M]\,\underline{\ddot{x}} + [R]\,\underline{\dot{x}} + [K]\,\underline{x} = \underline{0}$$

In order to highlight the excitation term and the free independent variables whose response has to be evaluated, it is necessary to perform a *matrix partitioning*.

The approach is based on the distinction of the mutual effect that the constrained variables have on the free *dofs* and vice versa and allows to get the expression:

$$\begin{bmatrix}[M_{CC}] & [M_{CF}]\\ [M_{FC}] & [M_{FF}]\end{bmatrix}\begin{Bmatrix}\underline{\ddot{x}}_C\\ \underline{\ddot{x}}_F\end{Bmatrix} + \begin{bmatrix}[R_{CC}] & [R_{CF}]\\ [R_{FC}] & [R_{FF}]\end{bmatrix}\begin{Bmatrix}\underline{\dot{x}}_C\\ \underline{\dot{x}}_F\end{Bmatrix} + \begin{bmatrix}[K_{CC}] & [K_{CF}]\\ [K_{FC}] & [K_{FF}]\end{bmatrix}\begin{Bmatrix}\underline{x}_C\\ \underline{x}_F\end{Bmatrix} = \underline{0}$$

In particular the first row of this expression can be used for the computation of the reaction forces in correspondence of the constrained variables $\underline{x}_C$, while the second one relates the free *dofs* response to the constraint excitement.

Knowing from equation 3.3.4 that the sub matrix $[M_{FC}]$ is null, the second row leads to the final expression:

$$[M_{FF}]\,\underline{\ddot{x}}_F + [R_{FF}]\,\underline{\dot{x}}_F + [K_{FF}]\,\underline{x}_F = -[R_{FC}]\,\underline{\dot{x}}_C - [K_{FC}]\,\underline{x}_C \tag{3.3.5}$$

The equation of motion has been numerically integrated by menas of the *Matlab* tool *ode45*. In order to downgrade the system to a first order differential equation, a further identity has been coupled to the equation 3.3.5:

$$\begin{cases}[M_{FF}]\,\underline{\ddot{x}}_F \;=\; -[R_{FF}]\,\underline{\dot{x}}_F \;-[K_{FF}]\,\underline{x}_F \;-[R_{FC}]\,\underline{\dot{x}}_C \;-[K_{FC}]\,\underline{x}_C\\ [I]\,\underline{\dot{x}}_F \;=\; [I]\,\underline{\dot{x}}_F\end{cases} \tag{3.3.6}$$

The equation 3.3.6 can be rewritten in matrix notation leading to the expression:

$$\underline{\dot{v}} \;=\; [A]\,\underline{v} \;+\; [B_C]\,\underline{u}_C \tag{3.3.7}$$

Where the *state vector* $\underline{v} = \{\underline{\dot{x}}_F;\, \underline{x}_F\}$ collects the degrees of freedom and their derivatives; the vector of the external excitement $\underline{u}_C = \{\underline{\dot{z}}_C;\, \underline{z}_C\}$ contains the constraint motion and their derivatives; the *state matrix* of the system $[A]$ and of the external excitement $[B_C]$ are defined as follow:

$$[A] = \begin{bmatrix}-[M_{FF}]^{-1}[R_{FF}] & -[M_{FF}]^{-1}[K_{FF}]\\ [I] & [0]\end{bmatrix} \qquad [B_C] = \begin{bmatrix}-[M_{FF}]^{-1}[R_{FC}] & -[M_{FF}]^{-1}[K_{FC}]\\ [0] & [0]\end{bmatrix} \tag{3.3.8}$$

This procedure has been applied to the data set of a passenger railway vehicle [30] that can be collected in the following table:

Car body	$m_A = 34\,250\ kg$ $J_A = 2\,000\,000\ kn\ m^2$	Bogie frame	$m_B = 3\,000\ kg$ $J_B = 2\,200\ kg\ m^2$
Primary suspension	$k_I = 2\,400\,000\ N/m$ $c_I = 5\,000\ Ns/m$	Secondary suspension	$k_{II} = 500\,000\ N/m$ $c_{II} = 40\,000\ Ns/m$
Length	$L = 24.5\ m$ $2a = 19\ m$ $2b = 2.5\ m$		
First bending mode	$\omega_1 = 53.2\ rad/s$ $f_1 = 8.5\ Hz$ $\xi_1 = 0.0181$	Second bending mode	$\omega_2 = 146.6\ rad/s$ $f_2 = 23.3\ Hz$ $\xi_2 = 0.0498$

Table 3.5: First configuration data set

3.3.2 Natural frequencies and mode shapes

After the definition of the *state matrix* $[A]$ in equation 3.3.8, whose dimension is 16×16 consistently with the *state vector* $\underline{v}$, the *natural frequencies* and the *mode shapes* of the system can be computed.

The *eigenvalues* associated to the matrix $[A]$ are 16 complex conjugate numbers, whose imaginary part directly gives the 8 natural frequencies ω_0:

	$\omega_0\ [rad/s]$	$f\ [Hz]$	ξ
Carbody bounce	5.0672	0.8065	0.1880
Carbody pitch	6.2821	0.9998	0.2394
Bogie frame bounce	41.0144	6.5277	0.2113
Bogie frame pitch	58.2793	9.2754	0.0609
First bending mode	52.7633	8.3975	0.0360
Second bending mode	146.4580	23.3095	0.0505

Table 3.6: Natural frequencies of first configuration

Moreover the ratio between the *real* and the *imaginary* part of the *eigenvalues* provides an estimation of the damping ratio associated to the mode, as shown in the table 3.6.

The correspondence between the *dofs* and the *natural frequencies* has been figured out by looking at the *eigenvectors* of the *state matrix* $[A]$ associated to each *eigenvalue*.

The *eigenvector* matrix has the same dimension 16×16 of the *state matrix* $[A]$ and its columns, which are complex conjugate, contain the mode shapes: the first rows refer to the velocity, while the last to the displacement, according to the *state vector* $\underline{v}$ definition.

The absolute value of the *eigenvector* directly provides the amplitude of the displacements of the independent variables in the specific *mode shape*, while the ratio of the *imaginary* over the *real* part contain the information about the *phase* $\tan\phi = \Im/\Re$.

The resulting *mode shapes* are summarized in the following table: the amplitudes are obtained from to the normalized *eigenvector* in order to highlight the dominant contribute; the phases are expressed as difference respect to the dominant *dof*.

	z_{B1}	θ_{B1}	z_{B2}	θ_{B2}	z_A	θ_A	G_1	G_2
In phase bogie bounce	0.7056	0	0.7056	0	0.0405	0	0.0518	0
$f = 6.5790\,Hz\ -\ \xi = 0.2103$	0°	213°	0°	−56°	240°	253°	112°	85°
Counter phase bogie bounce	0.7071	0	0.7071	0	0	0.0066	0	0
$f = 6.4763\,Hz\ -\ \xi = 0.2122$	0°	29°	180°	123°	258°	65°	254°	269°
Bogie pitch	0	0.9784	0	0.2069	0	0	0	0
$f = 9.2754\,Hz\ -\ \xi = 0.0609$	144°	0°	101°	234°	8°	174°	256°	216°
Bogie pitch	0	0.2320	0	0.9727	0	0	0	0
$f = 9.2754\,Hz\ -\ \xi = 0.0609$	−97°	30°	−74°	0°	78°	−42°	−8°	−74°
Carbody bounce	0.0956	0	0.0956	0	0.9908	0	0.0090	0
$f = 0.8065\,Hz\ -\ \xi = 0.1880$	21°	177°	21°	−20°	0°	21°	201°	201°
Carbody pitch	0.5650	0	0.5650	0	0	0.6012	0	0.0020
$f = 0.9998\,Hz\ -\ \xi = 0.2394$	207°	267°	27°	158°	206°	0°	206°	207°
First bending mode	0.4320	0	0.4320	0	0.0322	0	0.7910	0
$f = 8.3975\,Hz\ -\ \xi = 0.0360$	−66°	−164°	−66°	−144°	−249°	−248°	0°	−67°
Second bending mode	0.0274	0	0.0274	0	0	0.0007	0	0.9992
$f = 23.3095\,Hz\ -\ \xi = 0.0505$	90°	273°	270°	197°	90°	89°	90°	0°

Table 3.7: Mode shapes of the first configuration

For the sake of simplicity, the displacements lower than $1e-6$ are neglected.

Focusing on the mode shape dominated by the first bending mode, it is possible to detect the involvement of the in phase bounce of the bogie frames: this is consistent with the mode shape represented in figure 3.3, where the support points move synchronously in the odd modes. The synchronous bogie bounce movement also activates the coach bounce, thus the latter always appears together with the first bending mode.

The same happens for the second bending mode appearing always coupled with the carbody pitch, since both are activated by the counter phase bounce of the bogie frames. Again this is consistent with the mode shapes of figure 3.3: in the even modes, the support points have opposite sign.

For what concern the bogie frame bounce, a small difference in the excitement frequency depending on the phase can be observed: if the bogies undergo a synchronous motion, the natural frequency is slightly higher and the carbody bounce and first bending mode are activated; on the contrary when the bogies move in counter phase, the natural frequency is slightly lower and second bending mode and carbody pitch appear.

For what concern the bogie pitch, its activation is completely decoupled from the other *dofs*: as already explained, it may appear useless, but on the contrary it is needed for the computation of the primary suspension elongation and thus of the controlled force.

The pitch of the bogie frame would be on the contrary involved in the longitudinal displacement of the carbody, but this mathematical model of the vehicle only accounts for the vertical dynamics.

3.3.3 Frequency response function

With the definition of the equation of motion, the response in case of a monoharmonic excitement can be computed, feasible under the assumption of dealing with an harmonic railway irregularity.

Before computing the *transfer function*, it is important to briefly focus on the wheelset displacement z_{Cij}: given the defect wavelength λ_D, the wheelbase p_k and the vehicle velocity v, in case of monoharmonic irregularity it is possible to refer to the wheel position in terms of delay, represented by a phase, respect to the position of a reference wheel.

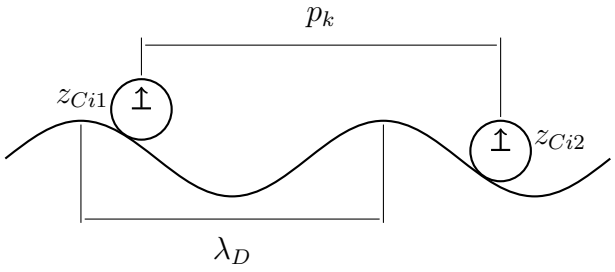

Figure 3.7: Track irregularity with monoharmonic profile

In particular by introducing the notion of the vector rotating in the complex plane, the displacement along the railway profile can be described as:

$$z(s) = A\, e^{j\,\Omega_D s} \quad \text{with} \quad \Omega_D = \frac{2\pi}{\lambda_D} \tag{3.3.9}$$

Where $s = s_0$ for the reference wheel, assumed to be the rear one; while for the other wheels $s = s_0 + p_k$. In particular the values of the wheelbase are: for $z_{C12} \implies 2b$; for $z_{C21} \implies 2a$; for $z_{C22} \implies 2(a+b)$. Thus from equation 3.3.9 it is possible to state:

$$z_k(s) = A\, e^{j\,\Omega_D (s_0 + p_k)} = A\, e^{j\,\Omega_D s_0}\, e^{j\,\Omega_D p_k} \implies z_k(s) = z(s_0)\, e^{j\phi_k} \tag{3.3.10}$$

Where the phase delay is $\phi_k = \Omega_D\, p_k = \frac{2\pi}{\lambda_D}\, p_k$. The equation 3.3.10 allows to rewrite the vector of the constraint motion $\underline{x}_C$ in case of monoharmonic irregularity as follow:

$$\underline{x}_C = \begin{Bmatrix} z_{C11} \\ z_{C12} \\ z_{C21} \\ z_{C22} \end{Bmatrix} = \begin{Bmatrix} z_{C11} \\ z_{C11}\, e^{j\phi_1} \\ z_{C11}\, e^{j\phi_2} \\ z_{C11}\, e^{j\phi_3} \end{Bmatrix} = \underline{\phi}\, z_{C11} \tag{3.3.11}$$

Moreover the equation 3.3.10 allows to introduce the definition of the *real* excitement frequency. In fact by moving the constrain displacement $z(s)$ from the spatial s to the time t domain with the relationship $s = vt$, it is possible to observe that:

$$z(s) = A\, e^{j\Omega_D s} \implies z(t) = A e^{j\Omega_D v t} = A e^{j\Omega t}$$

Thus the *real* excitement angular frequency is $\Omega = \Omega_D v = 2\pi \frac{v}{\lambda_D}$. This mean that it depends on both the vehicle velocity v and the irregularity characteristic λ_D; thus in order to excite the system about its resonances, those two aspects have to be tuned.

Knowing the vehicle natural frequencies from table 3.6 and defined the relationship of the excitement frequency $f = \frac{v}{\lambda_D}$, it is possible to compute the *critical velocities map* summarizing the $(v,\ \lambda_D)$ combination able to excite the system in resonance.

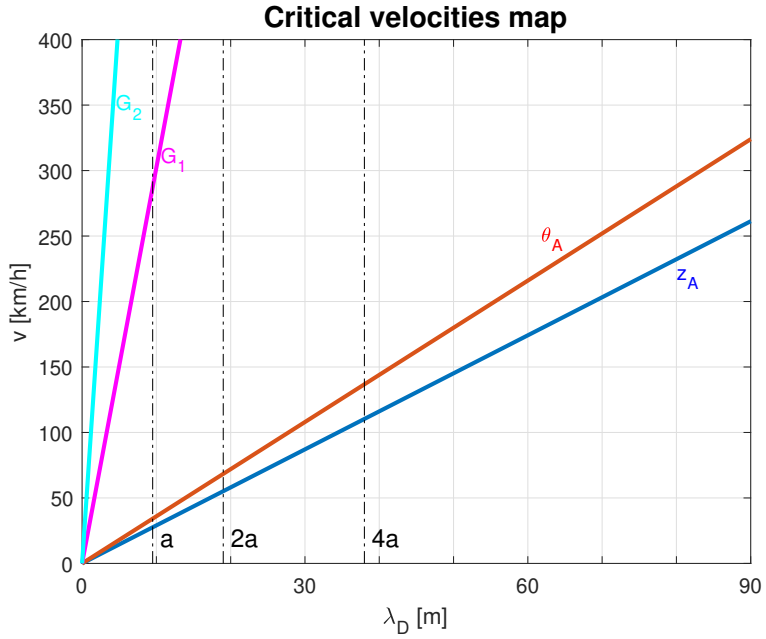

Figure 3.8: Critical velocities map for the first configuration

The vertical dotted lines of figure 3.8 highlight the main wheelbase in between the two bogie frames: when $\lambda_D = 2a$ the bogie frames move in phase, thus there is the maximum *lagrangian* component on the excitement of $(z_A;\ G_1)$ independent variables; when $\lambda_D = 4a$ the bogie frames move in counter phase, thus there is the maximum *lagrangain* component on the excitement of $(\theta_A;\ G_2)$ independent variables.

Those considerations stress that for generating *virtual work* δL and exciting the system, to have a force is not sufficient: a non zero *lagrangian* is furthermore necessary.

The synergy between the *lagrangain* of the mode shapes and the excitation frequency is even more clear by looking at the spectrum of the frequency response function.

For computing the frequency response function, it is necessary to move the equations of motion 3.3.5 from the *time* to the *frequency* domain. By imposing an harmonic input $\underline{z}_C(t) = \underline{z}_{C0}\, e^{j\Omega t}$ and assuming an harmonic response $\underline{x}_F(t) = \underline{x}_{F0}\, e^{j\Omega t}$ it is possible to get:

$$\left(-\Omega^2[M_{FF}] + j\Omega[R_{FF}] + [K_{FF}]\right)\underline{x}_{F0} = -\left(j\Omega[R_{FC}] + [K_{FC}]\right)\underline{x}_{C0}$$

Considering the relationship $\underline{x}_C = \underline{\Phi}\, z_C$ from equation 3.3.11, the final expression is:

$$\left(-\Omega^2[M_{FF}] + j\Omega[R_{FF}] + [K_{FF}]\right)\underline{x}_{F0} = -\left(j\Omega[R_{FC}] + [K_{FC}]\right)\underline{\Phi}\, z_{C0} \tag{3.3.12}$$

Where, considering the relationship $\Omega = v\Omega_D$ and the delay defined in equation 3.3.10, the phase vector $\underline{\Phi}(\Omega)$ results a function of the excitement frequency as well:

$$\Phi_k(\Omega) = e^{j\,2\pi\frac{p_k}{\lambda_D}} = e^{j\,\frac{p_k}{v}\Omega}$$

The frequency response has been computed by fixing the vehicle velocity v and by varying the defect wavelength λ_D in order to get all the excitation frequencies $f = \frac{v}{\lambda_D}$.

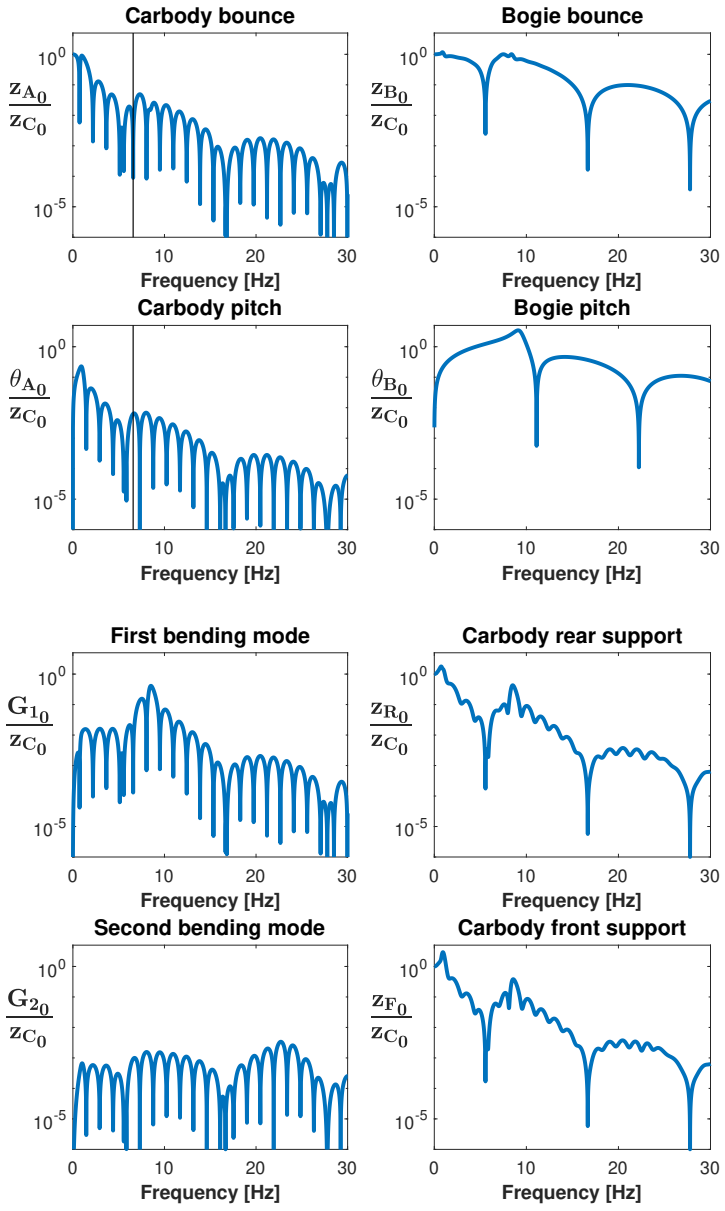

Figure 3.9: Frequency response function of the first configuration with $v = 100\,km/h$

The two bending modes (G_1; G_2) and the bounce and pitch of both carbody (z_A; θ_A) and bogie frame (z_{Bi}; θ_{Bi}) are reported. In addition there are the responses of the carbody supporting points, obtained through *superimposition* of the (z_A; θ_A; G_1; G_2) *dofs*.

The first important thing to highlight, is the presence of the lobes: as long as the defect wavelength λ_D is varying together with the excitation frequency Ω, its value may excite the bogie frame in phase, maximizing the *lagrangain* component of the carbody bounce and of the first bending mode while minimizing the *lagrangian* component of the carbody pitch and of the second bending mode, or in counter phase, with a dual effect.

This appear more clear noticing that the nodes in the response of the carbody bounce correspond to middle of the carbody pitch lobes, and vice versa: it is possible to demonstrate that the frequencies causing a drop in the response of the carbody pitch correspond to a synchronous excitement of the bounce of the bogie frames by comparing the wavelength of the irregularity λ_D and the distance of the bogie frames $2a = 19\,m$:

$f\ [Hz]$	7.31	8.77	10.23	11.70	13.16	14.62
$\lambda_D = v/f\ [m]$	3.80	3.17	2.72	2.37	2.11	1.90
$2a/\lambda_D$	5.0	6.0	7.0	8.0	9.0	10.0

Table 3.8: Defect wavelength leading to a null *lagrangian* component on the carbody pitch

When the bogie wheelbase $2a$ is an integer multiple of the wavelength of the irregularity λ_D, the bogie frames move in phase leading to a null *lagrangian* component on the carbody pitch, whose response drops; at the same time, this condition ensures the maximum *lagrangian* for the carbody bounce. The vertical line in figure 3.9 shows that in correspondence of the bounce node there is a pitch peak, and vice versa.

The lobes of the bogie frame response are wider than the lobes of the carbody response: this effect is due to a larger fundamental frequency $f = \frac{v}{2b}$ as long as the wheelbase of the bogie supports is shorter compared to the wheelbase of the carbody supports $2b < 2a$.

In the same way, the fundamental frequency of the lobe $f = \frac{v}{\lambda_D}$ will increase with a larger vehicle velocity v, leading to wider lobes, and vice versa.

Even if the figure 3.9 gives an idea of the resonant frequencies of the mode shapes, the peaks can be easier detected through the frequency response computed with a fixed irregularity wavelength $\lambda_D = 2a/1.75 = 10.86\,m$ and variable vehicle velocity $v = f\,\lambda_D$.

The ratio $2a/\lambda_D = 1.75$ has been chosen considering a value equally spaced from 1.5, which would excite the bogie frames in counter phase, and 2, which would excite the bogie frames in phase: in this way, all of the mode shapes are supposed to be excited.

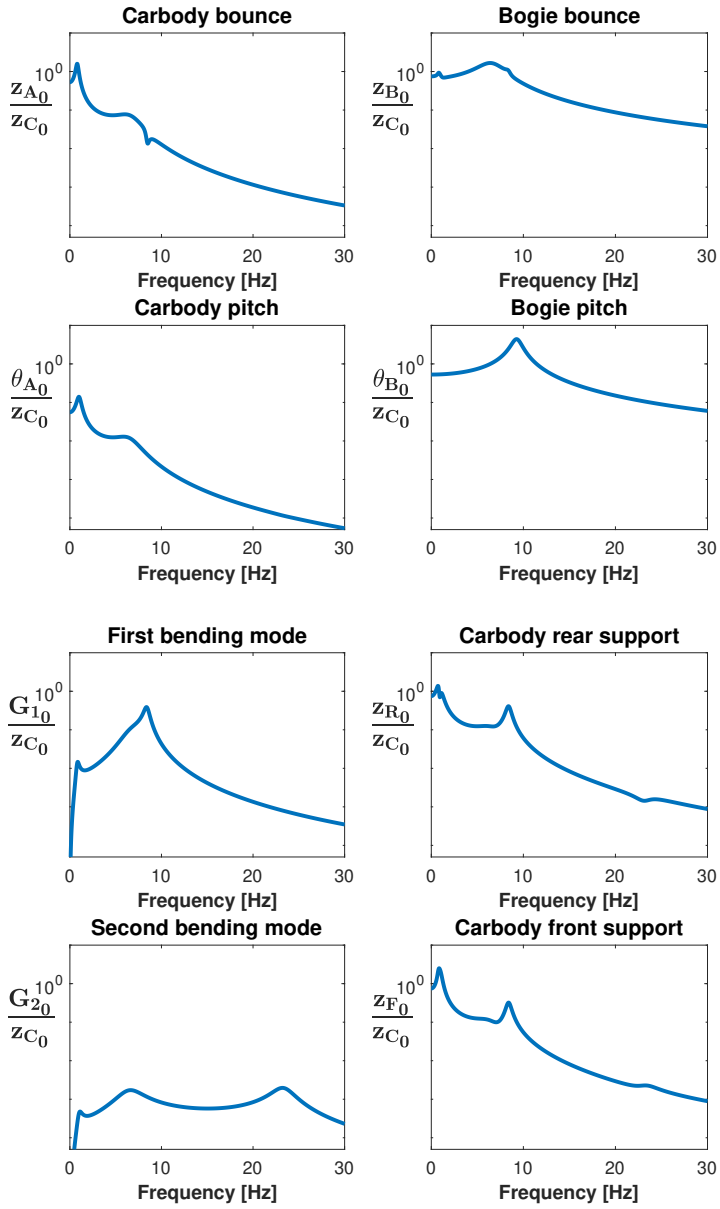

Figure 3.10: Fist configuration frequency response function with $\lambda_D = 10.86\,m$

The peaks are consistent with the computed natural frequencies, summarized in table 3.6: the carbody pitch and bounce are about 1 Hz; the bogie pitch about 9 Hz and the bounce about 7 Hz; the first bending mode is at 8 Hz while the second at 23 Hz.

Moreover the figure 3.10 highlights the mutual interaction of the mode shapes, consistently with the summarizing table 3.7.

3.3.4 Equations of motion for the controlled system

In the passive configuration shown in figure 3.1, the primary suspension consists in a spring and a damper with constant characteristic (k_I; c_I). In the controlled configuration, the passive damper is replaced by a semi active element with variable damping coefficient:

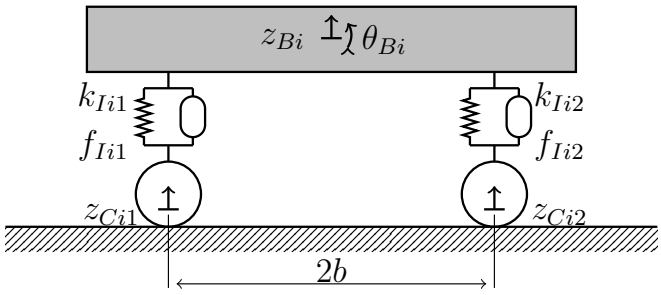

Figure 3.11: Primary suspension with semi active damper in controlled configuration

The semi active element generate a dissipative force f_{Iij} function of the suspension elongation velocity $\Delta\dot{L}_{I_{ij}}$ and of the variable damping coefficient $[c_{min} \div c_{max}]$, where the first index i refers to the front or rear bogie frame while the second index j to the front or rear wheelset. Without a fixed damping $c_{I_{ij}}$, it is no longer possible to define the matrix $[R_I]$ of equation 3.2.7 providing the primary suspension contribution to the system damping. Thus the force f_{Iij} has to be treated as an internal force applied to the suspension ends.

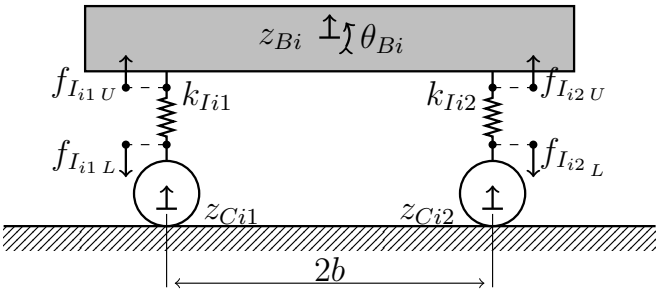

Figure 3.12: Modelling of the control force generated in the semi active primary suspension

For computing the *lagrangian* $\delta L = \underline{Q}_I^T \delta\underline{q}$ of the virtual work $\delta L = \overrightarrow{F} \times \delta\overrightarrow{s}_I = \underline{u}_f^T\, \delta\underline{s}_I$ generated by the control force on the primary suspension, it is necessary to introduce the vector $\underline{u}_f$, collecting the control forces computed a part by the controller, and the vector $\delta\underline{s}_I$ of the virtual displacements.

Considering that $f_{I_{ij\,L}} = -f_{I_{ij\,U}}$, the following reorganization can be arranged:

$$\underline{u}_f = \begin{Bmatrix} f_{I_{11\,U}} \\ f_{I_{11\,L}} \\ f_{I_{12\,U}} \\ f_{I_{12\,L}} \\ f_{I_{21\,U}} \\ f_{I_{21\,L}} \\ f_{I_{22\,U}} \\ f_{I_{22\,L}} \end{Bmatrix} = \begin{bmatrix} 1 & 0 & 0 & 0 \\ -1 & 0 & 0 & 0 \\ 0 & 1 & 0 & 0 \\ 0 & -1 & 0 & 0 \\ 0 & 0 & 1 & 0 \\ 0 & 0 & -1 & 0 \\ 0 & 0 & 0 & 1 \\ 0 & 0 & 0 & -1 \end{bmatrix} \begin{Bmatrix} f_{I_{11}} \\ f_{I_{12}} \\ f_{I_{21}} \\ f_{I_{22}} \end{Bmatrix} = [\Lambda_{u_{fF}}]\, \underline{u}_F \tag{3.3.13}$$

Focusing on the vector of the virtual displacements $\delta \underline{s}_I$, it is possible to notice that the lower application point directly experiences the wheelset displacement, while the upper lays on the bogie frame and its motion can be computed by means of the *superimposition* principle as follow:

$$\delta s_{I_{ij\,L}} = \delta z_{Cij} \qquad\qquad \delta s_{I_{ij\,U}} = \delta z_{Bi} \pm b\delta\theta_{Bi} \tag{3.3.14}$$

Since the virtual displacement $\delta s_{I_{ij}}$ is a function of the system independent variables $\delta \underline{x}$, it can be expressed in matrix notion as $\delta \underline{s}_I = [\Lambda_{\delta s_I}]\, \delta \underline{x}$, given the *jacobian* $[\Lambda_{\delta s_I}]$:

$[\Lambda_{\delta s_I}]$	z_{C11}	z_{C12}	z_{C21}	z_{C22}	z_{B1}	θ_{B1}	z_{B2}	θ_{B2}	z_A	θ_A	G_1	G_n
$\delta s_{I_{11\,U}}$					1	-b						
$\delta s_{I_{11\,L}}$	1											
$\delta s_{I_{12\,U}}$					1	b						
$\delta s_{I_{12\,L}}$		1										
$\delta s_{I_{21\,U}}$							1	-b				
$\delta s_{I_{21\,L}}$			1									
$\delta s_{I_{22\,U}}$							1	b				
$\delta s_{I_{22\,L}}$				1								

Table 3.9: *Jacobian* of the virtual displacements of the primary suspension

At this point, the *lagrangian* component of the control force can be computed:

$$\delta L \;=\; \underline{Q}_I^T\, \delta \underline{x} \;=\; \underline{u}_f^T\, \delta \underline{s}_I \qquad \Longrightarrow \qquad \underline{Q}_I^T \;=\; \left([\Lambda_{u_{fF}}]\, \underline{u}_F\right)^T [\Lambda_{\delta s_I}] \;=\; \underline{u}_F^T [\Lambda_{u_{fF}}]^T [\Lambda_{\delta s_I}]$$

The resulting $\underline{Q}_I$ is a row vector; so by transposing it is possible to get:

$$\underline{Q}_I \;=\; [\Lambda_{\delta s_I}]^T\, [\Lambda_{u_{fF}}]\, \underline{u}_F \;=\; [Q_I]\, \underline{u}_F \tag{3.3.15}$$

Leading to the final expression of the equations of motion:

$$\begin{bmatrix} [M_{CC}] & [M_{CF}] \\ [M_{FC}] & [M_{FF}] \end{bmatrix} \begin{Bmatrix} \ddot{\underline{x}}_C \\ \ddot{\underline{x}}_F \end{Bmatrix} + \begin{bmatrix} [R_{CC}] & [R_{CF}] \\ [R_{FC}] & [R_{FF}] \end{bmatrix} \begin{Bmatrix} \dot{\underline{x}}_C \\ \dot{\underline{x}}_F \end{Bmatrix} + \begin{bmatrix} [K_{CC}] & [K_{CF}] \\ [K_{FC}] & [K_{FF}] \end{bmatrix} \begin{Bmatrix} \underline{x}_C \\ \underline{x}_F \end{Bmatrix} = \begin{bmatrix} [Q_I^C] \\ [Q_I^F] \end{bmatrix} \underline{u}_F$$

It is important to remind that: the damping matrix $[R] = [R_{II}] + [R_m]$ doesn't have the primary suspension contribution $[R_I]$, ensured by the forces vector $\underline{u}_F$; the stiffness and mass matrix are the same of the passive configuration, from equation 3.3.2 and 3.3.4.

Following the same procedure of the passive configuration, is furthermore possible to define the *state matrix* notion already shown in equation 3.3.7:

$$\dot{\underline{v}} \;= [A]\, \underline{v} \;+\; [B_C]\, \underline{u}_C \;+\; [B_F]\, \underline{u}_F \tag{3.3.16}$$

Where the *state matrices* $[A]$ and $[B_C]$ are the same of equation 3.3.8 while $[B_F]$ is:

$$[A] = \begin{bmatrix} -[M_{FF}]^{-1}[R_{FF}] & -[M_{FF}]^{-1}[K_{FF}] \\ [I] & [0] \end{bmatrix} \qquad [B_C] = \begin{bmatrix} -[M_{FF}]^{-1}[R_{FC}] & -[M_{FF}]^{-1}[K_{FC}] \\ [0] & [0] \end{bmatrix}$$

$$[B_F] = \begin{bmatrix} -[M_{FF}]^{-1}[Q_I^F] \\ [0] \end{bmatrix} \tag{3.3.17}$$

3.4 Equations of the second configuration

The model of the second configuration has the same layout of the previous, reported in figure 3.1, with the only difference that it includes a *submodel* for the description of the secondary suspension dynamic behaviour.

The secondary suspension of the railway vehicles, whose role is to support the carbody preventing the transmission of the high frequency excitements, is usually an air spring.

Figure 3.13: Air spring for the secondary suspension of railway vehicles

The basic structure on an air suspension consists in:

- a deformable *rubber bellow*, collecting the air;
- a *laminated rubber* as security device for avoiding impacts an the end of the stroke;
- an auxiliary *air reservoir* where the air flowing from the rubber bellow is directed during the suspension compression;
- an *orifice*, which rules the air flow from the rubber bellow to the reservoir, controlling the pressure losses and thus the dissipation of energy.

The modelling of the suspension is fundamental in order to get accurate results, especially from a dynamic point of view. In fact the air spring has its own dynamics, with resonance and inertia effects, a non linear energy dissipation, a thermodynamic state of the filling air to be characterized [31].

For this study case, the so called *Nishimura model [32]* has been used.

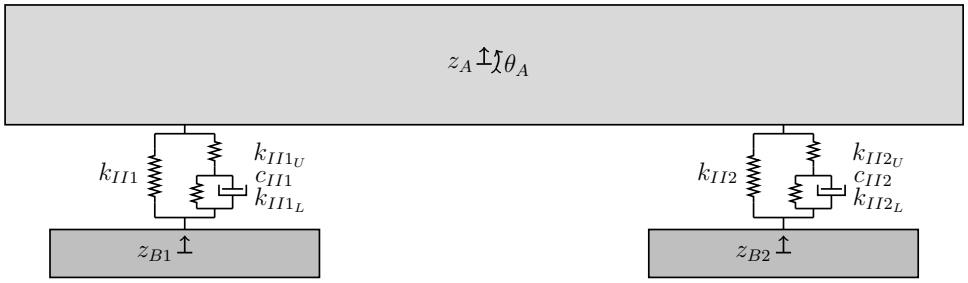

Figure 3.14: Secondary suspension with *Nishimura* air spring model

3.4.1 Model of the air spring

The model involves ideal linear spring and damper, connected so that: the damper c_{II} is in parallel to the lower spring k_{II_L}, both in series with the upper spring k_{II_U}; this complex element is finally in parallel with the main secondary spring k_{II}.

In order to describe the transmitted force, it is necessary to know the elongation of every element, starting from the position of the three highlighted points (z_L; z_M; z_U).

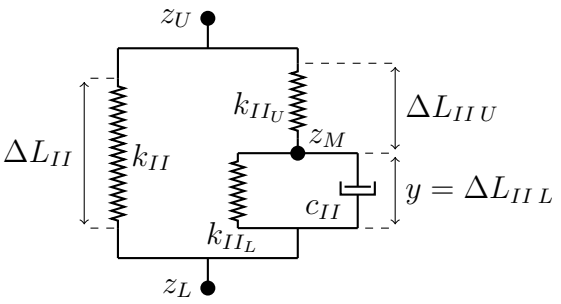

Figure 3.15: *Nishimura* air spring model

Assuming a convention positive during tensile deformation, the elongations are:

$$\begin{cases} \Delta L_{II} = z_U - z_L \\ \Delta L_{II\,L} = z_M - z_L = y \\ \Delta L_{II\,U} = z_U - z_M = (z_U - z_L) - (z_M - z_L) = \Delta L_{II} - y \end{cases} \tag{3.4.1}$$

Since $\Delta L_{II\,U}$ is the difference of the other two elongations ($\Delta L_{II} - y$), the generated force and the transfer function can be defined as function of (ΔL_{II}; y) only.

By referring to the system of figure 3.14, it is possible to state that: ΔL_{II} corresponds to the standard elongation of the secondary suspension introduced in equation 3.2.5, which is a function of the independent coordinates $\underline{x}$ of equation 3.3.1; on the contrary, an additional set of independent variable $\underline{y}$, needed for the description of the state of the *Nishimura* model of the air spring, has to be integrated in the independent variables set:

$$\underline{x} = \{z_{C11};\ z_{C11};\ z_{C11};\ z_{C11};\ z_{B1};\ \theta_{B1};\ z_{B2};\ \theta_{B2};\ z_A;\ \theta_A;\ G_1;\ G_2;\ y_1;\ y_2\} \tag{3.4.2}$$

The force transmitted with this modelling, is given by the equation:

$$\begin{aligned} F &= -k_{II}\Delta L_{II} - k_{II_U}\,(\Delta L_{II} - y) \\ &= -k_{II}\Delta L_{II} - k_{II_L}\,y - c_{II}\,\dot{y} \end{aligned} \tag{3.4.3}$$

The substitution of the right hand side is possible thanks to the *continuity* condition about the node z_M, that lead to the following balance of the vertical forces:

$$-k_{II_U}\,(\Delta L_{II} - y) = -k_{II_L}\,y - c_{II}\,\dot{y} \tag{3.4.4}$$

Under the assumption of harmonic excitement $\Delta L_{II}(t) = \Delta L_{II_0}\,e^{j\,\Omega t}$, the frequency response function of the generated force can be computed by moving the equation 3.4.3 from the time to the frequency domain.

In order to solve the dependency on y, the expression of equation 3.4.4 in the frequency domain can be substituted as long as it provides the relationship between (ΔL_{II}; y):

$$y_0 = \frac{k_{II_U}}{(k_{II_L} + k_{II_U}) + j\,\Omega\,c_{II}}\,\Delta L_{II_0}$$

The final expression of the frequency response function of the generated force for a given suspension elongation ΔL_{II_0} after the substitution is:

$$F_0 = -\frac{(k_{II} + k_{II_L} + k_{II_U}) + j\,(k_{II} + k_{II_U})\,\Omega\,c_{II}}{(k_{II_L} + k_{II_U}) + j\,\Omega\,c_{II}}\,\Delta L_{II_0} \tag{3.4.5}$$

In order to verify the system frequency response, the transfer function has been implemented in *MatLab* with the data set of a high speed *Shinkansen* train [23].

Main stiffness	$k_{II} = 67\,400\ [N/m]$	Upper stiffness	$k_{II_U} = 2\,740\,000\ [N/m]$
Damping	$c_{II} = 58\,800\ [Ns/m]$	Lower stiffness	$k_{II_L} = 1\,150\,800\ [N/m]$

Table 3.10: Data set of the *Nishimura* model of the air sping

The figure 3.16 represents the response $F_0/\Delta L_{II\,0}$ in a frequency range of $[0 \div 40]\ Hz$ and clearly highlights that the dynamic behaviour of the air spring model is non linear: there is no correspondence respect to the trend of the traditional suspension consisting of linear spring and damper in parallel.

Moreover, in order to compute an exhaustive study of the behaviour of the model, the effect of the variation of the damping coefficient has been investigated.

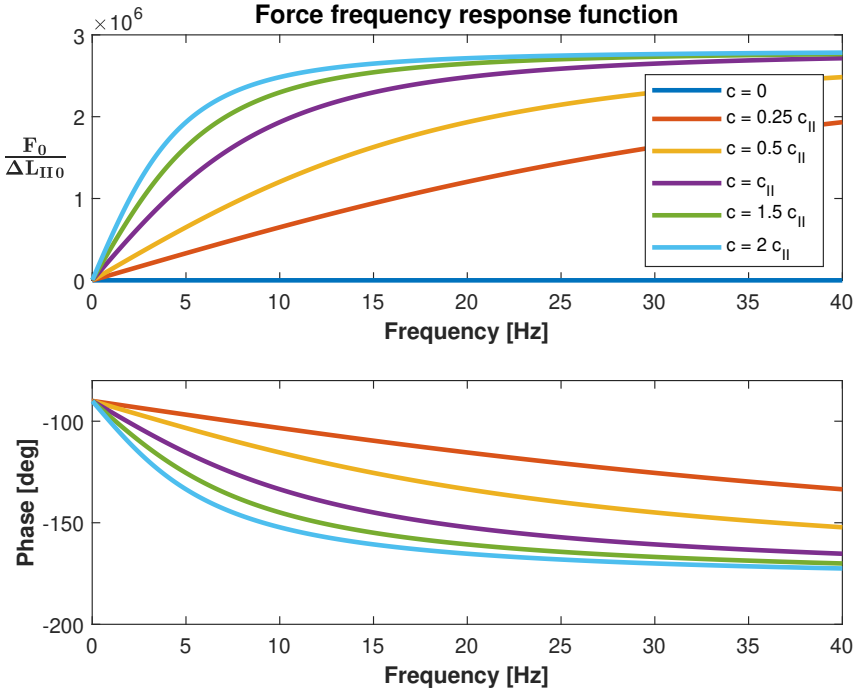

Figure 3.16: FRF of the force transmitted by *Nishimura* model of the air spring

By increasing the damping, the contribution $-c_{II}\dot{y}$ and consequently the generated force have a greater magnitude. The difference gets smaller when the frequency effect Ω becomes dominant and the transfer function of equation 3.4.5 goes to a steady state value $F_0 \to (k_{II} + k_{II_U})\,\Delta L_{II_0}$.

The transfer function of the transmitted force in equation 3.4.5 is furthermore important as long as it allows to characterize the performances of an equivalent suspension simply made of a damper c_{eq} and a spring k_{eq} in parallel.

In fact as long as there is no inertia contribution, the real content of the force fully derives from the stiffness while the imaginary content comes from the damper:

$$k_{eq} = \Re\left\{\frac{F_0}{\Delta L_{II_0}}\right\} \qquad \Omega c_{eq} = \Im\left\{\frac{F_0}{\Delta L_{II_0}}\right\}$$

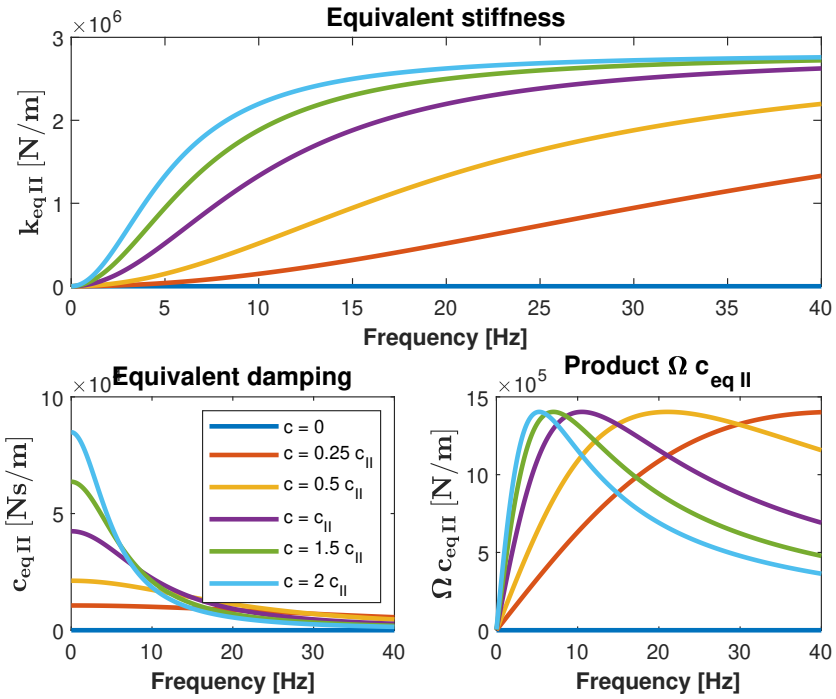

Figure 3.17: Equivalent stiffness and damping of the *Nishimura* air spring model

The figure 3.17 represents the variation of the damping $c_{eq\,II}$ and stiffness $k_{eq\,II}$ parameter of the equivalent suspension, highlighting once more the non linear dynamic properties.

The equivalent stiffness increases with the frequency, showing a slope proportional to the damping of the air spring c_{II}; on the contrary the equivalent damping has its maximum value, which is proportional to the damping of the air spring c_{II}, at low frequency and drops at high frequency, with a slope again proportional to the damping coefficient c_{II}.

3.4.2 *Lagrangian* component of the force of the air spring

As long as for the air spring state description two additional independent variables $(y_1; y_2)$ are needed, one for the front and one for the rear suspension, the vector collecting the independent variables has to be redefined according to the equation 3.4.2.

Assuming to consider only the first two bending mode, its final expression is:

$$\underline{x} = \{\underline{x}_C \ \underline{x}_F; \ \underline{y}\} \qquad where \quad \begin{cases} \underline{x}_C = \{z_{C11};\ z_{C12};\ z_{C21};\ z_{C22}\} \\ \underline{x}_F = \{z_{B1};\ \theta_{B1};\ z_{B2};\ \theta_{B2};\ z_A;\ \theta_A;\ G_1;\ G_2\} \\ \underline{y} = \{y_1;\ y_2\} \end{cases}$$

The layout of the longitudinal vehicle model is the same of figure 3.1: the only difference appears in the secondary suspension arrangement, including the variables $(y_1;\ y_2)$:

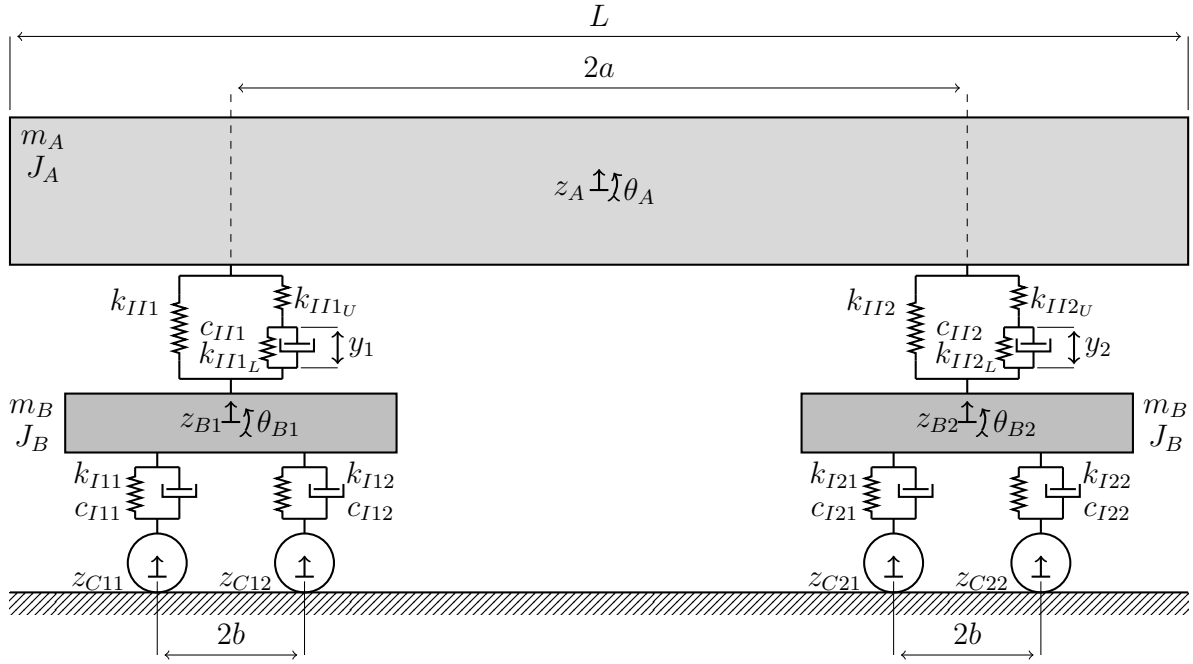

Figure 3.18: Model of the vertical dynamics of the vehicle with *Nishimura* air spring

Since there are no differences on the primary suspension, the equations 3.2.3 and 3.2.4 defining the contributions on the stiffness and damping matrix still hold:

$$[K_I] = [\Lambda_{\Delta L_I}]^T [k_I] [\Lambda_{\Delta L_I}] \qquad [R_I] = [\Lambda_{\Delta L_I}]^T [c_I] [\Lambda_{\Delta L_I}] \tag{3.4.6}$$

Where $[k_I] = diag\{k_I;\ k_I;\ k_I;\ k_I\}$ and $[c_I] = diag\{c_I;\ c_I;\ c_I;\ c_I\}$, while the *jacobian* of the elongations $[\Lambda_{\Delta L_I}]$ remain the very same as previously defined in table 3.3:

$[\Lambda_{\Delta L_I}]$	z_{C1}	z_{C2}	z_{C3}	z_{C4}	z_{B1}	θ_{B1}	z_{B2}	θ_{B2}	z_A	θ_A	G_1	G_2
ΔL_{I11}	-1				1	$-b$						
ΔL_{I12}		-1			1	b						
ΔL_{I21}			-1				1	$-b$				
ΔL_{I22}				-1			1	b				

Table 3.11: *Jacobian* of he elongations of the primary suspension

A different approach is needed in order to account for the secondary suspension: just like it has been done in the controlled configuration for the control force, the secondary suspension effect can be described as an internal force applied on its connection points:

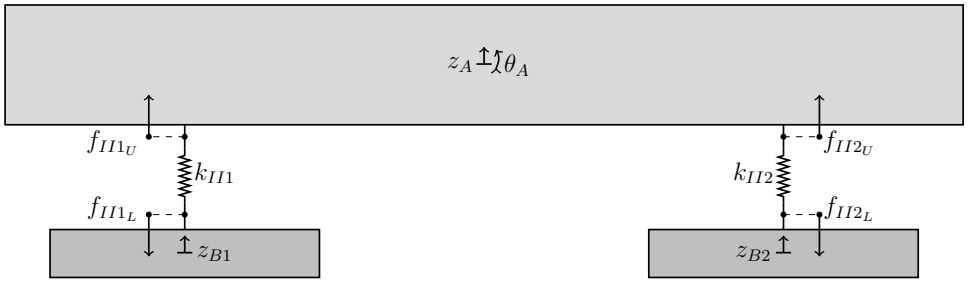

Figure 3.19: Modelling of the force generated by the air spring of the secondary suspension

As long as the main spring k_{II} is a linear element directly placed in between the bogie frame and the car body, its contribute can be included by using the usual equation 3.2.6:

$$[K_{II}] \;=\; [\Lambda_{\Delta L_{II}}]^T \, [k_{II}] \, [\Lambda_{\Delta L_{II}}] \tag{3.4.7}$$

Given $[k_{II}] = diag\{k_{II};\, k_{II}\}$ and recalling the *jacobian* matrix $[\Lambda_{\Delta L_{II}}]$ from table 3.4:

$[\Lambda_{\Delta L_{II}}]$	z_{C1}	z_{C2}	z_{C3}	z_{C4}	z_{B1}	θ_{B1}	z_{B2}	θ_{B2}	z_A	θ_A	G_1	G_2
ΔL_{II1}					-1				1	-a	Φ_{1R}	Φ_{nR}
ΔL_{II2}							-1		1	a	Φ_{1F}	Φ_{nF}

Table 3.12: *Jacobian* of the elongations of the secondary suspension

For what concern the force generated by the remaining part of the suspension, consisting in the arrangement of the elements (k_{II_L}; c_{II}; k_{II_U}), it is necessary to proceed with the description of the virtual work:

$$\delta L = \overrightarrow{\underline{F}}_{II} \times \delta \overrightarrow{\underline{s}}_{II}$$

Where $\underline{F}_{II}$ collects the internal forces (f_{IIi_L}; f_{IIi_U}) and $\delta \underline{s}_{II}$ the virtual displacements of their application points. The *superimposition principle* allows to compute the contribution of each *dofs* in the definition of the virtual displacements, leading to the generic expression:

$$\delta s_{IIi_L} = \delta z_{Bi} \qquad\qquad \delta s_{IIi_U} = \delta z_A \pm a\delta\theta_A + \Phi_{1i}\delta G_1 + \Phi_{2i} G_2$$

That can be expressed in matrix notion $\delta \underline{s}_{II} = [\Lambda_{\delta s_{II}}] \, \delta \underline{x}$ as result of the product of a *jacobian* matrix $[\Lambda_{\delta s_{II}}]$ and the vector of the independent variables $\delta \underline{x}$:

$[\Lambda_{\delta s_{II}}]$	δz_{C11}	δz_{C12}	δz_{C21}	δz_{C22}	δz_{B1}	$\delta\theta_{B1}$	δz_{B2}	$\delta\theta_{B2}$	δz_A	$\delta\theta_A$	δG_1	δG_n
δs_{II1_U}									1	-a	Φ_{1R}	Φ_{nR}
δs_{II1_L}					1							
δs_{II2_U}									1	a	Φ_{1F}	Φ_{nF}
δs_{II2_L}							1					

Table 3.13: *Jacobian* of virtual displacement of the air spring forces

For what concern the forces, thanks to the equilibrium condition 3.4.4 it is possible to state that $f_{II i_U} = -f_{II i_L}$. Thus, for sake of simplicity, $\underline{F}$ can be rearranged as follow:

$$\underline{F}_{II} = \begin{Bmatrix} f_{II_1\,U} \\ f_{II_1\,L} \\ f_{II_2\,U} \\ f_{II_2\,L} \end{Bmatrix} = \begin{bmatrix} 1 & 0 \\ -1 & 0 \\ 0 & 1 \\ 0 & -1 \end{bmatrix} \begin{Bmatrix} f_{II_1\,U} \\ f_{II_2\,U} \end{Bmatrix} = [\Lambda_{Ff}]\,\underline{f}_{II}$$

Where $\underline{f}_{II_U} = -k_{II\,U}\,\underline{\Delta L}_{II_U}$. The elongation $\Delta L_{II i_U}$ of the upper part of the air spring model, shown in figure 3.15 and computed in equation 3.4.1, is given by the difference of the overall elongation ΔL_{II_i} and the independent variable y_i:

$$\Delta L_{II i_U} = \Delta L_{II i} - y_i = [(z_A \pm b\theta_A + \Phi_{1i} G_1 + \Phi_{2i} G_2) - z_{Bi}] - y_i \tag{3.4.8}$$

Since the elongation $\Delta L_{II_{i\,U}}$ is a function of the independent variable vector $\underline{x}$ and of the state variables of the air spring model $\underline{y}$, by introducing the matrix notion it is possible to state that $\underline{\Delta L}_{II\,U} = [\Lambda^x_{\Delta L_{II\,N}}]\underline{x} + [\Lambda^{\overline{y}}_{\Delta L_{II\,N}}]\underline{y}$ and so:

$$\underline{f}_{II} = -k_{II_U}\,\underline{\Delta L}_{II_U} = -k_{II_U}\,\left(\,[\Lambda^x_{\Delta L_{II\,N}}]\,\underline{x} + [\Lambda^y_{\Delta L_{II\,N}}]\,\underline{y}\,\right)$$

Where the *jacobian* matrices $[\Lambda^x_{\Delta L_{II\,N}}]$ and $[\Lambda^y_{\Delta L_{II\,N}}]$ are defined from equation 3.4.8:

	$[\Lambda^x_{\Delta L_{II\,N}}]$												$[\Lambda^y_{\Delta L_{II\,N}}]$	
	z_{C11}	z_{C12}	z_{C21}	z_{C22}	z_{B1}	θ_{B1}	z_{B2}	θ_{B2}	z_A	θ_A	G_1	G_n	y_1	y_2
$\Delta L_{II_{1U}}$					-1				1	-a	Φ_{1R}	Φ_{nR}	-1	
$\Delta L_{II_{2U}}$							-1		1	a	Φ_{1F}	Φ_{1F}		-1

Table 3.14: *Jacobian* of the elongation of the *Nishimura* model of the air spring

At this point is finally possible to compute the *lagrangian* component of the forces generated by the air spring, defined as follow:

$$\delta L = \underline{Q}^T_{II}\,\delta\underline{x} = \underline{F}^T_{II}\,\delta\underline{s}_{II} \quad \Longrightarrow \quad \underline{Q}^T_{II} = -k_{II_U}\left[\left(\underline{x}^T\,[\Lambda^x_{\Delta L_{II\,N}}]^T + \underline{y}^T\,[\Lambda^y_{\Delta L_{II\,N}}]^T\right)[\Lambda_{Ff}]^T\right]\,[\Lambda_{\delta s_{II}}]$$

The resulting $\underline{Q}_{II}$ is a row vector; with a transposition, it becomes:

$$\underline{Q}_{II} = -k_{II_U}\,\left([\Lambda_{\delta s_{II}}]^T\,[\Lambda_{Ff}]\,[\Lambda^x_{\Delta L_{II\,N}}]\,\underline{x} + [\Lambda_{\delta s_{II}}]^T\,[\Lambda_{Ff}]\,[\Lambda^y_{\Delta L_{II\,N}}]\,\underline{y}\right)$$

$$\underline{Q}_{II} = [Q^x_{II}]\,\underline{x} + [Q^y_{II}]\,\underline{y} \tag{3.4.9}$$

Once all of the contributes of the primary and secondary suspension has been defined, it is possible to proceed in the equation of motion assembly.

3.4.3 Equations of motion for the passive system

Since there is no inertia associated to the *Nishimura* model of the air spring, the mass matrix of the new model is the same of the previous model, given in equation 3.3.4 by the sum of the contribution of the rigid *dofs* $[M_d]$ and of the modal matrix accounting for the inertia of the transverse bending deformation $[M_m]$ from equation 3.1.6:

$$[M] = [M_d] + [M_m] \tag{3.4.10}$$

For what concerns the stiffness matrix, there are three contributions: $[K_I]$ accounting for the primary suspension, defined in equation 3.4.6; $[K_{II}]$ accounting for the main spring of the secondary suspension, defined in equation 3.4.7; $[K_m]$ accounting for the carbody bending rigidity, which is defined in equation 3.1.8 just like in the previous model:

$$[K_1] = [K_I] + [K_{II}] + [K_m]$$

The damping matrix has just two contributions: $[R_I]$ for the primary suspension, given in equation 3.4.6; $[R_m]$ for the modal damping, shown in equation 3.1.9.

$$[R] = [R_I] + [R_y] \tag{3.4.11}$$

At the end, by recalling the *lagrangain* component of the air spring model from equation 3.4.9, it is finally possible to define the equation of motion:

$$[M]\,\underline{\ddot{x}} \;+\; [R]\,\underline{\dot{x}} \;+\; [K_1]\,\underline{x} \;=\; [Q^x_{II}]\,\underline{x} \;+\; [Q^y_{II}]\,\underline{y}$$

From this expression, the stiffness matrix can be redefined by collecting $\underline{x}$:

$$[K] = [K_1] - [Q^x_{II}] \tag{3.4.12}$$

In order to evaluate the response of the free independent variables and to highlight the excitement term, the usual *matrix partitioning* can be performed:

$$\begin{bmatrix}[M_{CC}] & [M_{CF}]\\ [M_{FC}] & [M_{FF}]\end{bmatrix}\begin{Bmatrix}\underline{\ddot{x}}_C\\ \underline{\ddot{x}}_F\end{Bmatrix} + \begin{bmatrix}[R_{CC}] & [R_{CF}]\\ [R_{FC}] & [R_{FF}]\end{bmatrix}\begin{Bmatrix}\underline{\dot{x}}_C\\ \underline{\dot{x}}_F\end{Bmatrix} + \begin{bmatrix}[K_{CC}] & [K_{CF}]\\ [K_{FC}] & [K_{FF}]\end{bmatrix}\begin{Bmatrix}\underline{x}_C\\ \underline{x}_F\end{Bmatrix} = \begin{bmatrix}[Q^y_{II_C}]\\ [Q^y_{II_F}]\end{bmatrix}\underline{y}$$

The first row of this expression can be used for the computation of the reaction forces in correspondence of the constrained variables $\underline{x}_C$, while the second one relates the free *dofs* response to the constraint excitement.

Knowing that $[M_{FC}]$ is null, the second row leads to the final expression:

$$[M_{FF}]\,\underline{\ddot{x}}_F \;+\; [R_{FF}]\,\underline{\dot{x}}_F \;+\; [K_{FF}]\,\underline{x}_F \;=\; -[R_{FC}]\,\underline{\dot{x}}_C \;-\; [K_{FC}]\,\underline{x}_C \;+\; [Q^y_{II_F}]\,\underline{y} \tag{3.4.13}$$

A brief consideration has to be done about the independent variables $\underline{y}$ characterizing the air spring state: with the introduction of this new variables, in the equations of motion 3.4.13 the equations are fewer than the unknowns, leading to an underdetermined system.

For this reason in order to define the value of $(y_1;\ y_2)$, the two continuity equation 3.4.4 of the *Nishimura* model relating $\underline{y}$ and $\underline{x}$, has to be added to the system:

$$\begin{cases} c_{II}\,\dot{y}_1 \;+\; k_{II_L}\,y_1 \;=\; k_{II_U}\Delta L_{II1_U}\\ c_{II}\,\dot{y}_2 \;+\; k_{II_L}\,y_2 \;=\; k_{II_U}\Delta L_{II2_U}\end{cases}$$

Knowing the elongation $\Delta L_{IIi_U} = \Delta L_{IIi} - y_i = [(z_A \pm a\theta_A + \Phi_{1i}G_1 + \Phi_{2i}G_2) - z_{Bi}] - y_i$ from equation 3.4.8, the additional equations can be reorganized as follow:

$$\begin{cases} c_{II}\,\dot{y}_1 - k_{II_U}\,(z_A - a\theta_A + \Phi_{1R}G_1 + \Phi_{2R}G_2 - z_{B1}) + (k_{II_U} + k_{II_L})\,y_1 = 0 \\ c_{II}\,\dot{y}_2 - k_{II_U}\,(z_A + a\theta_A + \Phi_{1F}G_1 + \Phi_{2F}G_2 - z_{B2}) + (k_{II_U} + k_{II_L})\,y_2 = 0 \end{cases}$$

Leading to a generic matrix expression:

$$[N_1]\,\underline{\dot{y}} \;+\; [N_2]\,\underline{x}_F \;+\; [N_3]\,\underline{y} \;=\; \underline{0} \tag{3.4.14}$$

At this point, by coupling 3.4.13 and 3.4.14, it is possible to get the complete expression of the final equations of motion:

$$\begin{cases} [M_{FF}]\,\underline{\ddot{x}}_F \;+\; [R_{FF}]\,\underline{\dot{x}}_F \;+\; [K_{FF}]\,\underline{x}_F \;=\; -[R_{FC}]\,\underline{\dot{x}}_C \;-\; [K_{FC}]\,\underline{x}_C \;+\; [Q^y_{II_F}]\,\underline{y} \\ [N_1]\,\underline{\dot{y}} \;+\; [N_2]\,\underline{x}_F \;+\; [N_3]\,\underline{y} \;=\; \underline{0} \end{cases} \tag{3.4.15}$$

For the numerical integration of the equations of motion, the *Matlab* tool *ode45* has been used. Thus for downgrading the system to a first order differential equation, a further identity has been coupled to the equation 3.3.5:

$$\begin{cases} [M_{FF}]\,\underline{\ddot{x}}_F \;+\; [R_{FF}]\,\underline{\dot{x}}_F \;+\; [K_{FF}]\,\underline{x}_F \;=\; -[R_{FC}]\,\underline{\dot{x}}_C \;-\; [K_{FC}]\,\underline{x}_C \;+\; [Q^y_{II_F}]\,\underline{y} \\ [I]\,\underline{\dot{x}}_F \;=\; [I]\,\underline{\dot{x}}_F \\ [N_1]\,\underline{\dot{y}} \;+\; [N_2]\,\underline{x}_F \;+\; [N_3]\,\underline{y} \;=\; \underline{0} \end{cases} \tag{3.4.16}$$

The equation 3.4.16 can be rewritten in matrix notation leading to the expression:

$$\underline{\dot{v}} \;=\; [A]\,\underline{v} \;+\; [B_C]\,\underline{u}_C \tag{3.4.17}$$

Where: the *state vector* $\underline{v} = \{\underline{\dot{x}}_F;\ \underline{x}_F;\ \underline{y}\}$ collects the free degrees of freedom, their derivatives and the state variables of the air spring; the vector of the external excitement $\underline{u}_C = \{\underline{\dot{z}}_C;\ \underline{z}_C\}$ contains the constraint motion and its derivatives; the *state matrix* of the system $[A]$ and of the external excitement $[B_C]$ are defined as follow:

$$[A] = \begin{bmatrix} -[M_{FF}]^{-1}[R_{FF}] & -[M_{FF}]^{-1}[K_{FF}] & [M_{FF}]^{-1}[Q^y_{II_F}] \\ [I] & [0] & [0] \\ [0] & -[N_1]^{-1}[N_2] & -[N_1]^{-1}[N_3] \end{bmatrix} \qquad [B_C] = \begin{bmatrix} -[M_{FF}]^{-1}[R_{FC}] & -[M_{FF}]^{-1}[K_{FC}] \\ [0] & [0] \\ [0] & [0] \end{bmatrix}$$

This procedure has been applied to the same data set used for the characterization of the *Nishimura* model for the air spring, referring to an high speed *Shinkansen* train [23]:

Car body	$m_A = 27\,000\ kg$ $J_A = 1\,840\,000\ kn\,m^2$	Bogie frame	$m_B = 2\,860\ kg$ $J_B = 1\,360\ kg\,m^2$
Primary suspension	$k_I = 17\,600\,000\ N/m$ $c_I = 123\,000\ Ns/m$	Secondary suspension	$k_{II} = 67\,400\ N/m$ $c_{II} = 58\,800\ Ns/m$
Nishimura model	$k_{II_U} = 2\,740\,000\ N/m$ $N = k_{II_L}/k_{II_U} = 0.42$ $k_{II_L} = 1\,150\,800\ N/m$	Length	$L = 24.5\ m$ $2a = 17.5\ m$ $2b = 2.5\ m$
First bending mode	$\omega_1 = 51.5\ rad/s$ $f_1 = 8.2\ Hz$ $\xi_1 = 0.072$	Second bending mode	$\omega_2 = 142.0\ rad/s$ $f_2 = 22.6\ Hz$ $\xi_2 = 0.198$

Table 3.15: Second configuration data set

3.4.4 Natural frequencies and mode shapes

With the first two bending modes, the *state matrix* $[A]$ of equation 3.4.17 has dimension 18×18, due to the introduction of the state variables of the air spring (y_1; y_2). The 18 *eigenvalues* associated to the matrix $[A]$ are complex conjugate: excluding the two *eigenvalues* related to $\underline{y}$, the remaining 16 related to $\underline{x}_F$ contain the information of the natural frequencies ω_0 in the imaginary part:

	$\omega_0\,[rad/s]$	$f\,[Hz]$	ξ
Carbody bounce	14.3457	2.2832	0.0139
Carbody pitch	18.3383	2.9186	0.0385
Bogie frame bounce	107.3725	17.0889	0.3804
Bogie frame pitch	143.0784	22.7716	0.9877
First bending mode	61.1638	9.7345	0.0342
Second bending mode	139.6980	22.2336	0.2003

Table 3.16: Natural frequencies of the second configuration

Analogously to the procedure applied for the first configuration, the damping ratio ξ associated to the mode shape can be estimated with the ratio of the *real* over the *imaginary* part of the *eigenvalues*.

In this configuration, the *eigenvector* are organized so that: the first rows refer to the velocity $\dot{\underline{x}}_F$, the central to the displacements $\underline{x}_F$ while the last to the air spring state $\underline{y}$. The resulting *mode shapes* are summarized in the following table:

	z_{B1}	θ_{B1}	z_{B2}	θ_{B2}	z_A	θ_A	G_1	G_2
In phase bogie bounce	0.7034	0	0.7034	0	0.0135	0	0.1013	0
$f = 17.0942\,Hz\ -\ \xi = 0.3780$	0°	99°	0°	−180°	−247°	−136°	108°	−239°
Counter phase bogie bounce	0.7063	0	0.7063	0	0	0.0017	0	0.0471
$f = 17.0835\,Hz\ -\ \xi = 0.3828$	−180°	99°	0°	−226°	39°	−243°	28°	−2°
Bogie pitch	0	0.0097	0	1.0000	0	0	0	0
$f = 22.7716\,Hz\ -\ \xi = 0.9877$	8°	−30°	52°	0°	−183°	−177°	107°	−174°
Bogie pitch	0	0.9013	0	0.4333	0	0	0	0
$f = 22.7716\,Hz\ -\ \xi = 0.9877$	−116°	0°	−206°	−28°	−219°	−70°	−21°	−185°
Carbody bounce	0.0703	0	0.0703	0	0.8815	0	0.4616	0
$f = 2.2832\,Hz\ -\ \xi = 0.0139$	−7°	251°	−7°	123°	0°	175°	176°	−4°
Carbody pitch	0.5723	0	0.5723	0	0	0.5611	0	0.1738
$f = 2.9186\,Hz\ -\ \xi = 0.0385$	168°	240°	−12°	91°	−36°	0°	142°	173°
First bending mode	0.0856	0	0.0856	0	0.0473	0	0.9915	0
$f = 9.7345\,Hz\ -\ \xi = 0.0342$	−41°	110°	−41°	157°	−14°	180°	0°	−21°
Second bending mode	0.0302	0	0.0302	0	0	0.0004	0	0.9991
$f = 22.2336\,Hz\ -\ \xi = 0.2003$	10°	233°	190°	107°	155°	−38°	125°	0°

Table 3.17: Mode shapes of the second configuration

For the sake of simplicity, the values lower than $1e-6$ are neglected.

The considerations about the coupling of the independent variable discussed for the first configuration still hold with the new system.

3.4.5 Frequency response function

At this point it is possible to investigate the *frequency response function*: since the equations of motion 3.4.15 consist in a first and in a second order differential equation, it is not possible to replicate the procedure of the previous configuration, but on the contrary it is necessary to work on the *state* notion of the equations of motion 3.4.17:

$$\dot{\underline{v}} \;=\; [A]\,\underline{v} \;+\; [B]\,\underline{u}_C$$

Before moving to the frequency domain, it is important to briefly focus on the constrained displacement vector $\underline{u}_C = \{\dot{\underline{x}}_C;\, \underline{x}_C\}$. In fact by imposing $\underline{x}_C$ to be an harmonic function $z_{Cij} = z_{C0}\, e^{j\Omega\, t}$, it is possible to rewrite $\underline{u}_C$ with the following matrix expression:

$$\underline{u}_C = \begin{Bmatrix} j\Omega\, z_{C11} \\ j\Omega\, z_{C12} \\ j\Omega\, z_{C21} \\ j\Omega\, z_{C22} \\ z_{C11} \\ z_{C12} \\ z_{C21} \\ z_{C22} \end{Bmatrix} = \begin{bmatrix} j\Omega & & & & & & & \\ & j\Omega & & & & & & \\ & & j\Omega & & & & & \\ & & & j\Omega & & & & \\ 1 & & & & & & & \\ & 1 & & & & & & \\ & & 1 & & & & & \\ & & & 1 & & & & \end{bmatrix} \begin{Bmatrix} z_{C11} \\ z_{C12} \\ z_{C21} \\ z_{C22} \end{Bmatrix} = [B_\Omega]\,\underline{x}_C \tag{3.4.18}$$

Moreover recalling the equation 3.3.11 relating the wheel distance with the excitation phase $\underline{x}_C = \underline{\Phi} z_{C0}$, it is finally possible to get the state equation in frequency domain:

$$(j\Omega\,[I] - [A]\,)\,\underline{v}_0 \;=\; [B]\,[B_\Omega]\,\underline{\Phi}\; z_{C0} \tag{3.4.19}$$

By recalling the definition of the *real* frequency of excitement $f = V/\lambda_D$, the *critical velocities map* of the second configuration, given in figure 3.20, can be computed and compared to the one of the first configuration, represented in figure 3.8: the larger natural frequencies summarized in table 3.16 leads to a greater slope of the curves.

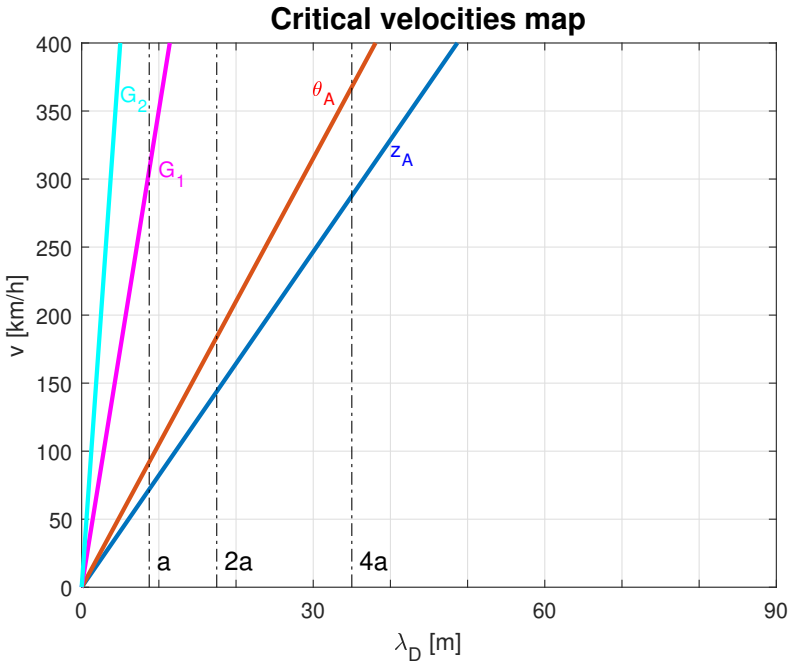

Figure 3.20: Critical velocities map for the second configuration

The considerations done about the *frequency response function* of the first configuration (figure 3.9) with fixed velocity and variable irregularity wavelength still hold.

For this reason just the dual response highlighting the natural frequencies is reported: the a irregularity wavelength $\lambda_D = 10.86\,m$ is fixed and equal to the previous FRF while the vehicle velocity is varied in order to match the excitation frequency $f = V/\lambda_D$.

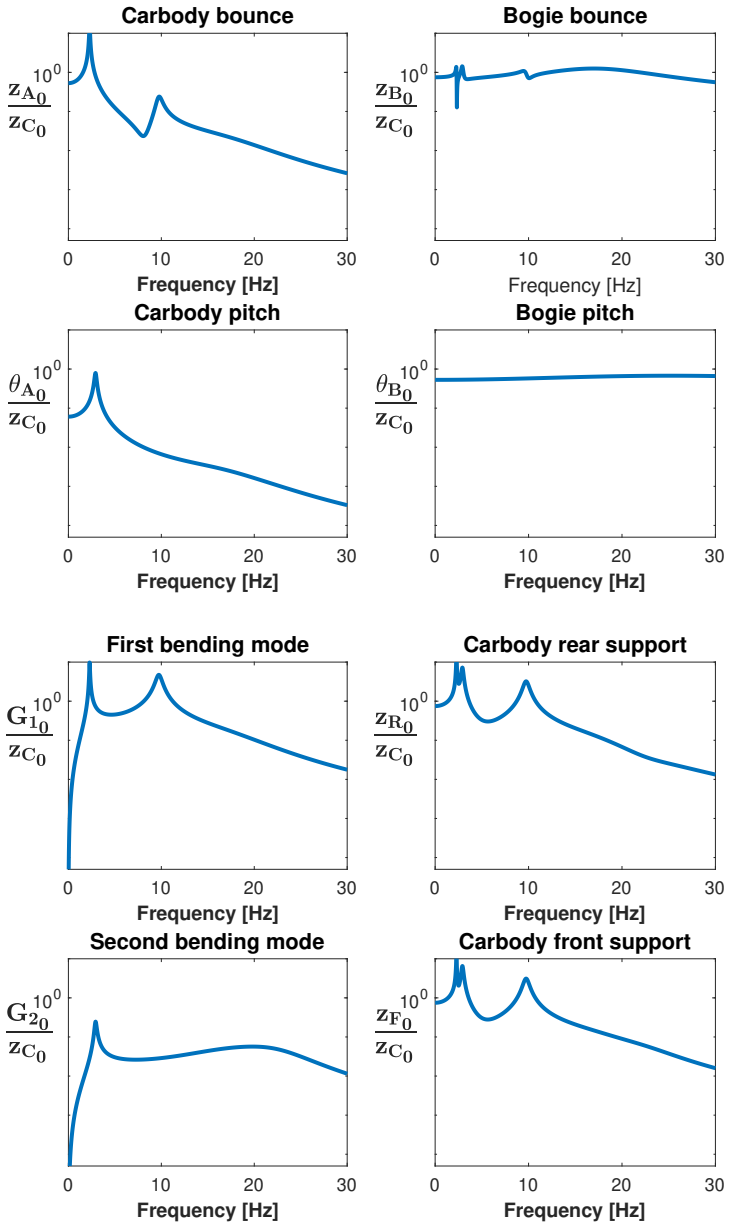

Figure 3.21: Second configuration frequency response function with $\lambda_D = 10.86\,m$

The resonant frequencies are consistent with the mode shapes shown in table 3.16: the modes dominated by the carbody pitch and bounce are at about $2.5\,Hz$; the mode shapes associated to the flexible modes at $10\,Hz$ and $22\,Hz$; for bogie frame modes there are the two modes dominated by the in phase and in counter phase bounce at $17\,Hz$ while the pitch at $23\,Hz$.

The peaks associated to the motion of the bogie frames are completely damped because of the large damping coefficient $c_I = 123\,000\ Ns/m$ of the primary suspension: in fact from table 3.16 it is possible to see that the damping ratio ξ of the mode shapes dominated by the bogie frame motion is always very large if compared to the other mode shapes. This aspect creates some doubt about the reliability of the data set taken from [23].

3.4.6 Equations of motion for the controlled system

As already discussed, in the controlled system the passive damper c_I of the primary suspension is replaced with a semi active element generating a force $f_{I_{ij}}$, function to the elongation velocity $\Delta L_{I_{ij}}$ and to the variable damping coefficient $[c_{min} \div c_{max}]$.

Consequently, the matrix $[R_I]$ computed in equation 3.4.6 can no longer be defined and the control force generated in the primary suspension has to be computed as an internal force applied in the suspension connection points, as shown in figure 3.12.

In order to compute the *lagrangian* component $\underline{Q}_I$ of the control force, the same procedure applied for the first configuration con be followed, leading to the final expression of equation 3.3.15:

$$\underline{Q}_I \ = \ [\Lambda_{\delta s_I}]^T \, [\Lambda_{u_{fF}}] \, \underline{u}_F \ = \ [Q_I] \, \underline{u}_F$$

By recalling from the passive system the already introduced mass matrix from equation 3.4.10 $[M] = [M_m] + [M_d]$, the damping matrix $[R] = [R_m]$ from equation 3.4.11 without the primary suspension contribution which is included in $[Q_I]$, the stiffness matrix with the contribution of the air spring model $[K] = [K_I] + [K_{II}] + [K_m] - [Q^x_{II}]$ from equation 3.4.12, the *lagrangian* component of the secondary suspension $[Q^y_{II}]\,\underline{y}$ from equation 3.4.9 and the *lagrangian* component of the control force $[Q_I]$ just computed, the final equations of motion of the controlled system can be finally computed:

$$\begin{bmatrix}[M_{CC}] & [M_{CF}] \\ [M_{FC}] & [M_{FF}]\end{bmatrix} \begin{Bmatrix}\ddot{\underline{x}}_C \\ \ddot{\underline{x}}_F\end{Bmatrix} + \begin{bmatrix}[R_{CC}] & [R_{CF}] \\ [R_{FC}] & [R_{FF}]\end{bmatrix} \begin{Bmatrix}\dot{\underline{x}}_C \\ \dot{\underline{x}}_F\end{Bmatrix} + \begin{bmatrix}[K_{CC}] & [K_{CF}] \\ [K_{FC}] & [K_{FF}]\end{bmatrix} \begin{Bmatrix}\underline{x}_C \\ \underline{x}_F\end{Bmatrix} = \begin{bmatrix}[Q^C_I] \\ [Q^F_I]\end{bmatrix} \underline{u}_F + \begin{bmatrix}[Q^y_{II_C}] \\ [Q^y_{II_F}]\end{bmatrix} \underline{y}$$

Thanks to the matrix partitioning and by coupling the equations of motion with the continuity equation 3.4.14 for the computation of the air spring state, it is possible to get:

$$\begin{cases} [M_{FF}]\,\ddot{\underline{x}}_F \ + \ [R_{FF}]\,\dot{\underline{x}}_F \ + \ [K_{FF}]\,\underline{x}_F \ = \ -[R_{FC}]\,\dot{\underline{x}}_C \ - [K_{FC}]\,\underline{x}_C \ + \ [Q^y_{II_F}]\,\underline{y} \ + \ [Q^F_I]\,\underline{u}_F \\ [N_1]\,\dot{\underline{y}} \ + \ [N_2]\,\underline{x}_F \ + \ [N_3]\,\underline{y} \ = \ \underline{0} \end{cases}$$

By repeating the same procedure for downgrading the equation to a first order differential equation explained for the passive configuration and by introducing the *state vector* $\underline{v} = \{\dot{\underline{x}}_F;\ \underline{x}_F;\ \underline{y}\}$, the constraint motion vector $\underline{u}_C = \{\dot{\underline{x}}_C;\ \underline{x}_C\}$ and the control force vector $\underline{u}_F = \{f_{I_{11}};\ f_{I_{12}};\ f_{I_{21}};\ f_{I_{22}}\}$, it is possible to get the final state formulation:

$$\dot{\underline{v}} \ = \ [A]\,\underline{v} \ + \ [B_C]\,\underline{u}_C \ + \ [B_F]\,\underline{u}_F \tag{3.4.20}$$

Where the state matrices are defined as follow:

$$[B_F] = \begin{bmatrix}[M_{FF}]^{-1}[Q^F_I] \\ [0] \\ [0]\end{bmatrix} \qquad [B_C] = \begin{bmatrix}-[M_{FF}]^{-1}[R_{FC}] & -[M_{FF}]^{-1}[K_{FC}] \\ [0] & [0] \\ [0] & [0]\end{bmatrix}$$

$$[A] = \begin{bmatrix}-[M_{FF}]^{-1}[R_{FF}] & -[M_{FF}]^{-1}[K_{FF}] & [M_{FF}]^{-1}[Q^y_{II_F}] \\ [I] & [0] & [0] \\ [0] & -[N_1]^{-1}[N_2] & -[N_1]^{-1}[N_3]\end{bmatrix} \tag{3.4.21}$$

3.5 Configuration comparison

From the mathematical point of view, the two configurations differ only for the model of the secondary suspension: the second configuration requires two additional variables (y_1; y_2) for the description of the air spring state and thus two additional equations.

Anyway, from the mechanical point of view the two system are very similar: the air spring model is just slightly affecting the response of the system.

Despite the similarity of the mode shapes, the corresponding natural frequencies are very different, as shown in the following comparative table 3.18: this represents the crucial difference of the two configurations.

	Configuration 1		Configuration 2	
	$f\,[Hz]$	ξ	$f\,[Hz]$	ξ
In phase bogie bounce	6.6	0.21	17.1	0.38
Counter phase bogie bounce	6.5	0.21	17.1	0.38
Bogie pitch	9.3	0.06	22.8	0.99
Carbody bounce	0.8	0.19	2.3	0.01
Carbody pitch	1.0	0.24	2.9	0.04
First bending mode	8.4	0.04	9.7	0.03
Second bending mode	23.3	0.05	22.2	0.20

Table 3.18: Natural frequencies comparison

This contrast is caused by the differences in the data set: while the inertia of the first configuration (table 3.5) are similar to the one of the second configuration (table 3.15), the stiffness of the second data set are one order of magnitude greater (at the primary suspension $k_{I_1} = 2.4e6$ against $k_{I_2} = 17.6e6$).

This pushes the natural frequencies to higher values.

The same happens for the damping, leading to higher damping ratio ξ especially in the modes dominated by the bogie frame motion and consequently by the first flexible modes (at the primary suspension $c_{I_1} = 5e3$ against $c_{I_2} = 123e3$).

Even in the value of c_{I_2} is off the chart, generating doubts on the reliability of the data set taken from [23], this configuration has been studied as long as its strong contrast allows to point out interesting considerations.

The aim of the following chapter is to figure out how this fundamental differences in the properties of the passive system affect the performances of the controller, thus understand the design features to consider for obtaining a good control system.

Control strategies for the primary suspension

The control strategy chosen for reduction of the excitement of the carbody through the management of the vibration transmitted by the bogie frame, is based on a replication of the ideal *SkyHook*, which from a theoretical point of view in suitable only for *full active* control system.

In order to show the main features of this solution, let's consider a simple system made of a mass supported on an irregular surface, which supposes to simulate the standard *quarter-car* model of a vehicle.

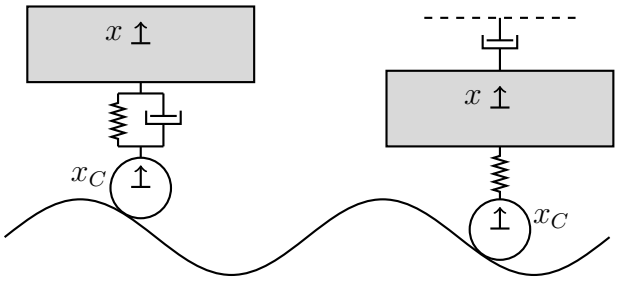

Figure 4.1: *SkyHook* main concept

In the passive configuration, depicted on the left, the sprung mass experiences a force:

$$F_1 \;=\; -c\,(\dot{x} - \dot{x}_C) \;- k\,(x - x_C)$$

In order to sustain the weight and to reduce the relative displacement between the mass and the road, a *stiff* suspension is required; on the other hand, in order to isolate the disturbances, a *soft* suspension would be preferred [26].

Supposing to connect the damper to an inertial reference, it would be possible to design a suspension as stiff as desired, but meanwhile to damp the absolute vibration as long as the sprung mass experiences a force:

$$F_2 \;=\; c\,\dot{x} \;- k(x - x_C)$$

The purpose of the control system is to generate a force simulating the effect of F_2 by commanding the semi active damper of the primary suspension.

4.1 Layout of the control system

The control system designed for this work supposes to model a control unit, which commands an *electro hydraulic* semi active damper, and to account for the dynamic of the current ruling the opening of the solenoid valve of the semi active damper itself.

In particular the dynamic of the response of the solenoid valve has been modelled as a simple first order system, similarly to the approach described in [21].

The architecture of the control system is fixed in all of the evaluated control strategies and it elaborates step by step several signals.

- The *command variable* u_R: it is the reference value of the control force, that is computed by the algorithm and that the variable damper should generate.
- The *intermediate variable* I_R: after the comparison and eventually the saturation of the required force u_R with the damper performance curve, a current value I_R is associated to the *command variable* u_R. It accounts for the setting of the characteristic parameter of the semi active damper and it is the signal sent to the semi active damper itself in real applications.
- The *actual command* I: in order to account for the dynamic of the current ruling the opening of the solenoid valve, the current I_R representing the required force is fed to a first order system whose output I represents the actual current in the solenoid valve and its actual opening, ruling the magnitude of the generated force.
- The *generated force* u_F: with a reverse process, the applied force is computed from the actual current I.

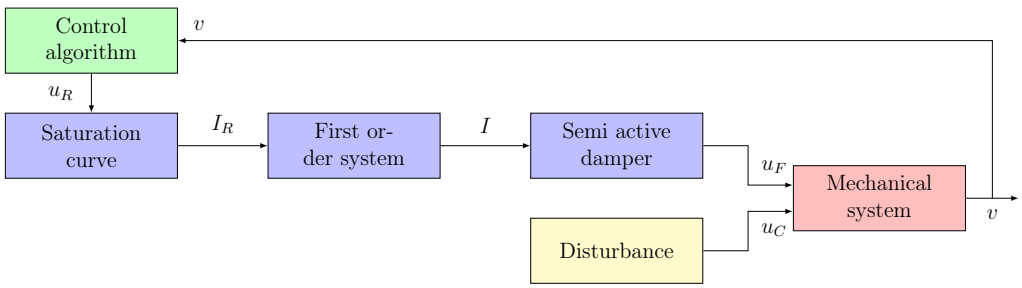

Figure 4.2: Chart of the workflow of the control system

The blue boxes standing for the general control system have been kept fixed in the several simulation computed; on the contrary the green box representing the control algorithm has been changed in order to evaluate the differences in the performance. The computation of the command variable u_R is obviously always based on the evaluation of the actual state v of the system.

4.2 Relevant features of the control system layout

The control system layout has been defined after studying and evaluating previous proposal [21] [23] [24] in order to point out strengths and weaknesses. In particular the most important new features consist in accounting for the current $\underline{I}$ and for the performance curve of the semi active damper, saturating the required force.

In order to understand the benefits provided by the introduction of the intermediate variable, the figure 4.3 is proposed: it represents in red color the time story of the required force u_R that the control unit asks to the semi active damper and the associated current I_R; in blue color the filtered current I accounting for the actual state of the solenoid valve opening affected by the dynamic of the response and the consequently generated force u_F.

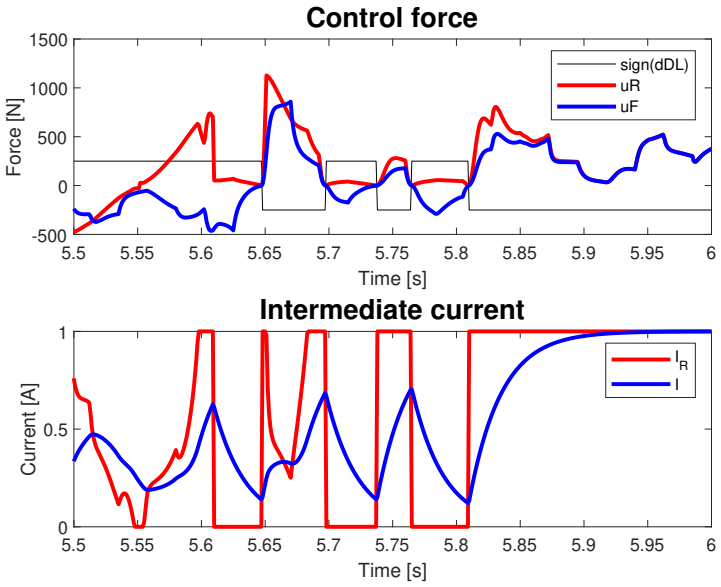

Figure 4.3: Comparison between the required and applied force

By looking at figure 4.3, it is worth to stress is that the applied force $\underline{u}_F$ is always opposite to the elongation velocity, consistently with the application of a semi active damper and independently from the sign of the command variable.

In fact the required force is not necessary dissipative: there is no evidence that the force u_R needed for the reduction of the absolute velocity of the unsprung mass has a direction opposite to the elongation velocity $\dot{\Delta L}$ of the suspension. For this reason, from a theoretical point of view, only a *full active* element would be able to obtain such a result.

This architecture of the control system allows to decouple the required u_R and the applied u_F force through the intermediate variable I, which carries only the information about the solenoid valve opening and indirectly about the amplitude of the force and removes the constrain of the direction of the required force u_R. This approach ensures:

- a proper modelling of the behaviour of a real semi active damper;
- an easy management of the issue related to the sign of the dissipative force u_F.

The figure 4.3 allows furthermore to enhance another strengths of the layout of the control system, resulting from the implementation of the dynamic behaviour of the current ruling the opening of the solenoid valve. In fact by comparing the required u_R and applied u_F forces, it is possible to notice that the discontinuity of the required force are damped in the applied force thanks to the first order filter effect, leading to a continuous and smooth actuation.

The continuous and smooth actuation is very important in order to avoid the impact caused by the application of a sudden forces, the related detrimental vibrations and to manage the non linear behaviour typical of a two state control algorithm.

For what concerns the introduction of the performance curve of the semi active damper, the important feature consists in the possibility to have a direct control on the applied force, allowing the challenging investigation of how the performances of the suspension affect the response. This aspect results very interesting considering that:

- in a passive suspensions, a larger damping coefficient improves the performances around the resonant frequency, but it is detrimental for the transmissibility at high frequencies, as shown in the figure 4.4 referred to the simple system of figure 4.1;
- in a *semi active* suspension, on the contrary, it is generally possible to use *semi active* damper able to generate larger forces because, thanks to their adjustability, the high frequency drawback is contained.

In order to characterize the effect of the performance of the *semi active* damper in the transmissibility at high frequencies and thus in the response of the carbody, a variable K_{PC} acting as a scale factor of the performance curve has been introduced.

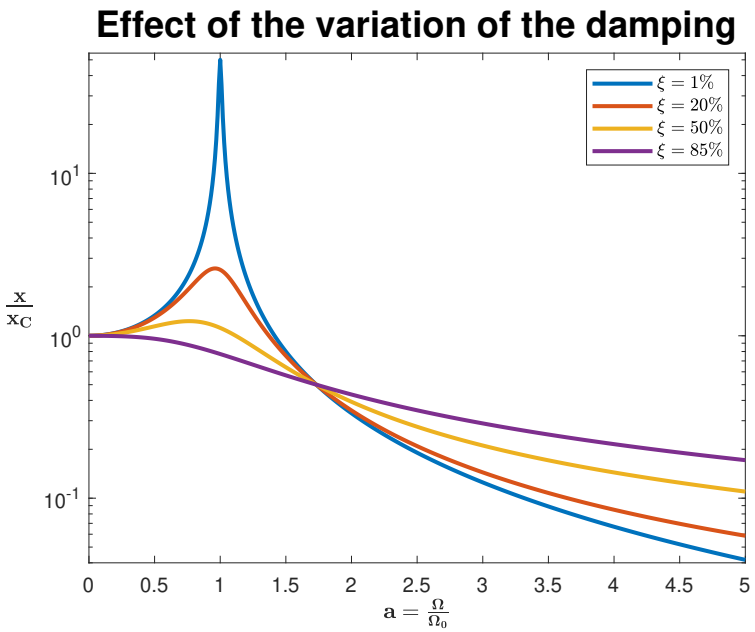

Figure 4.4: Effect of the damping in the response of the supported mass of figure 4.1

4.2.1 Performance curve of the semi active damper

The figure 4.5 shows the performance curve of the *semi active electro hydraulic* damper used as a reference for this work. The curve has been taken from the example reported in Sugahara's paper [24].

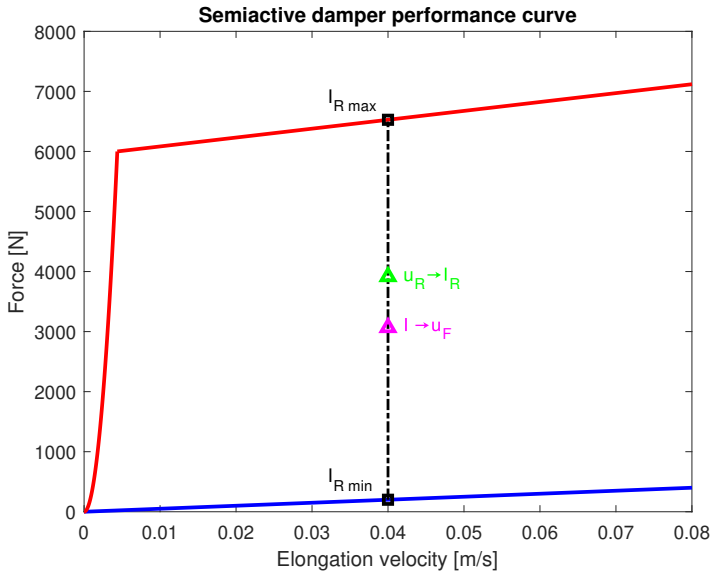

Figure 4.5: Semi active damper performance curve [24]

The semi active damper is able to generate a force $F = -c\,\dot{\Delta L}$ proportional to both its elongation velocity $\dot{\Delta L}$ and the variable damping coefficient $c \in [c_{min} \div c_{max}]$. Thus, for a given elongation velocity $\dot{\Delta L}$, the force can be adjusted by acting on the damping coefficient c, driving the system response and defining a two dimension working area.

The figure 4.5 shows that the lower limit of the performance curve follows a linear trend: at null current the damping coefficient is constant and equal to c_{min}, independently from the elongation velocity. On the contrary the upper limit follows a quadratic low for small elongation velocities, allowing to generate high forces even with small $\dot{\Delta L}$; than the trend shows a plateau with a soft linear trend so that the force saturates and even, reaching higher elongation velocities, it remains almost constant.

Furthermore the figure 4.5 proposes to show an example of how the intermediate current works: given the elongation velocity $\dot{\Delta L}$ of the considered time instant, the control algorithm compute the required force u_R and associate a current I_R to its value depending on the available range of forces $[F_{max};\ F_{min}]$:

$$I_R = \frac{u_R - F_{min}}{F_{max} - F_{min}}$$

Because of the dynamics of the current ruling the solenoid valve opening, the semi active damper does not directly receive the desired current value I_R, but the filtered I. At this point the process is reversed: given I, the amplitude of the force u_F that the semi active damper is able to generate with the actual elongation velocity is computed.

At the end it is furthermore important to highlight that the semi active damper behaviour is symmetrical in elongation and compression, thus just the axis with positive elongation velocity is depicted in figure 4.5.

4.2.2 First order system modelling the dynamic behaviour of the current

The dynamics between the reference current I_R and the one actually received by the semi active damper I is modelled as a simple first order system:

$$I = \frac{1}{1+\tau s} I_R \tag{4.2.1}$$

The time constant τ has been set to $25ms$, replicating the choice of [24]. Furthermore it has been investigated that this value offers a good compromise between the quickness of the response, thus the amplitude of the generated force respect to the required one, and the smoothness of the actuation: in fact the sudden variation of current and of the forces is detrimental because may lead to impacts and additional vibrations.

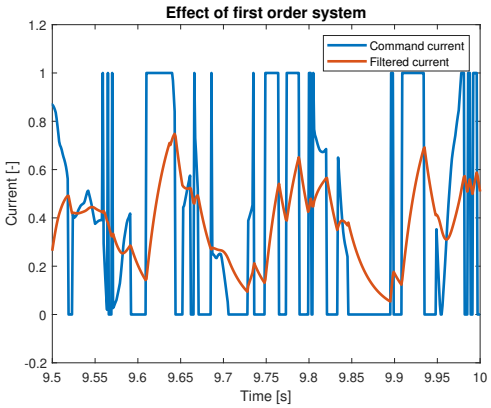

(a) Time constant $\tau = 25\,ms$

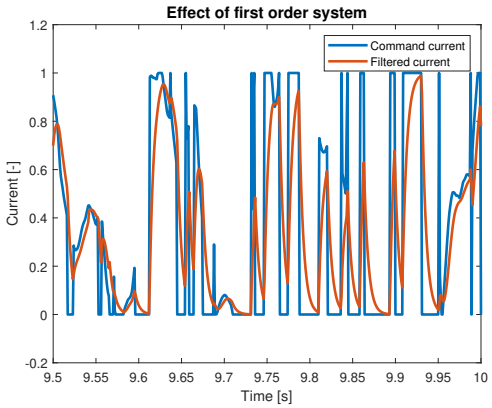

(b) Time constant $\tau = 5\,ms$

Figure 4.6: Effect of the time constant τ on the intermediate variable

As long as the control unit evaluates and actuates each semi active damper independently from the others, the current signal is made up four values, one for each suspension: $\underline{I}_R = \{I_{R_{11}};\ I_{R_{12}};\ I_{R_{21}};\ I_{R_{22}}\}$. The same considerations hold for the vector $\underline{I}$.

In order to get $\underline{I}$ from equation 4.2.1 and compute its dynamic behaviour, it is necessary to move to the time domain and to integrate the signal:

$$\tau \dot{I}_{ij} + I_{ij} = I_{R\,ij} \qquad \Longrightarrow \qquad \dot{I}_{ij} = -\frac{1}{\tau} I_{ij} + \frac{1}{\tau} I_{R\,ij} \tag{4.2.2}$$

The system made of the equations 4.2.2 accounting for all of the four signals I_{ij} can be furthermore expressed in matrix notation as follow:

$$\underline{\dot{I}} = -\tfrac{1}{\tau} \begin{bmatrix} 1 & & & \\ 0 & 1 & & \\ 0 & 0 & 1 & \\ 0 & 0 & 0 & 1 \end{bmatrix} \underline{I} + \tfrac{1}{\tau} \begin{bmatrix} 1 & & & \\ 0 & 1 & & \\ 0 & 0 & 1 & \\ 0 & 0 & 0 & 1 \end{bmatrix} \underline{I}_R = [D]\,\underline{I} + [D_R]\,\underline{I}_R \tag{4.2.3}$$

In order to solve the equation 4.2.3, it has to be coupled together with the equations of motion. By recalling the equation of motions of the first controlled configuration from equation 3.3.16 it is possible to get:

$$\begin{cases} [M_{FF}]\,\underline{\ddot{x}}_F + [R_{FF}]\,\underline{\dot{x}}_F + [K_{FF}]\,\underline{x}_F = -[R_{FC}]\,\underline{\dot{x}}_C - [K_{FC}]\,\underline{x}_C + [Q_I^F]\,\underline{u}_F \\ [I]\,\underline{\dot{x}}_F = [I]\,\underline{\dot{x}}_F \\ \underline{\dot{I}} = [D]\,\underline{I} + [D_R]\,\underline{I}_R \end{cases}$$

By introducing the new state vector $\underline{v} = \{\underline{\dot{x}}_F;\ \underline{x}_F;\ \underline{I}\}$ and recalling the external excitement vector $\underline{u}_C = \{\underline{\dot{x}}_C;\ \underline{x}_C\}$ it is possible to get the final state expression:

$$\underline{\dot{v}} \;=\; [A]\,\underline{v} \;+\; [B_C]\,\underline{u}_C \;+\; [B_I]\,\underline{I}_R \;+\; [B_F]\,\underline{u}_F \tag{4.2.4}$$

Where the required current signal $\underline{I}_R$ is computed by the control unit, which evaluates the system state, while $\underline{u}_F$ is the applied force obtained from the actual current signal $\underline{I}$, that is fed to the semi active actuator. The matrices are defined as follow:

$$[A] = \begin{bmatrix} -[M_{FF}]^{-1}[R_{FF}] & -[M_{FF}]^{-1}[K_{FF}] & [0] \\ [I] & [0] & [0] \\ [0] & [0] & [D] \end{bmatrix} \qquad [B_I] = \begin{bmatrix} [0] \\ [0] \\ [D_R] \end{bmatrix}$$

$$[B_C] = \begin{bmatrix} -[M_{FF}]^{-1}[R_{FC}] & -[M_{FF}]^{-1}[K_{FC}] \\ [0] & [0] \\ [0] & [0] \end{bmatrix} \qquad [B_F] = \begin{bmatrix} [M_{FF}]^{-1}[Q_I^F] \\ [0] \\ [0] \end{bmatrix}$$

The same procedure can be applied to the second configuration: by recalling the equations of motion 3.4.20 and coupling them with equations 4.2.3, it is possible to get:

$$\begin{cases} [M_{FF}]\,\underline{\ddot{x}}_F + [R_{FF}]\,\underline{\dot{x}}_F + [K_{FF}]\,\underline{x}_F = -[R_{FC}]\,\underline{\dot{x}}_C - [K_{FC}]\,\underline{x}_C + [Q^y_{II_F}]\,\underline{y} + [Q_I^F]\,\underline{u}_F \\ [I]\,\underline{\dot{x}}_F = [I]\,\underline{\dot{x}}_F \\ [N_1]\,\underline{\dot{y}} + [N_2]\,\underline{x}_F + [N_3]\underline{y} = \underline{0} \\ \underline{\dot{I}} = [D]\,\underline{I} + [D_R]\,\underline{I}_R \end{cases}$$

Defined the state vector $\underline{v} = \{\underline{\dot{x}}_F;\ \underline{x}_F;\ \underline{y};\ \underline{I}\}$, containing the state variable of the air spring as well, and recalled the other vectors ($\underline{u}_C;\ \underline{u}_F;\ \underline{I}_R$), the final state expression is:

$$\underline{\dot{v}} \;=\; [A]\,\underline{v} \;+\; [B_C]\,\underline{u}_C \;+\; [B_I]\,\underline{I}_R \;+\; [B_F]\,\underline{u}_F \tag{4.2.5}$$

Despite the similar expression, because of the different state vector the matrices are:

$$[A] = \begin{bmatrix} -[M_{FF}]^{-1}[R_{FF}] & -[M_{FF}]^{-1}[K_{FF}] & [M_{FF}]^{-1}[Q^y_{II_F}] & [0] \\ [I] & [0] & [0] & [0] \\ [0] & -[N_1]^{-1}[N_2] & -[N_1]^{-1}[N_3] & [0] \\ [0] & [0] & [0] & [D] \end{bmatrix} \qquad [B_I] = \begin{bmatrix} [0] \\ [0] \\ [0] \\ [D_R] \end{bmatrix}$$

$$[B_C] = \begin{bmatrix} -[M_{FF}]^{-1}[R_{FC}] & -[M_{FF}]^{-1}[K_{FC}] \\ [0] & [0] \\ [0] & [0] \\ [0] & [0] \end{bmatrix} \qquad [B_F] = \begin{bmatrix} [M_{FF}]^{-1}[Q_I^F] \\ [0] \\ [0] \\ [0] \end{bmatrix}$$

4.3 *SkyHook* strategy for the semi active damper

The first control logic investigated is the approximation proposed by Karnopp [26] in order to reproduce the *SkyHook* control strategy in a semi active control system.

The control strategy concept is based in the comparison of the direction of the suspension damping force, opposite to the elongation velocity, and the direction of the body velocity: if the force is acting in opposite direction respect to the body velocity, it is able to slow the mass down, leading to the desired effect; on the contrary if the force acts in the same direction of the body velocity, it is pushing the mass with a detrimental effect.

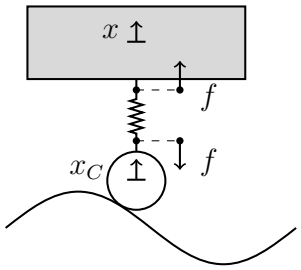

Figure 4.7: *Karnopp* main concept

	$\dot{x} > 0$	$\dot{x} < 0$	
$f < 0$	✓	✗	$\dot{\Delta L} > 0$
$f > 0$	✗	✓	$\dot{\Delta L} < 0$

Table 4.1: *Karnopp* approximation strategy

Under the assumption to keep the definition of the required force proposed in [23]:

$$u_{R\,ij} = -\frac{1}{2}(G_z\,\dot{z}_{Bi} \pm b\,G_\theta\,\dot{\theta}_{Bi})$$

where $G_z = 300\,000\ [Ns/m]$ and $G_\theta = 50\,000\ [Ns/m]$ are gains needed in order to divide the damping force in the contribution of the bogie frame bounce and pitch, allowing to drive the generated thrust toward the reduction of the vertical displacement of the bogie frame [23], it is possible to reduce the strategy of table 4.1 to the following simple generic rule:

$$u_{R\,ij} = \begin{cases} -\frac{1}{2}(G_z\,\dot{z}_{Bi} \pm b\,G_\theta\,\dot{\theta}_{Bi}) & \text{if } \dot{x}_i\dot{\Delta L}_{ij} > 0 \\ 0 & \text{if } \dot{x}_i\dot{\Delta L}_{ij} < 0 \end{cases} \tag{4.3.1}$$

The control law 4.3.1 is a simple two state algorithm. Usually in order to avoid discontinuity in the required force and non linear behaviour in the system response, more sophisticated algorithms are preferred, for example the *linear SH* [27] ; anyway this problem is avoided thanks to the control system layout: in fact the introduction of the filtered intermediate variable accounting for the dynamics of the solenoid valve ensures a continuous and smooth actuation.

4.4 Acceleration Driven Damper control

The second algorithm investigated is the *Acceleration Driven Damper* control (ADD) [28].

As suggested by the name, this algorithm is a counterpart of *SkyHook* control and, similarly to the *Karnopp* approximation, generates the control force depending on the direction of the deflection velocity of the suspension and of the acceleration of the suspended mass through the control law:

$$u_{R\,ij} = \begin{cases} -\frac{1}{2}(G_z\,\dot{z}_{Bi} \pm b\,G_\theta\,\dot{\theta}_{Bi}) & \text{if } \ddot{x}_i\,\dot{\Delta L}_{ij} > 0 \\ 0 & \text{if } \ddot{x}_i\,\dot{\Delta L}_{ij} < 0 \end{cases} \tag{4.4.1}$$

Again, the equation 4.4.1 is a two state control law, but the same considerations referred to the previous control law 4.3.1 hold: the non linearity issues caused by the sudden required force switch are managed by the filter on the intermediate variable accounting for the dynamics of the solenoid valve, ensuring a smooth and continuous actuation.

As it is possible to see from the conditions in equation 4.4.1, for the application of this algorithm, the information of the bogie frame acceleration is mandatory, whereas the state matrix formulation of equation 4.2.5 and 4.2.4 provides only $(\underline{\dot{x}}_F;\ \underline{x}_F)$.

Thus, in order to estimate $\underline{\ddot{x}}_F$ from $\underline{\dot{x}}_F$, it has been designed a filter $H(s) = s\,H^1(s)$ made of a second order *Butterworth* filter $H^1(s)$ with cutoff frequency at $100\,Hz$, providing v_{k+1} from $(v_k;\ v_{k-1})$, and a derivative block in series in order to move from v_{k+1} to a_{k+1}.

$$H(s) = s\,H^1(s)$$

$$H^1(s) = \frac{3.95e5}{s^2 + 888.6\,s + 3.95e5}$$

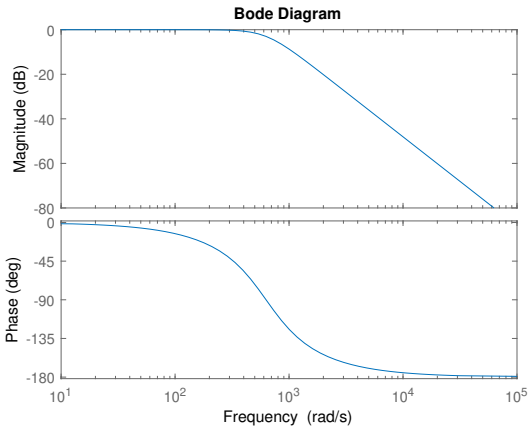

Figure 4.8: Bode diagram of $H(s)^1$

Every $1\,ms$ the integration is interrupted; the whole velocity time story is fed to the filter in order to remove the problem related to the initial transient and allowing to be more accurate; the last value of the filter output is used in the logic switch an is held constant in the following $1\,ms$ of integration as it would happen with a real sampled data.

No additional noise is consiedered.

The filter $H^1(s)$ is a *Butterworth* filter since no particular specifications are required for this application and it ensures a good tradeoff between the decay rate and the ripples in both the passing and stopping bandwidth.

From a practical point of view, referring the workflow chart of figure 4.2, the filter is placed before the *control algorithm* block processing the *mechanical system* output:

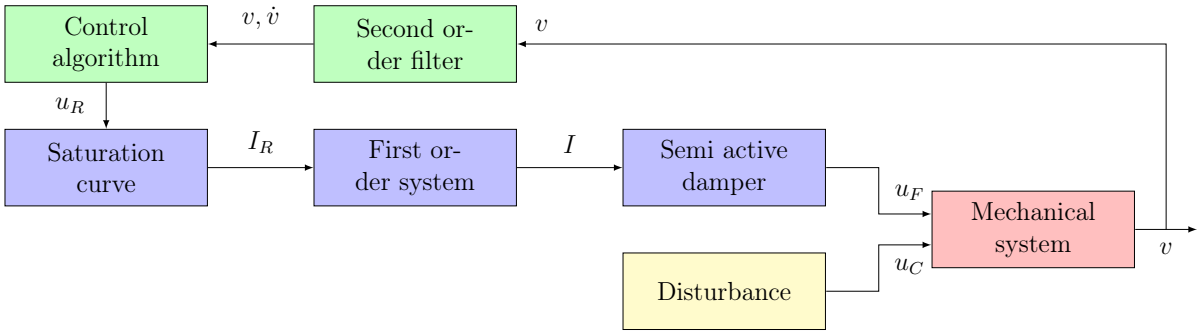

Figure 4.9: Chart of the workflow of the control system with *ADD* controller

In the previous strategy, the actuation was based on simple considerations about the force direction; in this approach [27], as long as the command variable is driven by the acceleration, given the discretization interval ΔT for refreshing the acceleration, the aim of the control algorithm is the minimization of:

$$\int_{k\,\Delta T}^{(k+1)\Delta T} |\ddot{x}(t)|\, dx$$

In absence of track preview, this algorithm is expected to perform a larger reduction of the vertical carbody accelerations if compared to the *SkyHook* strategy [27]:

- the *ADD* control should provide highest disturbance attenuation.
- the *ADD* control should be uniformly better than the passive in a wide frequency range, while the *SkyHook* one only about the natural frequency of the mode shape associated to the actuated degree of freedom.

Numerical simulation of semi active control system effects

In this chapter, a comparison is performed to assess the performance of the considered combinations of passive vehicles and control algorithms.

The main aim is to understand if the primary suspension control approach may have an engineering interest in order to improve the passenger comfort by reducing the carbody vibrations. In addition it is important to detect the relationship between the effectiveness of the control strategy and the dynamic properties of the passive vehicle in order to understand weaknesses and strengths of this semi active control approach.

In order to estimate the carbody vibration level, the accelerations of the front and rear points on the carbody connecting the latter to the secondary suspension have been evaluated. In fact they can be considered representative points of the overall effect as long as, by means of the *superimposition principle*, their response is given by the contribution of all of the independent variables of the carbody:

$$z_F = z_A - b\theta_A + \Phi_{1F} G_1 + \Phi_{2F} G_2$$
$$z_R = z_A + b\theta_A + \Phi_{1R} G_1 + \Phi_{2R} G_2$$

Furthermore for the evaluation and the comparison of the vibration disturbance, the *root mean square* value of both the displacement and the acceleration of the signals has been computed and taken as reference. In particular as long as the state vector $\underline{v}$ provides only the information about the displacements and the velocities ($\underline{x}_F$; $\dot{\underline{x}}_F$), the acceleration $\ddot{\underline{x}}_F$ has been computed backward from the state variables.

For the evaluation of the improvement, it has been introduced a variation rate between the *root mean square* value of the passive rms_P and of the controlled configuration rms_C:

$$variation\% = \frac{rms_P - rms_C}{rms_P}$$

To ensure the consistency of the comparison, of course the same track irregularity profile has been used for exciting the system in all simulations and, in order evaluate a wider working range, the same vehicle velocities have been tested:

$$V = [80;\ 130;\ 180;\ 230]\ km/h$$

The variable K_{PC} needed to scale linearly both $[u_R;\ F_{min};\ F_{max}]$ has been critically set in every simulation in order evaluate the dependency on the applied force.

5.1 First configuration with *SkyHook* strategy

The first test performed consists in the computation of the response of the first vehicle configuration with the *Karnopp* strategy approximating the *SkyHook* logic.

Before going through the results, it is important to recall the natural frequencies of the mode shapes from table 3.18: as it has been said, since the control force is not acting directly on the car body, there is a strong dependency between the response and the dynamic properties of the passive system.

For this reason it is fundamental to keep in mind the following values:

Bogie bounce	$f_{zB} = 6.6\ Hz$
Bogie pitch	$f_{\theta B} = 9.3\ Hz$
Carbody bounce	$f_{zA} = 0.8\ Hz$
Carbody pitch	$f_{\theta A} = 1.0\ Hz$
First bending mode	$f_{G1} = 8.4\ Hz$
Second bending mode	$f_{G2} = 23.3\ Hz$

Table 5.1: Natural frequencies of the mode shapes of the first configuration

For this simulation, the shape factor of the performance curve K_{PC} has been set to 0.45: this value leads to a control force whose average value of the *root mean square* for all of the velocities is $1\,309\,N$; in the same conditions the passive damper generates in average $419\,N$, with a ratio of 3.13. This can be demonstrated by the following figure, representing the damping force at the primary suspension for a vehicle velocity of $V = 80\ km/h$:

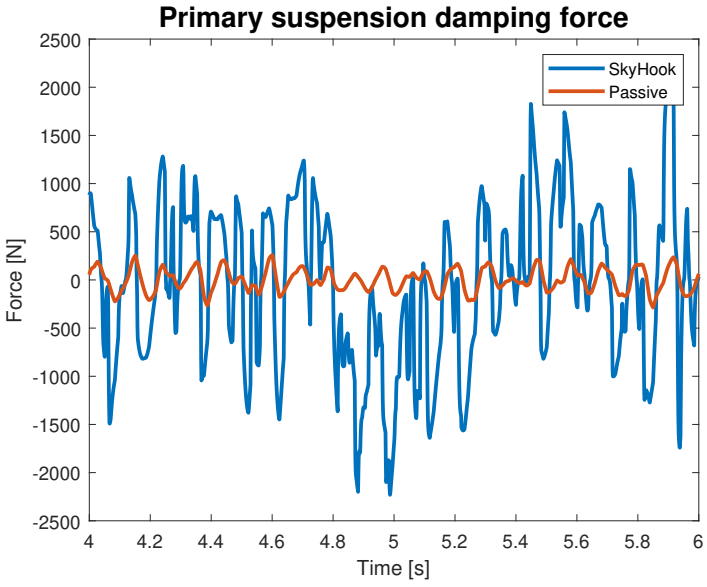

Figure 5.1: Primary suspension force comparison between controlled and passive system

This magnification of the forces is allowed by the adjustability of the semi active damper that contains the drawback ofthe transmissibility of the passive system in the *seismographic* region when the damping coefficient is increased, as shown in figure 4.4.

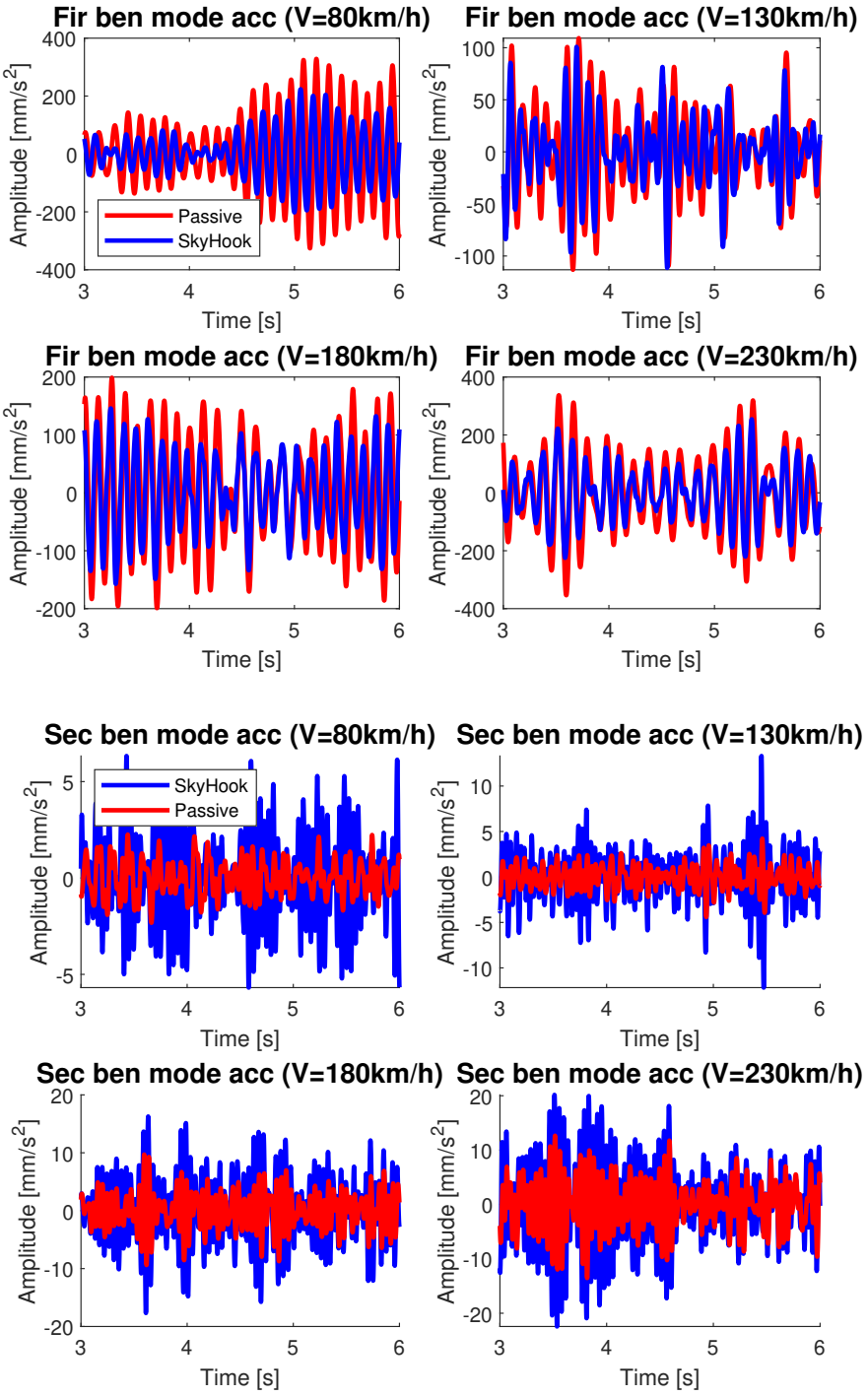

Figure 5.2: Time domain response of the accelerations of the independent variables of the flexible modes for the first configuration with the *SkyHook* approximation

By looking at the time domain response of the two flexible independent variables acceleration ($\ddot{G}_1$; $\ddot{G}_2$) in figure 5.2, it is possible to detect a dual trend, independently from the vehicle velocity:

- from one side the controller is able to reduce the first bending mode response;
- from the other side it is completely ineffective in reducing the second bending mode amplitudes, whose response shows furthermore high frequency components.

In order to understand the reason for this behaviour, it is helpful to investigate the *power spectra density* of the responses. In particular the acceleration of the carbody supporting points have been evaluated, since they are representative of the carbody overall behaviour. While going through this analysis, it is important to keep in mind that:

- the control system is acting on the primary suspension, thus it is expected to mostly affect the bogie frame response about the natural frequency associated to its bounce $f_{zB} = 6.6\,Hz$ with consequences on the vibration transmitted to the carbody in that frequency range;
- from table 5.1, it is possible to highlight that the frequency associated to the first bending mode $f_{G1} = 8.4\,Hz$ is very close to f_{zB}; the frequencies associated to the coach rigid modes are lower than f_{zB}, with $f_{zA} = 0.8\,Hz$ and $f_{\theta A} = 1.0\,Hz$; the frequency associated to the second bending mode is higher than f_{zB}, standing at $f_{G2} = 22.2\,Hz$.

By moving to the observation of the *power spectra density* of figure 5.3 it is possible to distinguish three areas depending on the difference respect to the passive response:

- a wide *seismographic* region for frequencies larger than $9.2\,Hz$ in which the controlled configuration has a worse transmissibility respect to the passive one; but since the amplitude of the vibrations in this range is very small (1/20 respect to the amplitudes at $10\,Hz$), from the global point of view there is almost no difference;
- a *quasi static* region at very low frequencies, in which the passive and the controlled configurations have similar behaviour as long as the response is dominated by the system stiffness, which is not affected by the controller;
- a very narrow *effective* region for frequencies about $f_{zB} = 6.5\,Hz$, as expected: here the response of the controlled configuration is better than the passive one.

The strong bond coupling the dynamic properties of the passive system and the performances of the controller can be enhanced from the *power spectra density* evaluation by knowing the relative position of the natural frequencies of the mode shapes.

In particular the closeness of f_{G1} and f_{zB} explains the beneficial effect on the reduction of the first bending mode response, evident in the acceleration time response of figure 5.2.

On the other hand, since f_{G2} is in a *seismographic* region respect to f_{zB}, it is definitely not possible to reduce the excitement of the secondary bending mode through a primary suspension control strategy on this passive mechanical system. This furthermore explains the detection of superharmonic components in the acceleration time response of the second bending mode in figure 5.2.

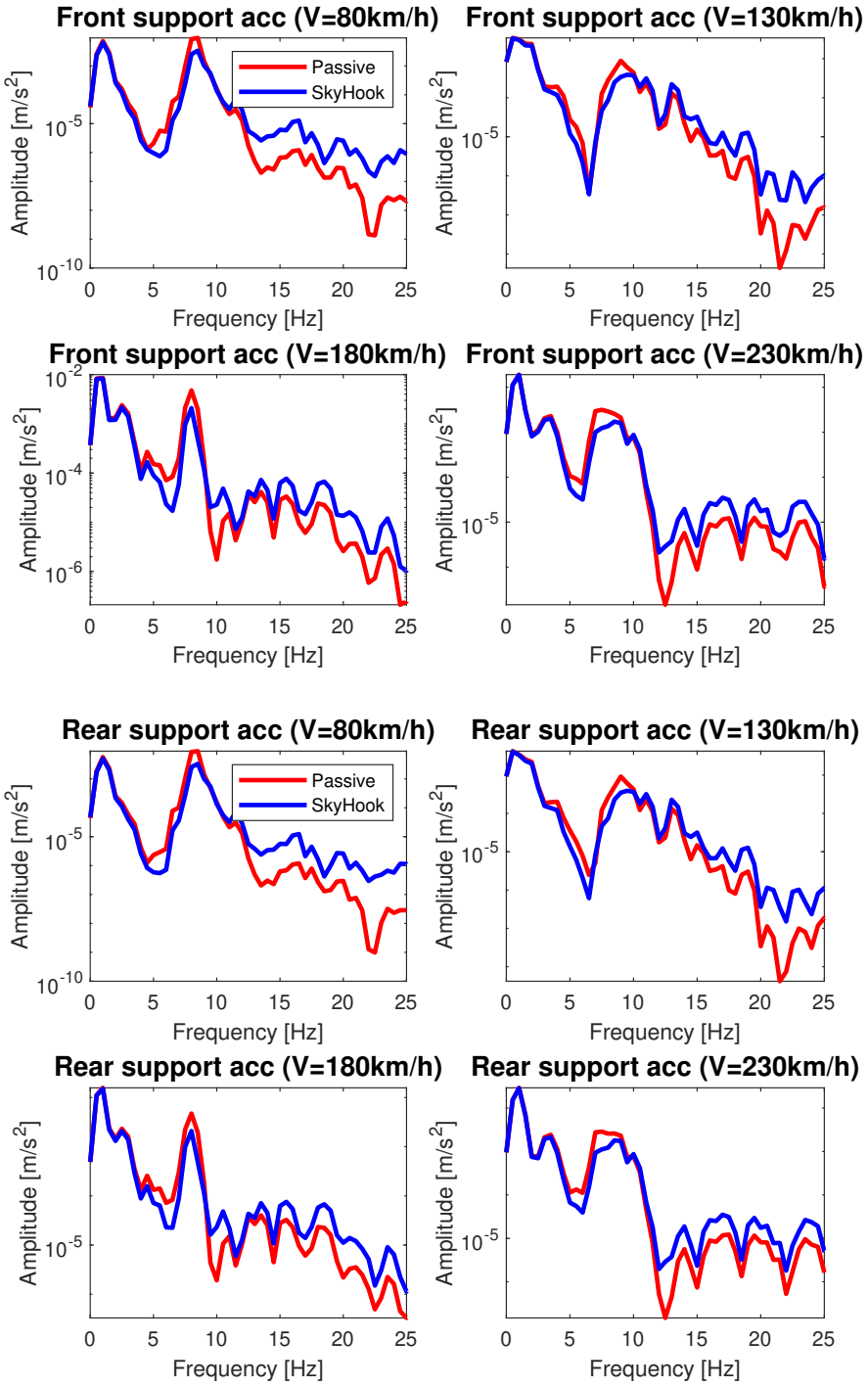

Figure 5.3: *PSD* of the accelerations of the carbody support points for the first configuration with the *SkyHook* approximation

The reason for the worse transmissibility in the *seismographic* region is mostly related to two factors:

- the use of a suspension with better performances, able to supply larger forces and thus leading to the same drawback of a suspension with too high damping coefficient (in this configuration, the control force is generally 3.13 times greater than the force generated by the passive damper on the same track profile).
- the non linear nature of the two state control system that, because of the sudden switch, may lead to the presence of superharmonic components in the response.

As already discussed, the filtering on the intermediate variable accounting for the dynamics of the current ruling the solenoid valve opening can partially manage the non linear response of the control system, as shown in figure 4.3.

Furthermore an additional issue that is related to the dynamic property of the passive vehicle itself and that is limiting the effectiveness of the control system, is represented by the low value of the natural frequency of the mode shape associated to the bogie frame bounce $f_{zB} = 6.5\,Hz$. In fact it is possible to see that the *effective* zone is limited about f_{zB}, thus the higher the frequency f_{zB} the wider the *effective* region is.

In conclusion, it is possible to state that this control system is poorly effective on the carbody rigid mode, works properly on the first bending mode and is detrimental on the second bending mode. In order to figure out if the overall effect is anyway advantageous, it is possible to evaluate the *root mean square* values of the responses.

In particular, figure 5.4 proposes a comparison of the *rms* values of both the displacements and the accelerations of the flexible independent variables and of the representative carbody supporting points. Apparently, despite the slightly worse response of the second bending mode, the figure 5.4 shows an overall vibration reduction. In order to quantify this effect, it is possible to compute the variation rate.

$$variation\,[\%] = \frac{rms_P - rms_C}{rms_P}$$

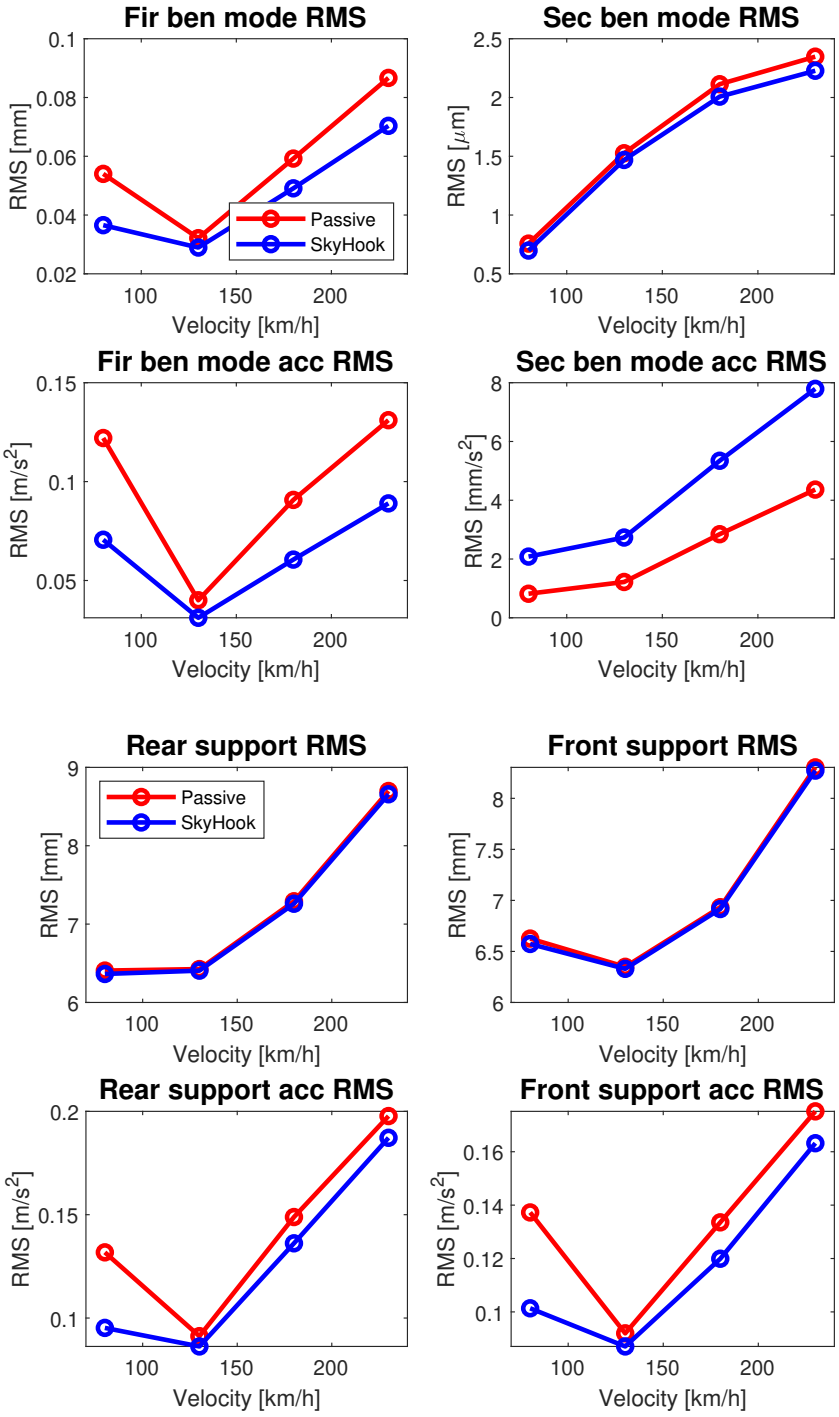

Figure 5.4: *rms* of the two flexible independent variables and of the carbody support points for the first configuration with the *SkyHook* approximation

	z_A	θ_A	G_1	G_2	R	F	
Passive	6.494	0.528	0.054	$0.8e-4$	6.407	6.626	
SkyHook	6.445	0.523	0.037	$7.0e-4$	6.364	6.573	displacements $[mm]$
Variation [%]	0.742	1.034	32.332	7.787	0.673	0.793	
Passive	0.081	$9.4e-3$	0.122	$8.2e-4$	0.132	0.137	
SkyHook	0.074	$8.6e-3$	0.071	$2.1e-3$	0.095	0.101	accelerations $[m/s^2]$
Variation [%]	8.293	8.003	42.141	-154.5	27.738	26.157	

Table 5.2: *RMS* of the simulation at $V = 80\,km/h$ of the first configuration with *SkyHook* approximation

	z_A	θ_A	G_1	G_2	R	F	
Passive	6.352	0.631	0.032	$1.5e-3$	6.456	6.349	
SkyHook	6.333	0.622	0.029	$1.5e-3$	6.406	6.330	displacements $[mm]$
Variation [%]	0.296	1.389	9.931	3.743	0.309	0.308	
Passive	0.082	0.019	0.040	$1.2e-3$	0.091	0.092	
SkyHook	0.078	0.018	0.031	$2.7e-3$	0.086	0.087	accelerations $[m/s^2]$
Variation [%]	4.650	4.039	22.159	-124.065	5.448	5.339	

Table 5.3: *RMS* of the simulation at $V = 130km/h$ of the first configuration with *SkyHook* approximation

	z_A	θ_A	G_1	G_2	R	F	
Passive	7.097	0.626	0.059	$2.1e-3$	7.291	6.933	
SkyHook	7.073	0.617	0.049	$2.0e-3$	7.260	6.916	displacements $[mm]$
Variation [%]	0.341	1.491	17.094	4.996	0.429	0.258	
Passive	0.127	0.026	0.091	$2.8e-3$	0.149	0.134	
SkyHook	0.120	0.025	0.061	$5.3e-3$	0.136	0.120	accelerations $[m/s^2]$
Variation [%]	5.637	5.382	33.258	-87.9	8.537	10.206	

Table 5.4: *RMS* of the simulation at $V = 180km/h$ of the first configuration with *SkyHook* approximation

	z_A	θ_A	G_1	G_2	R	F	
Passive	8.507	0.594	0.087	$2.3e-3$	8.699	8.303	
SkyHook	8.471	0.588	0.070	$2.2e-3$	8.657	8.272	displacements $[mm]$
Variation [%]	0.430	1.013	18.818	5.098	0.480	0.379	
Passive	0.178	0.029	0.131	$4.4e-3$	0.198	0.175	
SkyHook	0.168	0.028	0.089	$7.8e-3$	0.187	0.163	accelerations $[m/s^2]$
Variation [%]	5.594	5.646	32.100	-78.6	5.318	6.813	

Table 5.5: *RMS* of the simulation at $V = 230km/h$ og the first configuration with *SkyHook* approximation

The figure 5.4 and the summarizing table evaluating the *rms* of the response, lead to some expected conclusion and to some new consideration. In particular:

- as long as the natural frequency associated to the bogie bounce f_{zB} and to the first bending mode f_{G1} are very close, the latter independent variable experiences a very good improvement [22.2 % ÷ 42.1 %];
- as long as the natural frequency associated to the bogie bounce f_{zB} and the second bending mode f_{G2} are very far, the latter independent variable experiences a detrimental effect, even worse than 100 %; this is anyway not detrimental for the overall response since the absolute magnitude is still very small compared to the others;
- it is a nice surprise to see that, even if the natural frequencies of the mode shapes associated to the carbody rigid modes are at very low frequency, the controller has anyway a good effect on them [4.3 % ÷ 8.3 %].
- at the end, it is important to consider that the overall carbody response benefits of a good improvement [5.3 % ÷ 27.7 %].

5.1.1 Effect of the performances of the semi active damper

As already discussed, on the contrary with respect to the passive damper, by increasing the semi active damper performances it is expected to further improve the response about f_{zB} with few drawbacks on the *seismographic* region, thanks to its adjustability.

Thanks to the the introduction of scale factor of the performance curve, it is possible to evaluate the response trend while increasing the generated force, to characterize this phenomena and to detect strengths and weaknesses with respect to a passive configuration.

Thus a new simulation has been performed by holding all of the parameter except $K_{PC} = 0.8$, thus the 78 % more than the previous case: with this scale factor value, the semi active damper force has an *rms* value of 1 896 N, which is 4.53 times larger than the average force generated by the passive damper in the non controlled configuration (419 N).

By looking at the time responses of the accelerations of the independent variables of the bending modes in figure 5.5, it is possible to detect the same behaviour:

- the vibration of the first bending mode acceleration is generally reduced, but it is no longer appreciable in all of the evaluated working conditions;
- consistently with the expectations, the second bending mode acceleration response shows larger amplitudes.

The presence of the high frequency harmonic component is consistent with the use of a suspension whose transmitted force has a larger damping contribution: the fact that semi active damper is generating larger forces has an effect equivalent to the employment of a passive element with a larger damping coefficient. Thus the filtering properties of the suspension are negatively affected.

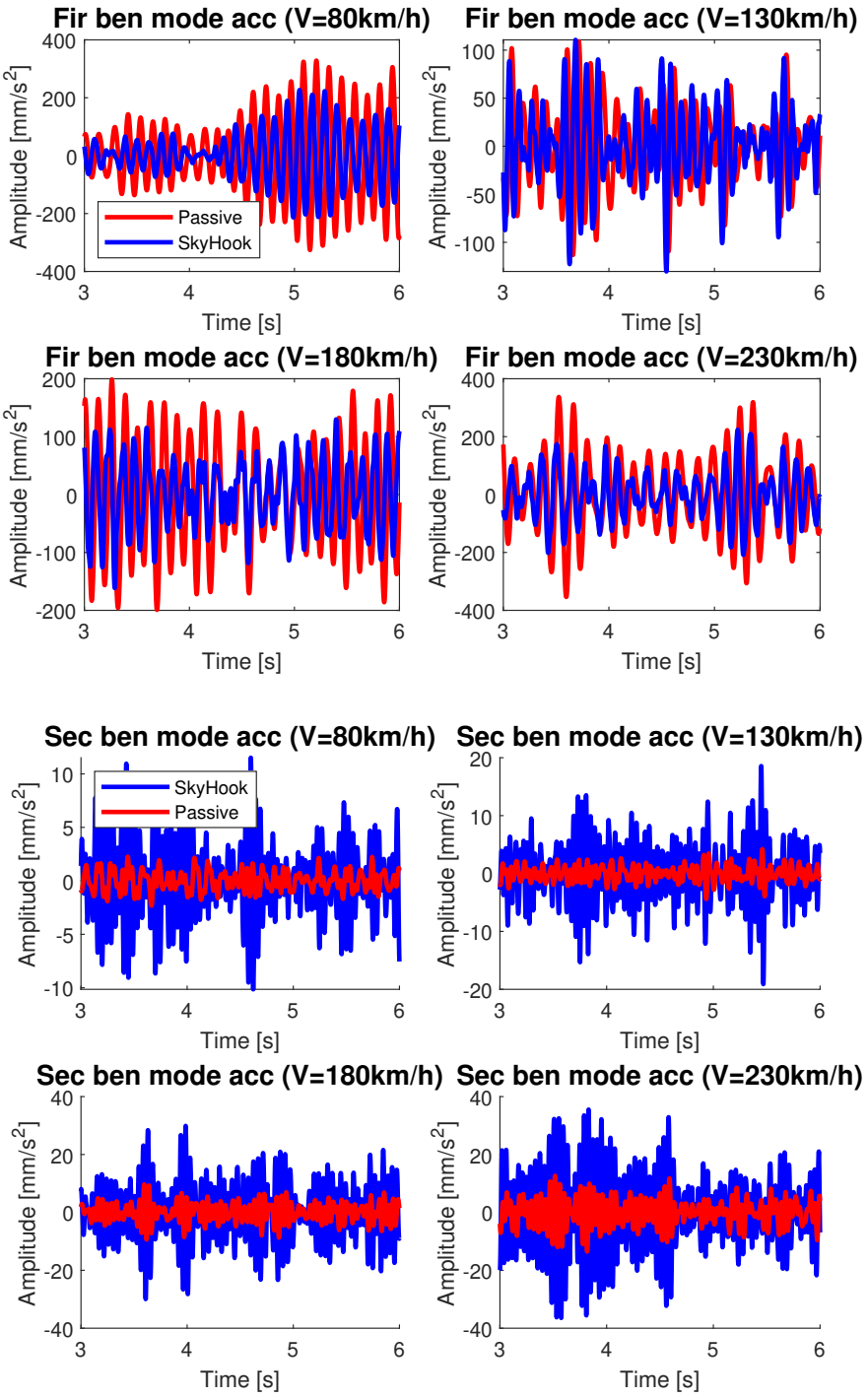

Figure 5.5: Time domain response of the accelerations of the independent variables of the flexible modes for the first configuration with *SkyHook* approximation for the evaluation of the performance curve effect

At this point, in order to evaluate the differences in the frequency response relate to the larger damping force generated, it is possible to move to the analysis of the *power spectra density* of the carbody support points, reported in figure 5.6:

- the *quasi static* region is still unaffected since the response is dominated by the system stiffness in that frequency range;
- in the *effective* range about $f_{zB} = 6.6\,Hz$, the response if further damped respect to the previous simulation;
- in the *seismographic* region, the usual detrimental drawback appears.

In order to evaluate the magnitude of the high frequency transmissibility issue, it is necessary to move to the observation of the *root mean square* values. From the summarizing tables at the end of this section, it is possible to highlight that:

- there is a strong benefit on the rigid modes of the carbody, with a reduction up to 10.4 %. This represent an important improvement with respect to the previous simulation as long as the rigid modes have a large weight in the overall vibration;
- the first bending mode has an improvement very similar to the one of the previous consideration, with a variation in the range $[8.5\,\% \div 40.5\,\%]$;
- a detrimental effect can be detected on the second bending mode, whose response may achieve amplitudes over 200 % larger, but still remains small in absolute value;
- the overall effect estimate from the evaluation of the coach support point is anyway positive, ensuring a reduction of $[2.5\,\% \div 12.1\,\%]$.

This comparison highlighted that, as expected, by employing a semi active damper with larger performances it is possible to achieve better results, thanks to its adjustability property: the worsening of the high frequency range is largely compensated by the improvements in the low frequency range.

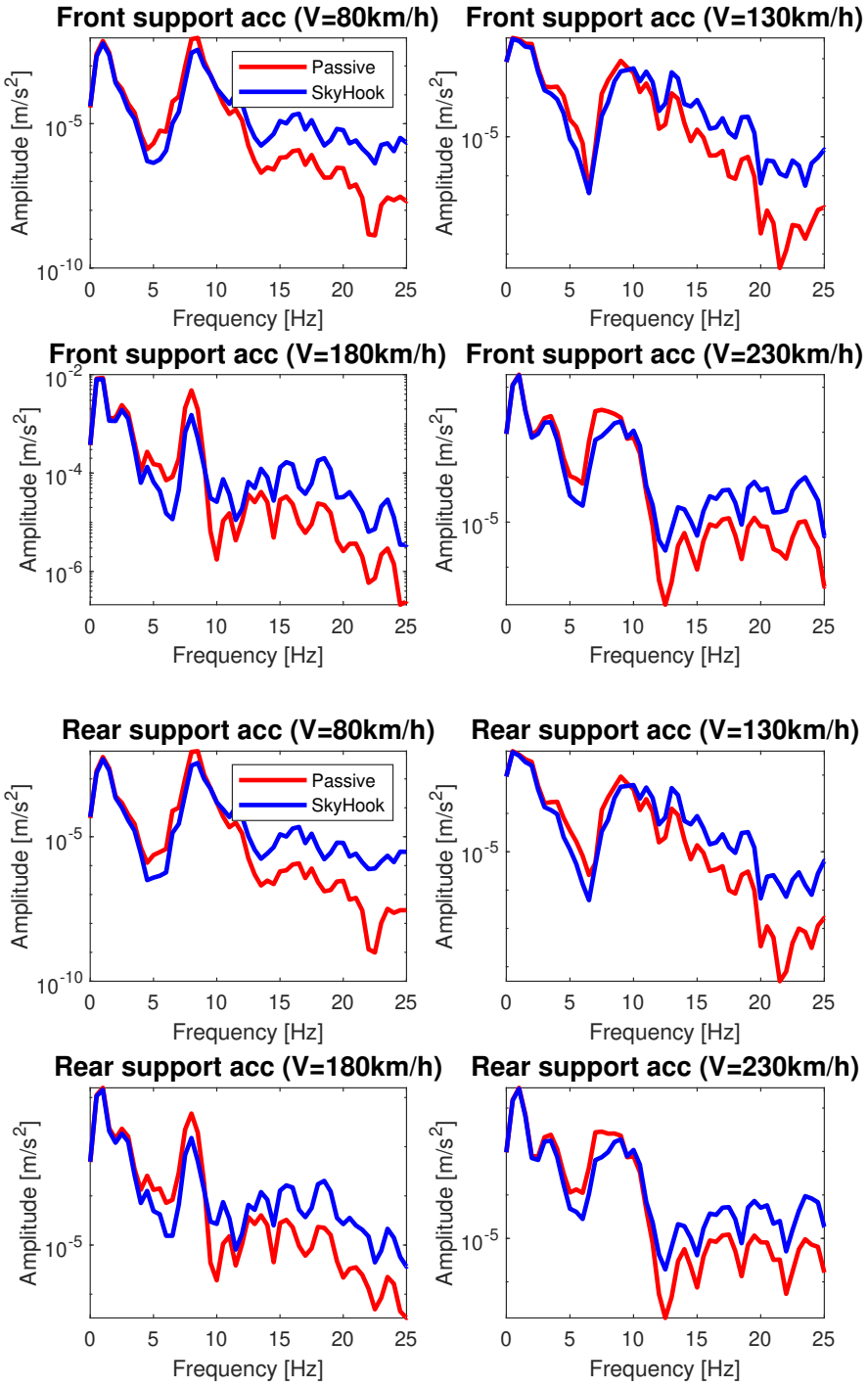

Figure 5.6: *PSD* of the accelerations of the carbody support points for the first configuration with *SkyHook* approximation for the evaluation of the performance curve effect

	z_A	θ_A	G_1	G_2	R	F	
Passive	6.494	0.528	0.054	$8.0e-4$	6.407	6.626	
SkyHook	6.416	0.516	0.037	$7.0e-4$	6.339	6.560	displacements $[mm]$
Variation [%]	1.193	2.233	32.103	8.450	1.062	1.303	
Passive	0.081	$9.4e-3$	0.122	$8.2e-4$	0.132	0.137	
SkyHook	0.072	$8.4e-3$	0.073	$3.4e-3$	0.096	0.102	accelerations $[m/s^2]$
Variation [%]	0.896	10.389	39.939	−317.7	27.279	26.075	

Table 5.6: *RMS* of first configuration simulation at $V = 80\,km/h$ with *SkyHook* approximation for the evaluation of the performance curve effect

	z_A	θ_A	G_1	G_2	R	F	
Passive	6.352	0.631	0.032	$1.5e-3$	6.456	6.349	
SkyHook	6.307	0.611	0.028	$1.4e-3$	6.378	6.302	displacements $[mm]$
Variation [%]	0.716	3.133	12.187	6.492	0.750	0.739	
Passive	0.082	0.019	0.040	$1.2e-3$	0.091	0.092	
SkyHook	0.077	0.018	0.037	$4.8e-4$	0.089	0.090	accelerations $[m/s^2]$
Variation [%]	6.953	7.704	8.456	−289.8	2.541	2.718	

Table 5.7: *RMS* of first configuration simulation at $V = 130\,km/h$ with *SkyHook* approximation for the evaluation of the performance curve effect

	z_A	θ_A	G_1	G_2	R	F	
Passive	7.097	0.626	0.059	$2.1e-3$	7.291	6.933	
SkyHook	7.039	0.605	0.046	$2.0e-3$	7.219	6.888	displacements $[mm]$
Variation [%]	0.816	3.366	22.218	6.071	0.995	0.655	
Passive	0.127	0.026	0.091	$2.8e-3$	0.149	0.134	
SkyHook	0.117	0.024	0.054	$9.3e-3$	0.133	0.117	accelerations $[m/s^2]$
Variation [%]	0.8340	8.343	40.481	−225.7	10.793	12.133	

Table 5.8: *RMS* of first configuration simulation at $V = 180\,km/h$ with *SkyHook* approximation for the evaluation of the performance curve effect

	z_A	θ_A	G_1	G_2	R	F	
Passive	8.507	0.594	0.087	$2.3e-3$	8.699	8.303	
SkyHook	8.423	0.579	0.066	$2.2e-3$	8.602	8.232	displacements $[mm]$
Variation [%]	0.991	2.535	24.125	5.735	1.115	0.858	
Passive	0.178	0.029	0.131	$4.4e-3$	0.198	0.175	
SkyHook	0.163	0.027	0.080	0.014	0.184	0.160	accelerations $[m/s^2]$
Variation [%]	8.438	8.918	38.986	−209.4	7.165	8.627	

Table 5.9: *RMS* of first configuration simulation at $V = 230\,km/h$ with *SkyHook* approximation for the evaluation of the performance curve effect

By testing a wide range of configurations varying the value K_{PC}, it is possible to compute the comparative *power spectra density* of figure 5.7 which allows to characterize the trend of this phenomena.

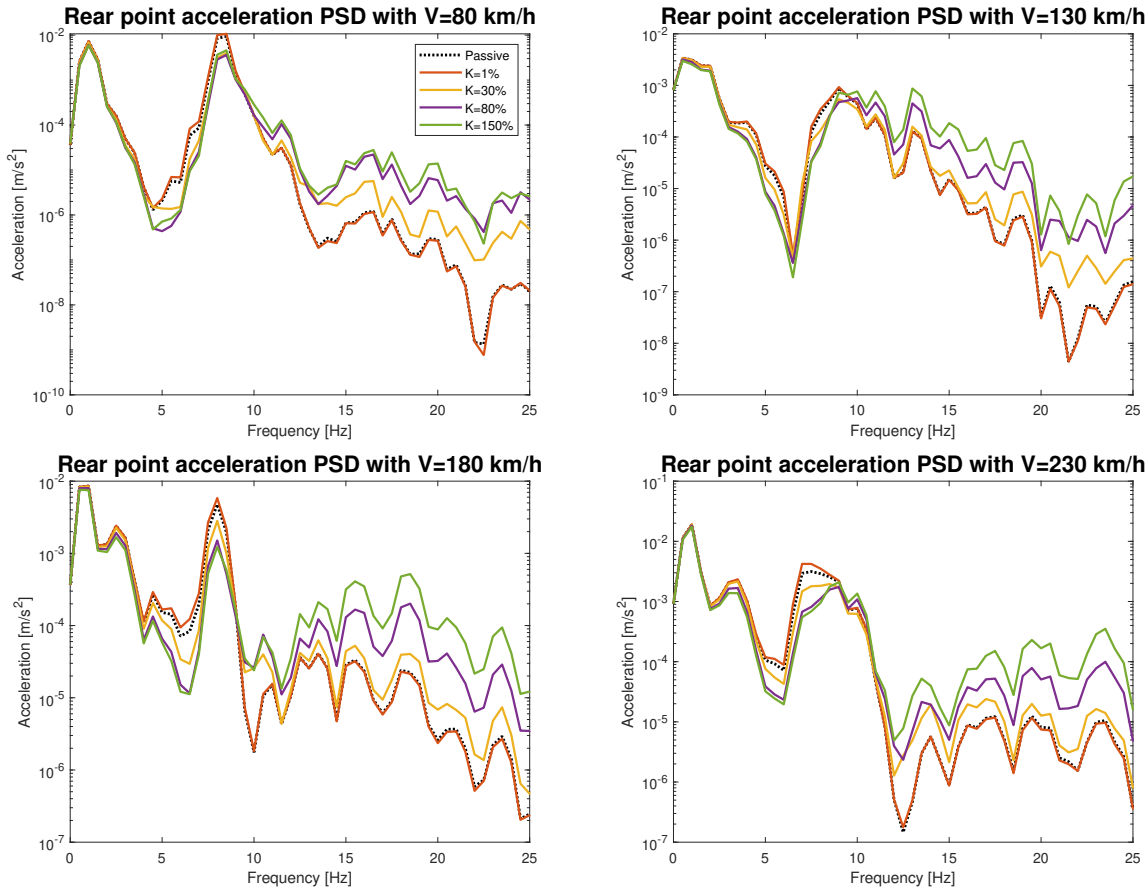

Figure 5.7: *PSD* of the accelerations of the carbody support points for the first configuration with *SkyHook* approximation for the evaluation of the effect of the performance curve

Furthermore the figure 5.7 shows that the K_{PC} value ensuring the best tradeoff between the low frequencies benefits and high frequency drawback is about 0.30. In particular with this coefficient the average control force applied is 990 N, thus 2.36 times larger than the passive one (419 N).

Thus in conclusion, consistently with the summarizing tables evaluating the *rms* variation in the simulations with $K_{PC} = 0.45$ and $K_{PC} = 0.8$, it is possible to state that to use a semi active damper generating larger force is functional to the reduction of the vibration of the carbody, but after a ratio of the control force over the passive one of 2.5 the benefits get slighter.

5.2 Second configuration with *SkyHook* strategy

In order to go back in the main topic and find out the effects of the passive system dynamics on the controller effectiveness, a comparative simulation has been performed with the second configuration data set, whose natural frequencies are very different respect to the previous example (aw shown in table 3.18):

Bogie bounce	$f_{zB} = 17.1\ Hz$
Bogie pitch	$f_{\theta B} = 22.8\ Hz$
Carbody bounce	$f_{zA} = 2.3\ Hz$
Carbody pitch	$f_{\theta A} = 2.9\ Hz$
First bending mode	$f_{G1} = 9.7\ Hz$
Second bending mode	$f_{G2} = 22.2\ Hz$

Table 5.10: Natural frequencies of the mode shapes of the second configuration

For ensuring the consistency of the results, all of the simulation parameters have been kept constant and the damper performance curve scale factor has been set to $K_{PC} = 150$.

In fact with this value the *rms* of the control force results $7\,834\ N$, which is again 2.98 times larger than the passive configuration, generating $2\,630\ N$. This magnification has been needed since the damping of the primary suspension in the second configuration has a value of $c_I = 123\,000\ Ns/m$, thus almost 25 times larger than the damper of the first configuration.

Under the same conditions, the same controller provides completely different effect on the second system: in fact by looking at the time domain response of the acceleration of the bending modes in figure 5.8, it is possible to see that both of them reduce their vibration amplitude with the controller, but the advantage is slighter.

Thus the dual trend with positive effect on the first bending mode and detrimental on the second is no longer present.

Furthermore respect to the other configuration, there is no additional disturbance caused by the superharmonic components in the response of the second bending mode.

Once more the key for understanding this behaviour can be found in the *power spectra density* of the representative support points of figure 5.9; but before going through their analysis it is as usual necessary to remind that:

- the controller is acting on the primary suspension; thus, as it has been demonstrated, an improvement about the natural frequency of the mode associated to the bogie bounce with $f_{zB} = 17.7\ Hz$ is expected;
- the natural frequencies of the mode shape associated to the bending modes are almost equally spaced respect to f_{zB}, with the first mode toward the *quasi static* range with $f_{G1} = 9.7\ Hz$ and the second mode toward the *seismographic* region with $f_{G2} = 22.2\ Hz$; the natural frequencies of the mode shapes associated to the carbody rigid modes are at low frequency, with $f_{zA} = 2.3\ Hz$ and $f_{\theta A} = 2.9\ Hz$.

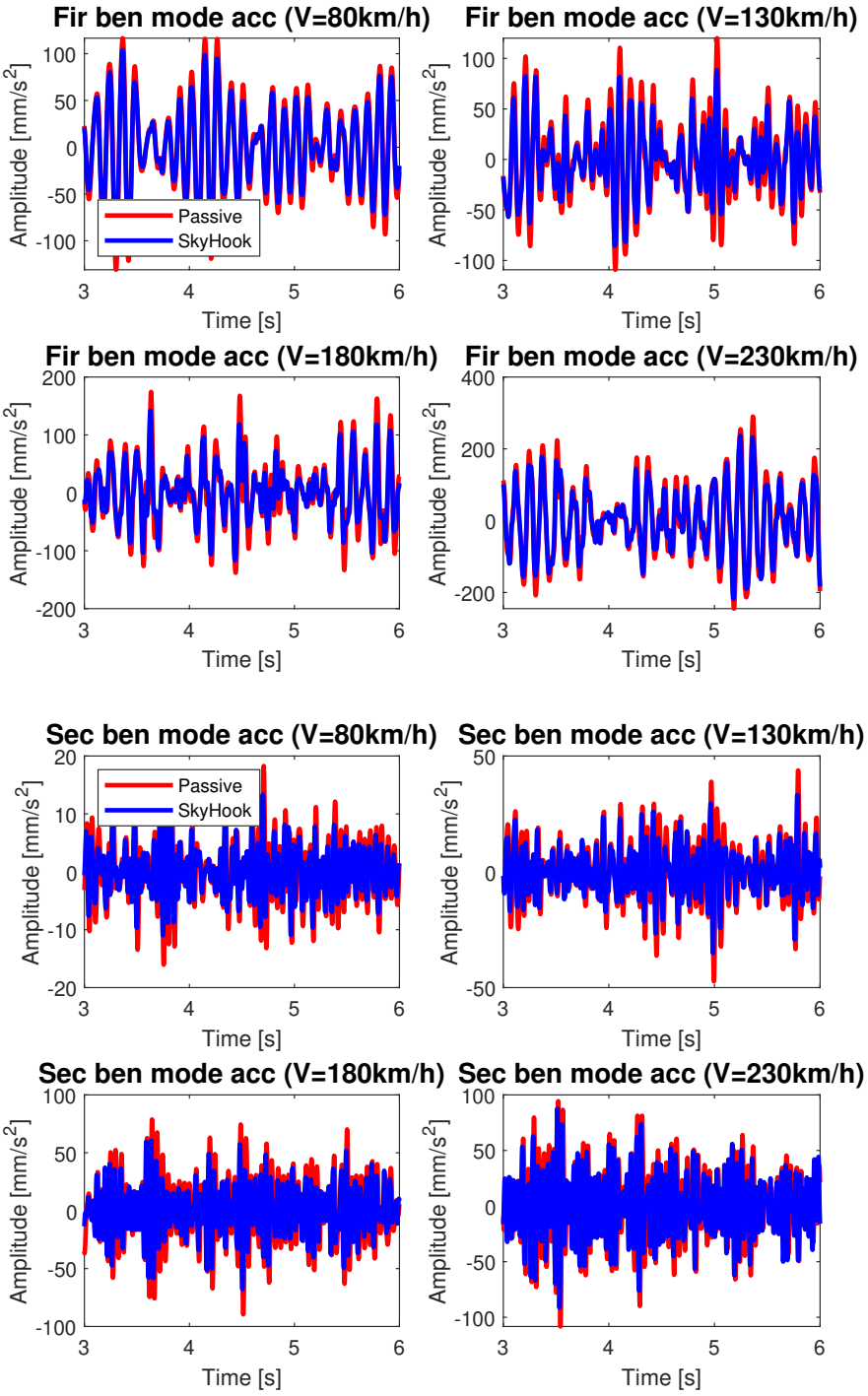

Figure 5.8: Time domain response of the flexible mode independent variables acceleration for second configuration with *SkyHook* approximation

So, by moving to the observation of the *PSD* in figure 5.9, it is possible to notice some peculiar difference respect to the corresponding simulation with the first configuration:

- first of all, the *effective* region is wider than before, going from about $8\,Hz$ till over $24.2\,Hz$. Thus both the natural frequencies of the modes associated to the carbody flexible modes stand in this range and benefit for the controller effect.

- consequently the *quasi static* region is wider as well, thus it is hardly possible to affect the carbody rigid modes starting from this passive system property. But anyway this does not represent a problem as long as in this range the response is almost equal to the passive, without additional detrimental effect carried by the control system.

- last but not least, the *seismographic* region is pushed in very high frequencies, where for energy reasons the amplitude of the vibrations is intrinsically small. For this reason in the time response it is no longer possible to detect the disturbance of the superharmonic components.

Proving that the same controller leads to completely different behaviour makes undeniable the bound between the the passive system dynamics and the controller effectiveness.

For example in the previous configuration there was no way to abate the second bending mode vibration; on the contrary with this configuration it is possible to reduce the overall response in the whole human perception frequency range, with large benefit for the passenger comfort.

The main relevant feature of the second configuration passive dynamics consists in the higher frequency of the mode shape dominated by the bogie bounce $f_{zB} = 17.7\,Hz$: this makes the *effective* region of the controller definitely wider than for the previous configuration ($f_{zB} = 6.6\,Hz$). This is even more relevant considering that the improvement takes place exactly in correspondence of the frequency range of interest $[0 \div 25\,Hz]$.

At this point it finally possible to move to the evaluation of the *rms* shown in figure 5.10. As already discussed, it is possible to detect a clear improvement of the flexible modes response in the whole velocity range considered; but at the end the overall effect estimated by the evaluation of the carbody supports point is very slight because of the large weight of the rigid independent variables of the varbody in the vibration contribution.

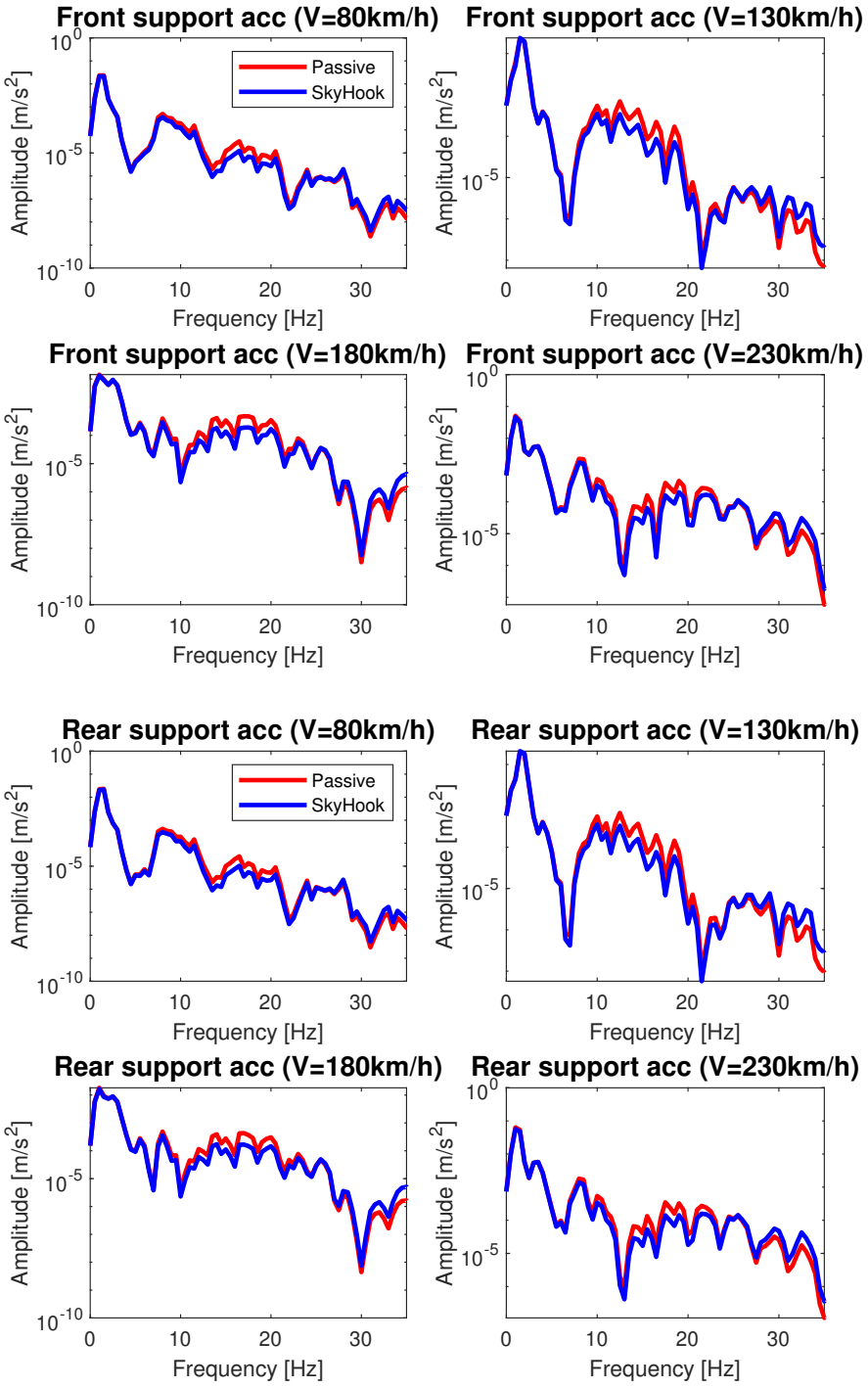

Figure 5.9: *Power spectra density* of the accelerations of the carbody support points for the second configuration with the *SkyHook* strategy

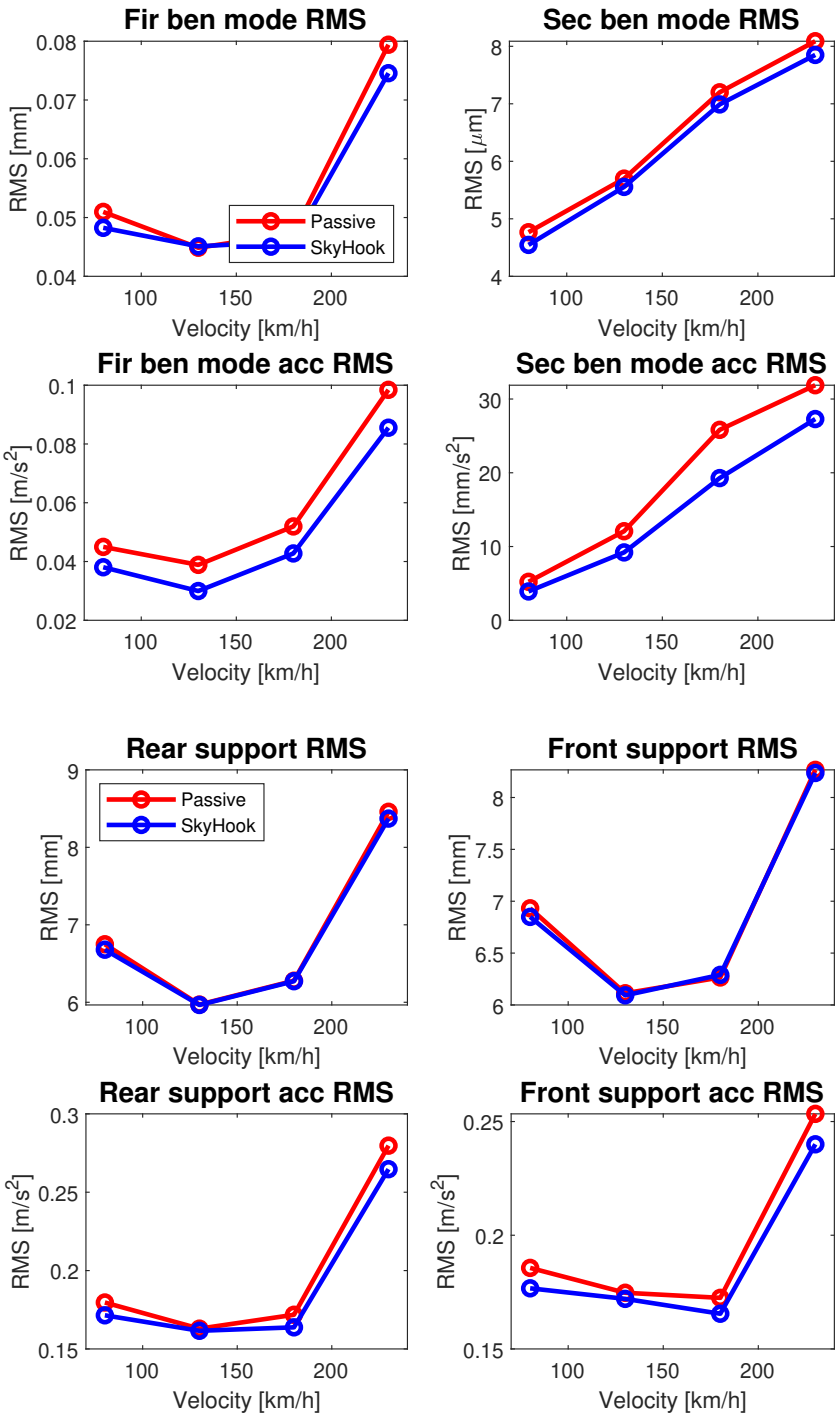

Figure 5.10: *RMS* of the accelerations of the carbody support pointsfor the second configuration with the *SkyHook* strategy

	z_A	θ_A	G_1	G_2	R	F	
Passive	6.826	0.513	0.051	$4.8e-3$	6.749	6.932	
SkyHook	6.748	0.508	0.048	$4.5e-3$	6.679	6.849	displacements $[mm]$
Variation [%]	1.135	1.041	5.319	4.624	1.039	1.195	
Passive	0.182	0.012	0.045	$5.2e-3$	0.180	0.186	
SkyHook	0.174	0.012	0.038	$3.9e-3$	0.172	0.177	accelerations $[m/s^2]$
Variation [%]	4.338	0.860	15.401	25.017	4.548	4.837	

Table 5.11: *RMS* of second configuration simulation at $V = 80\ km/h$ with *SkyHook* strategy

	z_A	θ_A	G_1	G_2	R	F	
Passive	5.997	0.656	0.050	$5.7e-3$	5.970	6.113	
SkyHook	5.987	0.638	0.045	$5.6e-3$	5.966	6.093	displacements $[mm]$
Variation [%]	0.164	2.667	−0.530	2.528	0.084	0.326	
Passive	0.163	0.028	0.039	0.012	0.163	0.175	
SkyHook	0.164	0.027	0.030	$9.2e-3$	0.162	0.172	accelerations $[m/s^2]$
Variation [%]	−0.572	3.485	22.914	23.795	0.837	1.538	

Table 5.12: *RMS* of second configuration simulation at $V = 130\ km/h$ with *SkyHook* strategy

	z_A	θ_A	G_1	G_2	R	F	
Passive	6.217	0.738	0.047	$7.2e-3$	6.278	6.265	
SkyHook	6.289	0.719	0.046	$7.0e-3$	6.272	6.290	displacements $[mm]$
Variation [%]	−0.194	2.481	2.843	2.931	0.098	−0.399	
Passive	0.161	0.047	0.052	0.026	0.172	0.173	
SkyHook	0.156	0.046	0.043	0.019	0.164	0.166	accelerations $[m/s^2]$
Variation [%]	2.640	2.119	17.697	25.332	4.668	4.050	

Table 5.13: *RMS* of second configuration simulation at $V = 180\ km/h$ with *SkyHook* strategy

	z_A	θ_A	G_1	G_2	R	F	
Passive	8.334	0.779	0.079	$8.1e-3$	8.459	8.266	
SkyHook	8.276	0.756	0.075	$7.9e-3$	8.371	8.237	displacements $[mm]$
Variation	0.698	2.957	6.101	2.944	1.036	0.360	
Passive	0.257	0.053	0.098	0.032	0.280	0.253	
SkyHook	0.245	0.052	0.086	0.027	0.265	0.240	accelerations $[m/s^2]$
Variation [%]	4.763	1.781	13.102	14.397	5.370	5.283	

Table 5.14: *RMS* of second configuration simulation at $V = 230\ km/h$ with *SkyHook* strategy

The summarizing tables lead to the conclusion that the *SkyHook* approximation control strategy is always effective on this configuration, ensuring a reduction of the vibration on all of the carbody mode shapes:

- the control strategy is equally effective on both the flexible modes, overtaking the performances of the first configuration. In particular the first bending mode experiences an improvement of $[13.1\,\% \div 22.9\,\%]$, while the second flexible mode of $[14.4\,\% \div 25.3\,\%]$.

- the response of the rigid *dofs* of the carbody is almost completely unaffected, stressing the limits of the primary suspension semi active control in the low frequency range: the variation is always below $4.8\,\%$.

- the overall response follows the trend of the rigid independent variables of the carbody stressing the dominant contribution of the latter. Despite the large improvement of the flexible modes, the variation is just about $[0.8\,\% \div 5.4\,\%]$.

At this point, by looking the numerical results of the two configuration working with the same controller, it s possible to point out a first rough comparison:

- from one side, there is a configuration whose natural frequency of mode shape associated to the controlled *dof* is at low frequency $f_{zB} = 6.6\,Hz$: the *effective* region of the control system is very narrow, but leads to great improvements. As long as the natural frequencies of the dominant modes are about the *effective* region, $(z_A;\, \theta_A;\, G_1)$ experience a good improvement. The overall effect is positive despite the detrimental effect on the second bending mode, whose natural frequency stands in the *seismographic* region.

- on the other side, there is a configuration whose natural frequency of mode shape associated to the controlled *dof* is at higher frequency $f_{zB} = 17.7\,Hz$: the *effective* region of the control system is consequently wider, but the improvements are slighter. As long as the natural frequencies of the flexible modes stand about the *effective* region, their response is improved; anyway the carbody rigid *dof* $(z_A;\, \theta_A)$ are unaffected because of their distance respect to f_{zB}. Thus, the overall effect is slightly lower.

The natural frequency of the mode shape associated to the controlled independent variable f_{zB} plays a central role. In conclusion, the passive system dynamics property may drive the controller effect toward a wider but slight improvement over the spectrum or on the contrary to a greater improvement but focused in a narrow frequency range.

During the design step, it is possible to take advantage of these considerations.

5.3 First configuration with *ADD* strategy

In order to prove the consistency of the benefits of the primary suspension semi active control strategy, a cross comparison between the *SkyHook* approximation and *ADD* control sstrategy has been performed.

The first test, described in section 5.1, has been repeated by applying the *ADD* control strategy. Of course the same simulation parameters have been kept constant.

The first important thing to notice is that despite the performance curve of the same semi active damper has the same scale factor $K_{SC} = 0.45$, with the *ADD* controller the applied force has an average value of $1\,006\,N$ against the $1\,309\,N$ of the *SkyHook* approximation approach. Thus in this configuration the system is dealing with forces generally 2.4 times greater than in the passive configuration ($419\,N$).

As usual, it is important to recall the passive system mode shapes natural frequencies:

Bogie bounce	$f_{zB} = 6.6\,Hz$
Bogie pitch	$f_{\theta B} = 9.3\,Hz$
Coach bounce	$f_{zA} = 0.8\,Hz$
Coach pitch	$f_{\theta A} = 1.0\,Hz$
First bending mode	$f_{G1} = 8.4\,Hz$
Second bending mode	$f_{G2} = 23.3\,Hz$

Table 5.15: Natural frequencies of the mode shapes of the first configuration

By looking at the acceleration response of the independent variables of the bending modes ($\ddot{G}_1$; $\ddot{G}_2$) in figure 5.11, it is possible to recognize the same trend already discussed:

- form one side, the response of the first bending mode in the controlled configuration is much more damped than the passive configuration, in the whole vehicle speed range.
- form the other side, the second bending mode response in the controlled configuration shows vibrations larger than in the passive configuration. This is consistent with the already detected detrimental effect that the primary suspension control approach causes to the high frequency components of the response.

In order to investigate if the dynamic properties of the passive system cause the same problems despite the different control strategy, it is necessary to move on to the observation of the *power spectra density* of the carbody support points in figure 5.12.

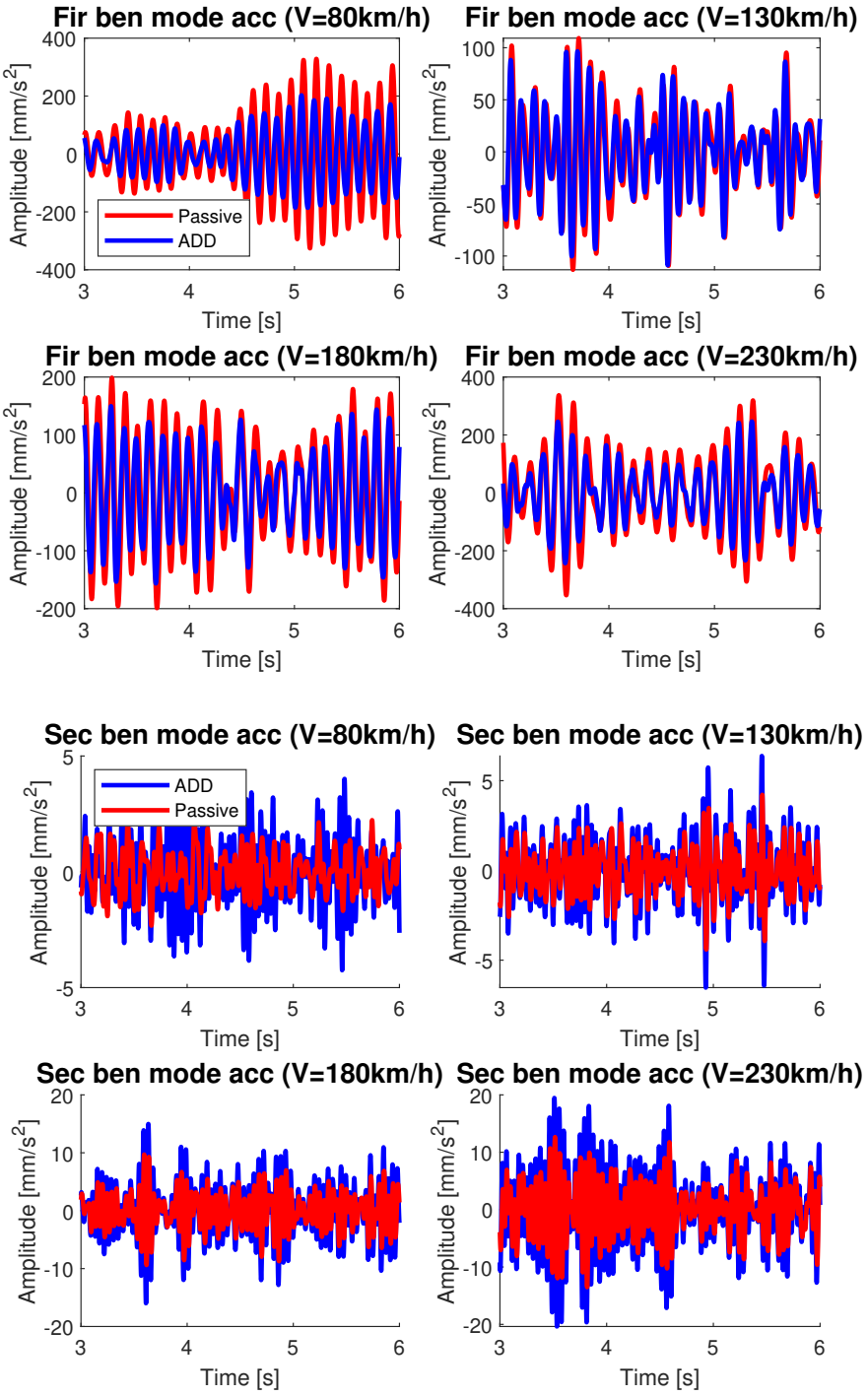

Figure 5.11: Time domain response of the acceleration of the flexible mode independent variables for the first configuration with *ADD* strategy

The first thing that is possible to appreciate is the reduction of the transmissibility in the high frequency range respect to the response with *SkyHook* approximation controller (figure 5.3). This effect may be caused by:

- the generation of a lower control force (an average value of $F_{ADD} = 1\,006\,N$ respect to $F_{SH} = 1\,309\,N$); from a practical point of view, this effect is similar to the use of a damper with a smaller damping coefficient in the passive configuration;
- intrinsic property of the control strategy: the *ADD* law is expected to provide a better response than the passive in the whole spectrum, while the *SkyHook* only about the resonand frequency of the controlled *dof* [27].

By observing the figure 5.12, it is possible to appreciate that the division in three region holds and their frequency range is the same respect to the results with the *SkyHook* strategy:

- the *quasi static* region, characterized by negligible difference between controlled and passive response, limited to frequencies below $3\,Hz$
- the *effective* region in about $f_{zB} = 6.6\,Hz$. It extends in a very narrow range, till about $9.2\,Hz$, and ensures and improvement in the vibrations reduction.
- the *seismographic* region takes place at higher frequencies than the *effective* region and it is very wide. In its range, a detrimental effect on the response can be detected.

The distribution of the three different areas with respect to the passive system natural frequencies, stresses once more the coupling between the control system effectiveness and the dynamic properties of the passive system, besides the control strategy.

The reason for this behaviour can be found in the control system layout: it is able to control the primary suspension, ruling the bogie response; thus the way the bogie frame motion is transmitted to the carbody and the dynamic property of the passive system play a central role. On the contrary the typical control system for the passenger comfort works at the secondary suspension level and for this reason it is able to directly affect the carbody response.

In order to asses a final comparison between the *SkyHook* logic and *ADD* control system, the *root mean square* values of the responses has been evaluated. From figure 5.13, it is possible to have the confirm that, over all the evaluated service velocity range:

- the first bending mode response is always damped.
- the second bending mode vibrations are always larger than the passive configuration, but still their absolute value is very small.
- the representative carbody support points always experience a vibration reduction.

But consistently with the previous considerations, the overall improvement is very slight because of the dominant contribution of the rigid modes.

In order to measure the improvement, the summarizing table showing the *percentage variation* have been computed for this study case as well.

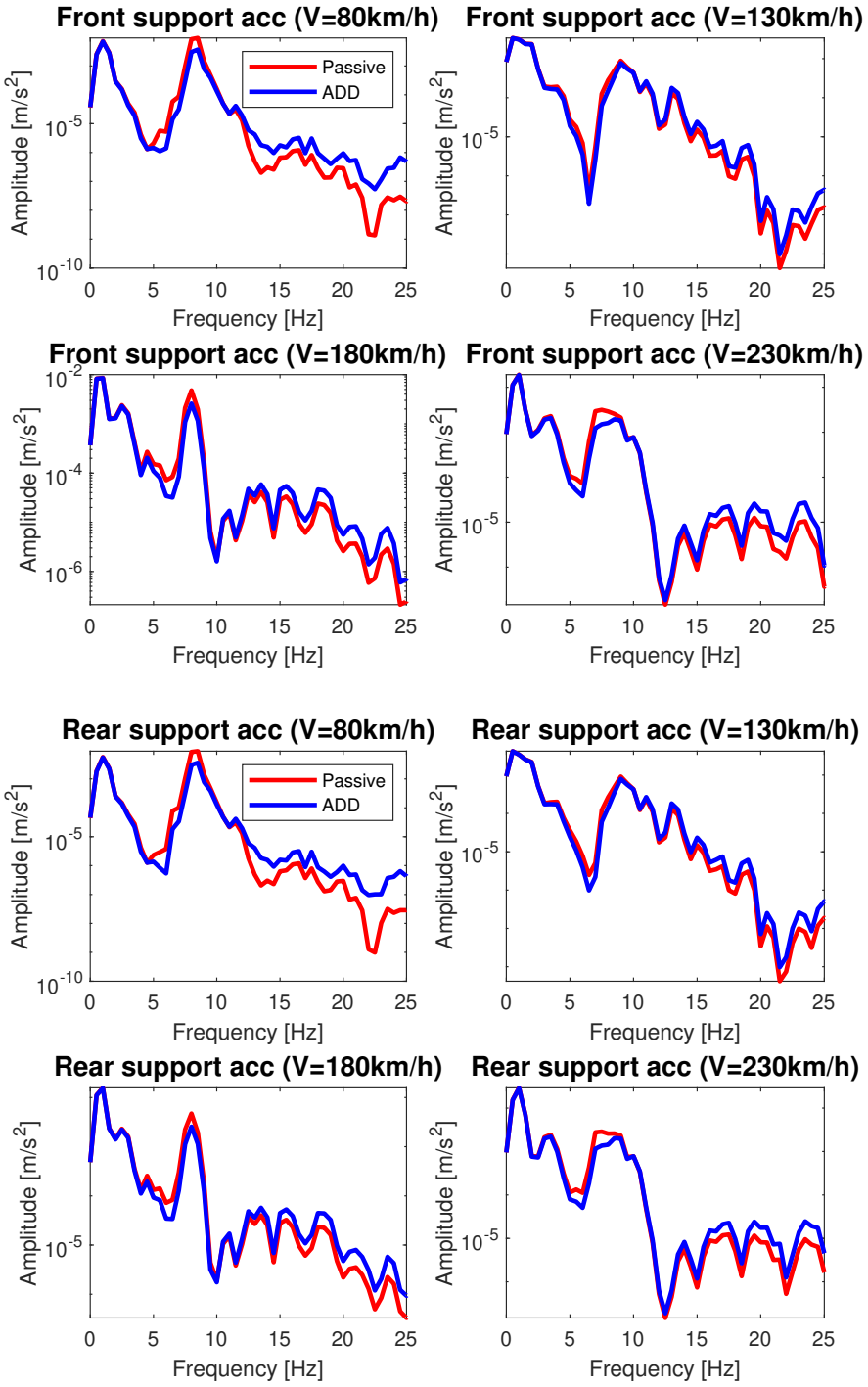

Figure 5.12: *Power pectra density* of the accelerations of the carbody support points for the first configuration with the *ADD* controller

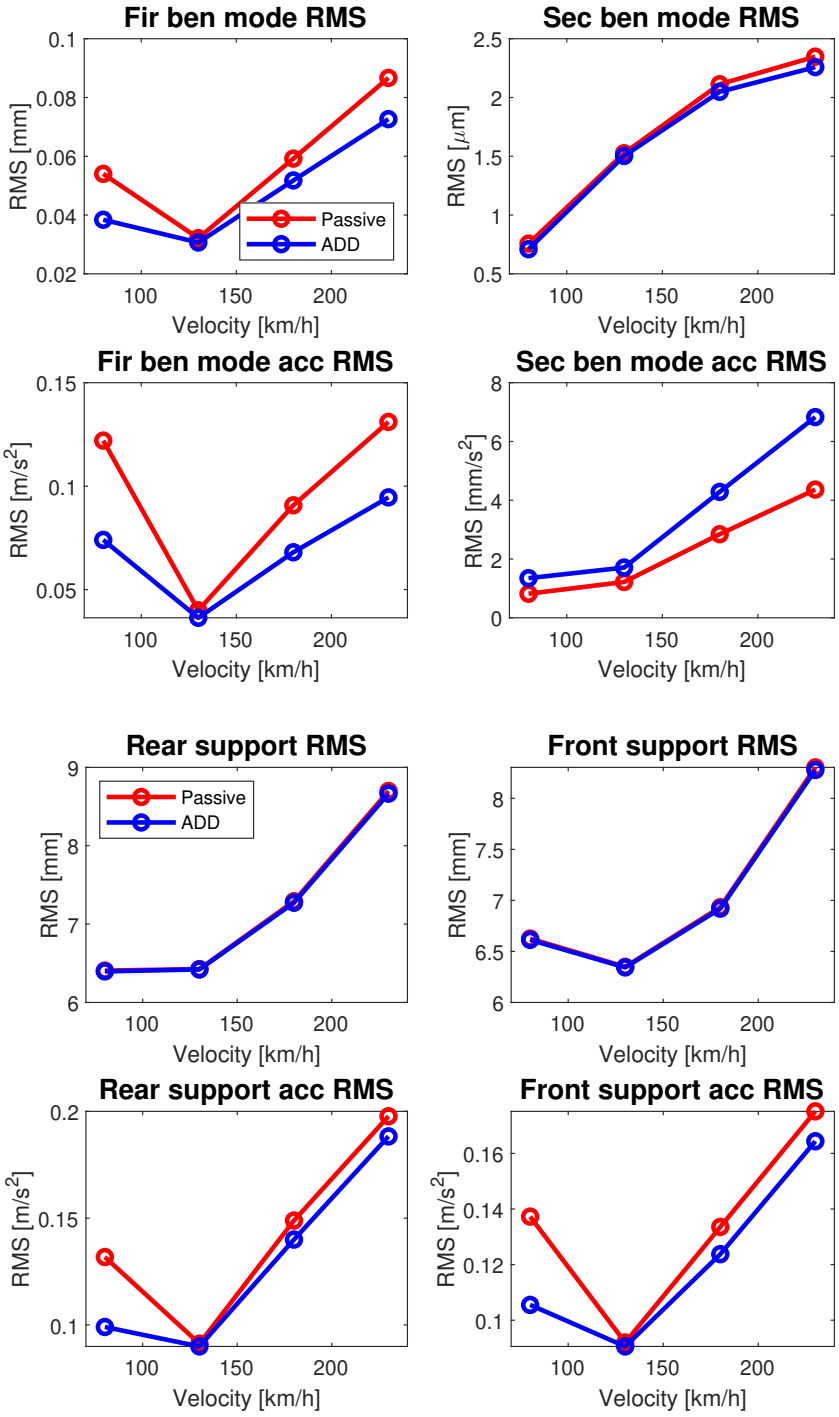

Figure 5.13: *rms* of the accelerations of the carbody support points for the first configuration with the *ADD* controller

	z_A	θ_A	G_1	G_2	R	F	
Passive	6.494	0.528	0.054	$0.8e-4$	6.407	6.626	
ADD	6.482	0.527	0.038	$6.4e-4$	6.397	6.613	displacements $[mm]$
Variation [%]	0.177	0.173	28.910	6.270	0.156	0.192	
Passive	0.081	$9.4e-3$	0.122	$8.2e-4$	0.132	0.137	
ADD	0.078	$8.9e-3$	0.074	$1.3e-3$	0.099	0.106	accelerations $[m/s^2]$
Variation [%]	4.308	5.798	39.326	−64.8	24.834	23.131	

Table 5.16: *RMS* of first configuration simulation at $V = 80\,km/h$ with *ADD* control

	z_A	θ_A	G_1	G_2	R	F	
Passive	6.352	0.631	0.032	$1.5e-3$	6.456	6.349	
ADD	6.347	0.628	0.031	$1.5e-3$	6.421	6.344	displacements $[mm]$
Variation [%]	0.75	0.392	4.575	1.517	0.068	0.098	
Passive	0.082	0.019	0.040	$1.2e-3$	0.091	0.092	
ADD	0.081	0.019	0.036	$1.7e-3$	0.090	0.091	accelerations $[m/s^2]$
Variation [%]	1.692	1.579	9.059	−40.206	1.440	1.537	

Table 5.17: *RMS* of first configuration simulation at $V = 130\,km/h$ with *ADD* control

	z_A	θ_A	G_1	G_2	R	F	
Passive	7.097	0.626	0.059	$2.1e-3$	7.291	6.933	
ADD	7.080	0.622	0.052	$2.0e-3$	7.273	6.919	displacements $[mm]$
Variation [%]	0.229	0.649	12.557	3.058	0.254	0.204	
Passive	0.127	0.026	0.091	$2.8e-3$	0.149	0.134	
ADD	0.123	0.026	0.068	$4.3e-3$	0.140	0.124	accelerations $[m/s^2]$
Variation [%]	3.514	3.143	25.010	−50.6	5.986	7.336	

Table 5.18: *RMS* of first configuration simulation at $V = 180\,km/h$ with *ADD* control

	z_A	θ_A	G_1	G_2	R	F	
Passive	8.507	0.594	0.087	$2.3e-3$	8.699	8.303	
ADD	8.478	0.590	0.073	$2.3e-3$	8.665	8.278	displacements $[mm]$
Variation [%]	0.349	0.712	16.190	3.788	0.387	0.307	
Passive	0.178	0.029	0.131	$4.4e-3$	0.198	0.175	
ADD	0.169	0.028	0.095	$6.8e-3$	0.188	0.164	accelerations $[m/s^2]$
Variation [%]	4.738	4.078	27.829	−56.5	4.772	6.146	

Table 5.19: *RMS* of first configuration simulation at $V = 230\,km/h$ with *ADD* control

The summarizing table allows to perform an important comparison between the *SkyHook* and *ADD* control strategy. In fact the results show that:

- the *ADD* effect on the first bending mode is relevant [9.1 % ÷ 39.3 %], but still smaller than the one ensured by the *SkyHook* approximation [22.2 % ÷ 42.1 %].
- the *ADD* controller manages better the high frequency detrimental effect related to the passive system dynamic characteristic. In fact, the variation is about −50 %, whereas it is over −100 % with the *SkyHook* control logic.
- both the *ADD* and *SkyHook* control law are not able to widely affect the carbody rigid independent variables, but the latter is still slightly better ([1.5 % ÷ 5.8 %] for this control strategy against [4.0 % ÷ 8.3 %] for the *SkyHook* one).

Given that none of the two control laws is able to affect the rigid modes, the overall improvement is very similar: [1.4 % ÷ 24.8 %] with *ADD* control strategy and [5.3 % ÷ 27.7 %] with *SkyHook* approach.

This results confirm that the *ADD* control strategy ensures a generally slight improvement all over of the spectrum, while on the contrary the *SkyHook* control strategy provides larger benefits focused on a narrower frequency range and some detrimental effect in the other frequencies.

This may suggest that:

- the *SkyHook* control strategy is more suitable for a mechanical system whose natural frequencies are very close one another and the natural frequency of mode shape associated to the actuated *dof* stands in this range, just like the system of the first configuration.
- the *ADD* control strategy is more suitable fora mechanical system whose natural frequencies are speaded over a relatively wide frequency band and the natural frequency of the mode shape associated to the actuated *dof* is quite far from the others.

In order to assess this statement, the last simulation of the second mechanical system coupled with the *ADD* control logic has been performed.

5.4 Second configuration with *ADD* stategy

As usual, the same simulation parameters have been kept constant between this test and the corresponding one with the second vehicle model coupled with the *SkyHook* strategy.

Given the saturation curve scale factor $K_{SC} = 150$, with the *ADD* controller an average control force of $6\,524\ N$ has been generated, which is 2.48 times larger than the passive one $2\,630\ N$. This time, the *ADD* controller generates larger forces with respect to the *SkyHook* one ($7\,834\ N$), with the resulting effect equivalent to a passive suspension whose damping coefficient is smaller.

The natural frequencies needed for a correct evaluation of the results, are as usual taken from table 3.18 and summarized as follow::

Bogie bounce	$f_{zB} = 17.1\ Hz$
Bogie pitch	$f_{\theta B} = 22.8\ Hz$
Coach bounce	$f_{zA} = 2.3\ Hz$
Coach pitch	$f_{\theta A} = 2.9\ Hz$
First bending mode	$f_{G1} = 9.7\ Hz$
Second bending mode	$f_{G2} = 22.2\ Hz$

Table 5.20: Natural frequencies of the mode shapes of the second configuration

By looking at the time domain response of the bending modes acceleration in figure 5.14, the same trend obtained with the first vehicle configuration is detected:

- both the first and the second bending modes shows a slight improvement in the whole service speed evaluated;
- the are no the disturbances of the superharmonic components.

Thus, apparently the same consideration should hold: despite the natural frequencies are spread in a wide frequency range, as long as f_{zB} has a large value all of the modes benefit of the controller introduction whose *effective* range extends up to almost $24.2\ Hz$.

Anyway by moving to the evaluation of the *power spectra density* of the acceleration of the representative support points of the carbody in figure 5.15, the usual detection of the three areas is definitely less evident and the difference between the passive and the controlled configuration is very slight.

Recalling the *ADD* feature to ensure an improvement wider in the frequency range but lower in the magnitude [27], this behaviour can be understood and the consistency of the results appreciated.

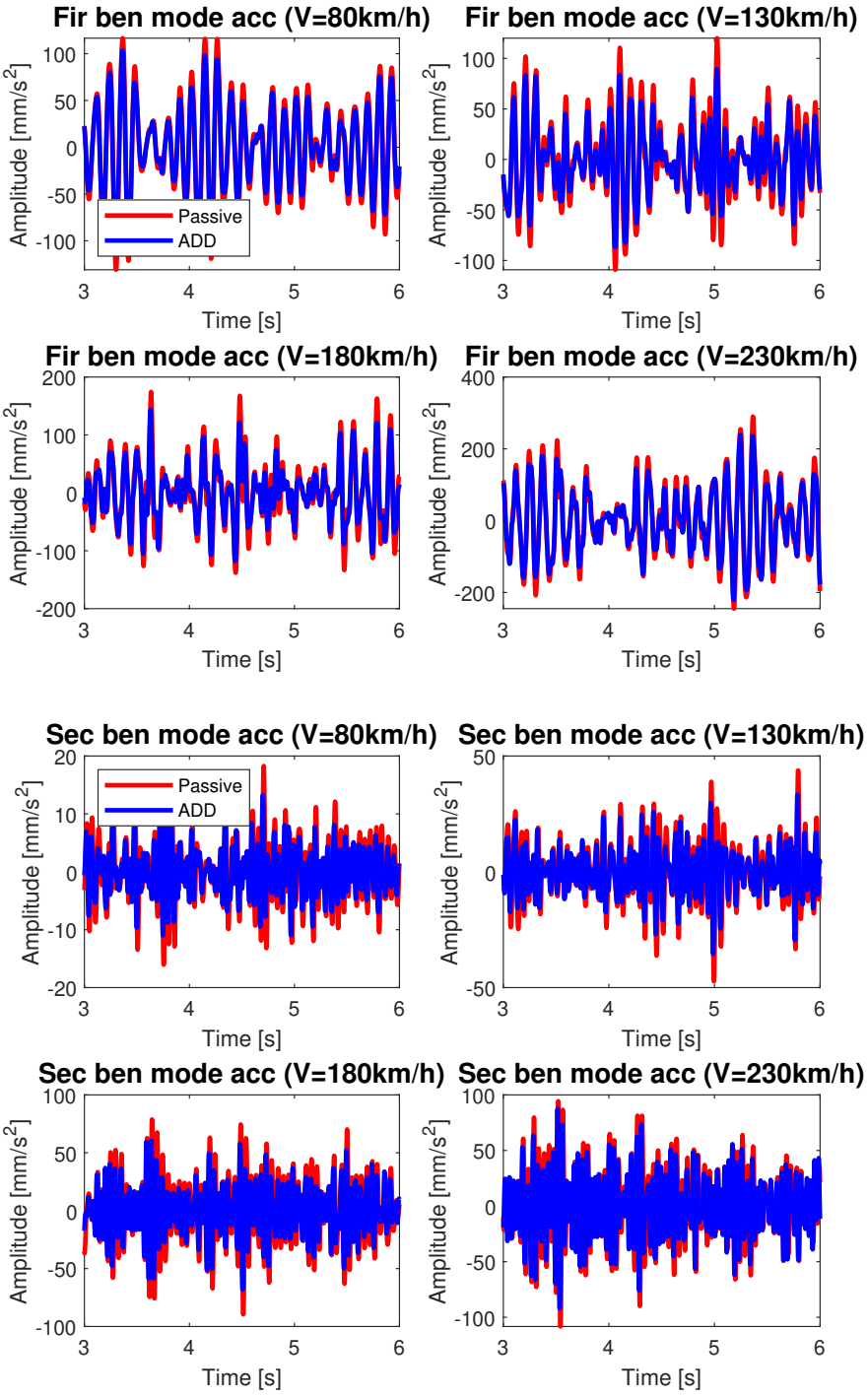

Figure 5.14: *Power spectra density* of the accelerations of the bending modes for the second configuration with *ADD* strategy

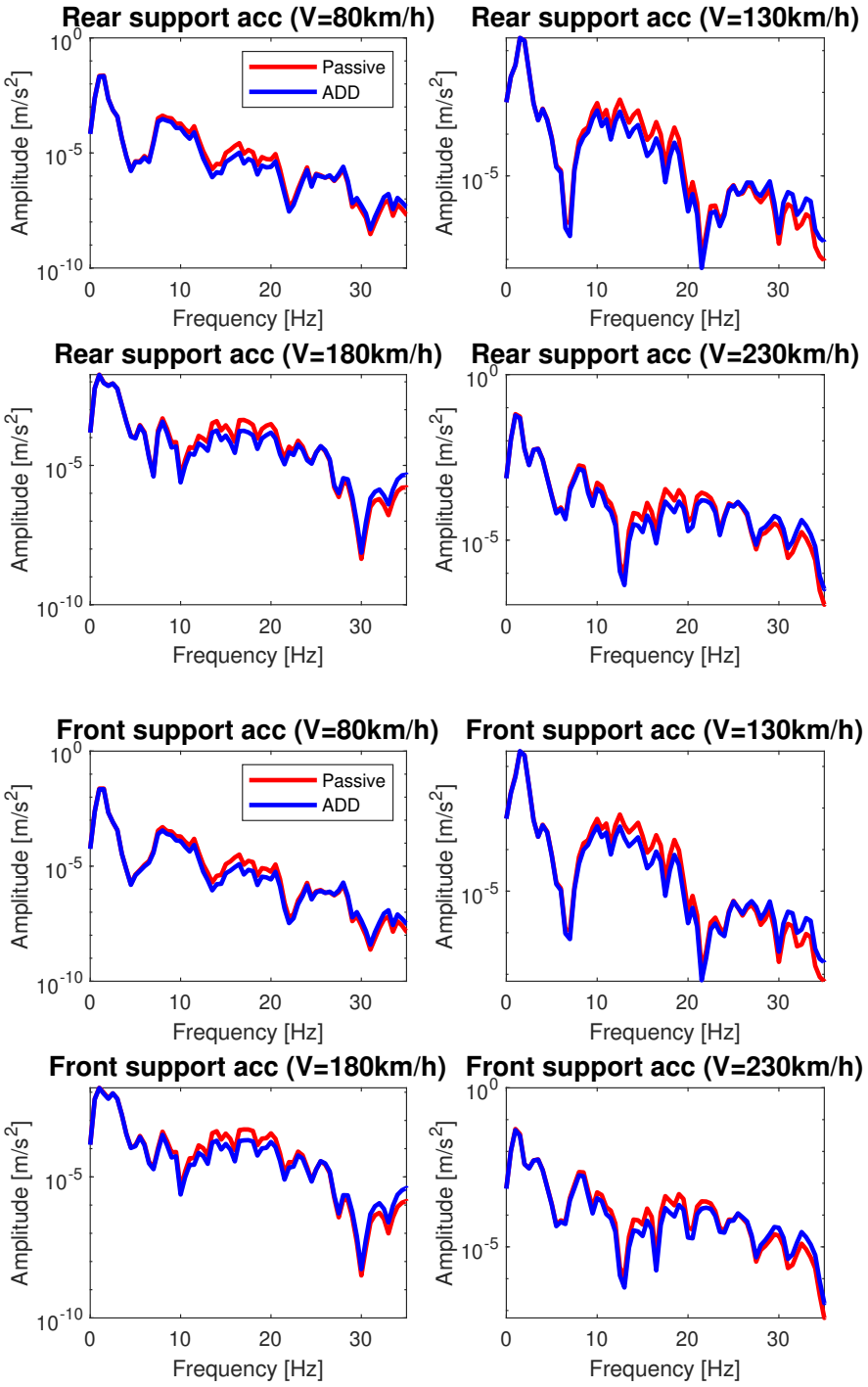

Figure 5.15: *Power spectra density* of the accelerations of the support points of the car-body for the second configuration with *ADD* strategy

At this point, in order to carry out a final evaluation, it is possible to move to the observation to the *root mean square* values. The figure 5.16 allows to consider that:

- both the first and the second bending mode experience a good improvement, consistently to the relative position of the natural frequencies associated to their mode respect to f_{zB};
- as it happens for all of the other simulation, the overall effect is slighter as long as the natural frequencies associated to the carbody rigid modes stand in the *quasi static* region and are almost completely unaffected by the controller.

To quantify the effectiveness of this control law, it is possible to refer to the tables at the end of the section. In conclusion:

- thanks to the positive effect spread over the whole spectrum, the *ADD* logic ensures a surely positive reduction of the carbody rigid modes vibrations $[0.7\,\% \div 4.0\,\%]$ respect to the *SkyHook* one whose effect is not always positive $[-0.6\,\% \div 4.8\,\%]$ in the evaluated range of service velocities;
- for what concerns the bending modes, there is no a large difference between the *ADD* $[11.7\,\% \div 25.6\,\%]$ and the *SkyHook* logic $[13.1\,\% \div 25.3\,\%]$ vibration reduction;
- the overall effect as well shows negligible differences, with the *ADD* providing a reduction in between $[2.3\% \div 5.0\%]$ while the *SkyHook* strategy about $[0.8\% \div 5.4\%]$.

Anyway the results of this last simulation shows that the improvement ensured by the *ADD* control logic implementation varies in a narrower range, thus is more uniform over the evaluated range if service speed and thus may be preferable.

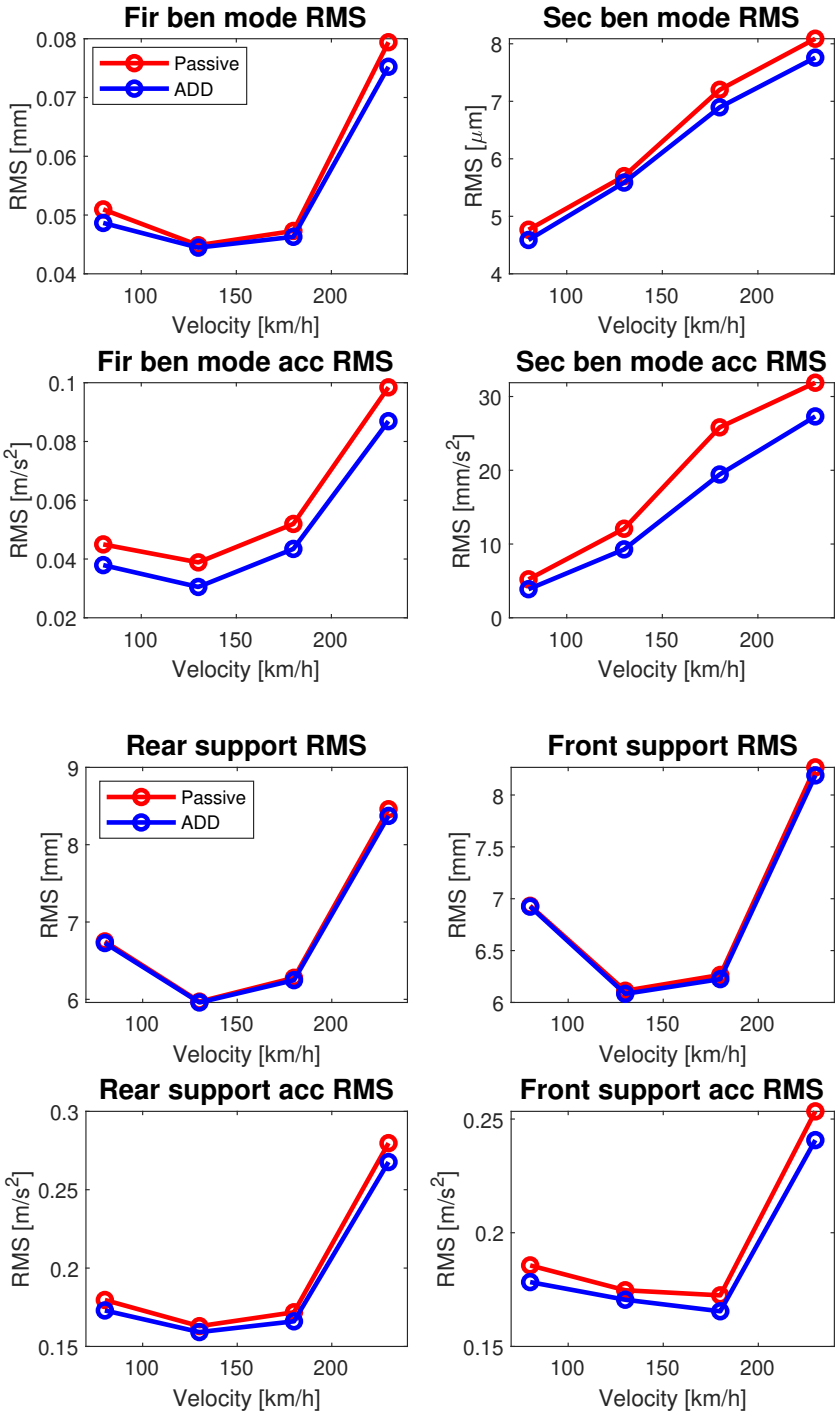

Figure 5.16: *RMS* of the accelerations of the coach support points and bending mode for the second configuration and *ADD* strategy

	z_A	θ_A	G_1	G_2	R	F	
Passive	6.826	0.513	0.051	$4.8e-3$	6.749	6.932	
ADD	6.810	0.516	0.049	$4.6e-3$	6.728	6.924	displacements $[mm]$
Variation [%]	0.230	−0.508	4.522	3.740	0.306	0.117	
Passive	0.182	0.012	0.045	$5.2e-3$	0.180	0.186	
ADD	0.175	0.012	0.038	$3.9e-3$	0.173	0.178	accelerations $[m/s^2]$
Variation [%]	3.437	0.715	15.680	25.652	3.712	3.956	

Table 5.21: *RMS* of second configuration simulation at $V = 80 km/h$ with *ADD* controller

	z_A	θ_A	G_1	G_2	R	F	
Passive	5.997	0.656	0.050	$5.7e-3$	5.970	6.113	
ADD	5.978	0.649	0.045	$5.6e-3$	5.960	6.083	displacements $[mm]$
Variation [%]	0.325	1.010	0.903	1.959	0.181	0.483	
Passive	0.163	0.028	0.039	0.012	0.163	0.175	
ADD	0.162	0.028	0.031	$9.3e-3$	0.159	0.171	accelerations $[m/s^2]$
Variation [%]	0.883	1.542	21.525	23.203	2.318	2.380	

Table 5.22: *RMS* of second configuration simulation at $V = 130\, km/h$ with *ADD* controller

	z_A	θ_A	G_1	G_2	R	F	
Passive	6.217	0.738	0.047	$7.2e-3$	6.278	6.265	
ADD	6.183	0.724	0.046	$6.9e-3$	6.248	6.225	displacements $[mm]$
Variation [%]	0.537	1.897	2.105	4.231	0.482	0.642	
Passive	0.161	0.047	0.052	0.026	0.172	0.173	
ADD	0.158	0.046	0.043	0.019	0.166	0.166	accelerations $[m/s^2]$
Variation [%]	1.870	3.063	16.380	24.754	3.362	4.060	

Table 5.23: *RMS* of second configuration simulation at $V = 180\, km/h$ with *ADD* controller

	z_A	θ_A	G_1	G_2	R	F	
Passive	8.334	0.779	0.079	$8.1e-3$	8.459	8.266	
ADD	8.252	0.767	0.075	$7.8e-3$	8.373	8.189	displacements $[mm]$
Variation	0.983	1.579	5.254	4.062	1.020	0.933	
Passive	0.257	0.053	0.098	0.032	0.280	0.253	
ADD	0.247	0.052	0.087	0.027	0.268	0.241	accelerations $[m/s^2]$
Variation [%]	4.022	2.320	11.705	14.336	4.312	4.994	

Table 5.24: *RMS* of second configuration simulation at $V = 230\, km/h$ with *ADD* controller

Conclusions

The common strategies employed in railway vehicle for the reduction of the vibrations of the carbody and the improvement of the passenger comfort are generally based on secondary suspension control strategies.

The purpose of this work has been the evaluation of an alternative to the more common layout, which would hopefully be easier to implement and lead to larger design flexibility.

The results obtained have proved that a semi active primary suspension control may be effective and represents an appealing solution to be investigated in the future.

The main strengths of this layout can be identified in:

- the simplicity of the installation, since it is sufficient to substitute the primary suspension damper with a semi active element and there is no requirement of special additional devices, like monitoring equipment or power supply;
- the possibility to use classical and smart control strategies;
- the involvement of semi active elements only, whose power consumption is negligible and that are light, robust, space-saving and can not cause instability;
- the possibility to leave free space around the secondary suspension for adding further devices or leaving larger design flexibility.

As described in chapter 3 and 4, this work has left a robust and realistic mathematical model for the analysis of the vertical dynamics of the vehicle with several advanced features:

- accurate description of the transverse bending vibration of the carbody;
- consistent and tough coupling of the flexible and rigid modes;
- implementation of an intermediate variable decoupling the required and the applied force;
- implementation of the first order system accounting for the dynamic behaviour of the current ruling the solenoid valve opening, which makes the actuation smoother;
- implementation of the performance curve of the semi active damper, which allows to have a direct control on the force generated by the control system.

From the numerical simulations, an overall vibration reduction up to 20 % has been obtained, despite the aim of this work was not focused on tuning the parameter to achieve the best improvements.

On the other hand, it has been detected a strong dependency between the primary suspension control effectiveness and the dynamic properties of the passive system. The reason for this behaviour has been identified in the layout of the control system: as long as it is controlling the primary suspension, ruling the bogie frame response, the way the excitement in transmitted from the bogie frame to the carbody plays a central role.

In particular this control layout excels in damping the bogie frame resonant response. As a consequence, the carbody vibration reduction is enhanced in the frequency range about the frequency of the mode shape associated to the bogie frame bounce. For this reason, it is possible to state that the control effectiveness itself can be fully exploited only provided that:

- it is applied on a passive system whose mode shapes natural frequencies are quite close one another: under this assumption all the system's resonances benefit of the isolating effect provided by the semi active suspension and the overall response is surely positive.
- the natural frequency of the mode shape associated to the bogie frame is at high frequencies, leading to a wider effective frequency range of the controller.

Consistently with these observations, the larger amplitude reduction, with values up to 40 %, has been observed on the first carbody bending mode, whose natural frequency is about the typical range in which it is possible to find the natural frequency of the mode shape associated to the bogie bounce.

The drawback of semi active control is related to the reduced effectiveness to control the modes whose natural frequencies are largely above the natural frequency of the mode shape associated to the bogie bounce. Anyway, this issue is not detrimental for the overall response as long as the contribution of those component is negligible in regard to ride comfort of passengers.

This work has furthermore lead to a a direct and detailed comparison of the *SkyHook* and *ADD - Acceleration Driven Damper* control strategies. As result, it is possible to summarize the following features:

- the *SkyHook* strategy ensures a significant improvement but focused on a narrow frequency range. For this reason, it is more suitable for those systems whose natural frequencies are very close one another;
- the *ADD* strategy ensures a slight improvement over a wide frequency range. For this reason it is more suitable for those system whose natural frequencies are spread along the spectrum.

Appendix

7.1 Slender beam bending vibration

7.1.1 Euler Bernoulli theory: Eq. 3.1.1

The *Euler Bernoulli theory* is valid under the assumptions of: small displacements; slender beam, with the length grater than the cross section; homogeneos, isotropic and linear elastic material; cross section constant in shape and size.

The partial differential equation roling the beam transverse vibration is obtained by copuling the *deflection line equation* and the *bending vibration equation.*

The *deflection line equation* relates the beam neutral axis transverse displacement w to the bendind moment M applied at the beam ends:

$$\frac{\partial^2 w}{\partial x^2} = \frac{M}{EJ}$$

The *bending vibration equation* results from a force equilibrium in the vertical direction that involves the shear forces generated by the bending moment and the inertia forces:

$$\frac{\partial T}{\partial x} = -\lambda \frac{\partial^2 w}{\partial t^2}$$

Adding the relationship $T = \frac{\partial M}{\partial x}$, it's possible to get the final equation 3.1.1:

$$\begin{cases} \frac{\partial^2 w}{\partial x^2} = \frac{M}{EJ} \\ \frac{\partial^2 M}{\partial x^2} = -\lambda \frac{\partial^2 w}{\partial t^2} \end{cases} \implies EJ\, \frac{\partial^4 w}{\partial x^4} = -\lambda\, \frac{\partial^2 w}{\partial t^2}$$

7.1.2 Standing wave solution: Eq. 3.1.2

The only way for the derivative respect to time to be equal to the derivative respect the the space, is to impose: that the variables are decopuled, so that the function $w(x,t)$ is the product of a function depending on the only space variable $\Phi(x)$ and a function depending on the only time variable $G(t)$; that the derivatives are equal to a constant γ^4.

$$w(x,t) = \Phi(x)G(t) \implies \begin{cases} \frac{\partial^4 w}{\partial x^4} = \Phi^{IV}(x)G(t) \\ \frac{\partial^2 w}{\partial t^2} = \Phi(x)\ddot{G}(t) \end{cases}$$

So the partial differential equation 3.1.1 can be reorganized as follow:

$$\frac{\Phi^{IV}}{\Phi} = -\frac{\lambda}{EJ}\frac{\ddot{G}}{G} = \gamma^4$$

And decopuled into two homogeneous differential equation:

$$\begin{cases} \ddot{G} + \omega^2 G = 0 \\ \Phi^{IV} - \gamma^2 \Phi = 0 \end{cases} \qquad with\, \omega^2 = \gamma^4 \frac{\lambda}{EJ}$$

At this point it's possible to get the solution of the homogeneous differential equations:

$$\begin{cases} \Phi(x) = A_1 \sin(\gamma x) + B_1 \cos(\gamma x) + C_1 \sinh(\gamma x) + D_1 \cosh(\gamma x) \\ G(t) = G_0 \cos(\omega t + \psi) \end{cases}$$

and to multiply them in order to obtain the standing wave solution 3.1.2:

$$w(x,t) = [A \sin(\gamma x) + B \cos(\gamma x) + C \sinh(\gamma x) + D \cosh(\gamma x)] \cos(\omega t + \psi)$$

7.1.3 Boundary conditions imposition: Eq. 3.1.4 and 3.1.5

As long as the beam has both the ends free, there are no informations about the displacements $w(0,t)$ and $w(L,t)$ or about the rotations $\frac{\partial w}{\partial x}|_{x=0}$ and $\frac{\partial w}{\partial x}|_{x=L}$.

Thus the proper boundary conditions are:

$$\begin{cases} T(0,t) = \frac{\partial M}{\partial x}|_{x=0} = EJ\, \frac{\partial^3 w}{\partial x^3}|_{x=0} = 0 \\ T(L,t) = \frac{\partial M}{\partial x}|_{x=L} = EJ\, \frac{\partial^3 w}{\partial x^3}|_{x=L} = 0 \\ M(0,t) = EJ\, \frac{\partial^2 w}{\partial x^2}|_{x=0} = 0 \\ M(L,t) = EJ\, \frac{\partial^2 w}{\partial x^2}|_{x=L} = 0 \end{cases}$$

That focusing on the space dependent function $\Phi(x)$ lead to the expression:

$$\begin{cases} \Phi^{III}(0) = \gamma^3 EJ\ [-A\cos(0) + B\sin(0) + C\cosh(0) + D\sinh(0)] = 0 \\ \Phi^{III}(L) = \gamma^3 EJ\ [-A\cos(\gamma L) + B\sin(\gamma L) + C\cosh(\gamma L) + D\sinh(\gamma L)] = 0 \\ \Phi^{II}(0) = \gamma^2 EJ\ [-A\sin(0) - B\cos(0) + C\sinh(0) + D\cosh(0)] = 0 \\ \Phi^{II}(L) = \gamma^2 EJ\ [-A\sin(\gamma L) - B\cos(\gamma L) + C\sinh(\gamma L) + D\cosh(\gamma L)] = 0 \end{cases}$$

With $\cosh 0 = \cos 0 = 1$ and $\sinh 0 = \sin 0 = 0$. The resulting matricial expression is:

$$\begin{bmatrix} -1 & 0 & 1 & 0 \\ -\cos(\gamma L) & \sin(\gamma L) & \cosh(\gamma L) & \sinh(\gamma L) \\ 0 & -1 & 0 & 1 \\ -\sin(\gamma L) & -\cos(\gamma L) & \sinh(\gamma L) & \cosh(\gamma L) \end{bmatrix} \begin{Bmatrix} A \\ B \\ C \\ D \end{Bmatrix} = \underline{0}$$

The first row suggests that $-A + C = 0$ and the third that $-B + D = 0$. Thus the system can be reduced as follow:

$$\begin{bmatrix} \cosh(\gamma L) - \cos(\gamma L) & \sinh(\gamma L) + \sin(\gamma L) \\ \sinh(\gamma L) - \sin(\gamma L) & \cosh(\gamma L) - \cos(\gamma L) \end{bmatrix} \begin{Bmatrix} AC \\ BD \end{Bmatrix} = \underline{0} \tag{7.1.1}$$

In order to avoid the trivial solution $\{AC;\ BD\} = \underline{0}$, there's the need to impose the determinant $det([H(\gamma)]) = 0$ to be null. This condition lead to the definition of the charateristic equation and of the parameter γ:

$$(\cosh \gamma L - \cos \gamma L)^2 - (\sinh \gamma L + \sin \gamma L)(\sinh \gamma L - \sin \gamma L) = 0$$

$$\cosh^2(\gamma L) - 2\cos(\gamma L)\cosh(\gamma L) + \cos^2(\gamma L) - \sinh^2(\gamma L) + \sin^2(\gamma L)$$

$$[\cosh^2(\gamma L) - \sinh^2(\gamma L)] - 2\cosh(\gamma L)\cos(\gamma L) + [\cos^2(\gamma L) + \sin^2(\gamma L)]$$

Considering that $\sin^2 x + \cos^2 x = 1$ and that $\cosh^2 x - \sinh^2 x = 1$, it's finally possible to get the well known charateristic equation:

$$\cosh(\gamma L)\cos(\gamma L) = 1$$

Once that $det([H(\gamma)]) = 0$ has been imposed, it's no longer possible to find both of the constants $\{AC;\ BD\}$. Anyway it's possible to compute one as function of the other in order to get the normalized mode shapes.

The amplitude becomes an unknown computed with the time funtion $G(t)$ integration.

At this point is possible to collect the constants BD of the system 7.1.1 and obtain:

$$\begin{cases} BD\{K[\cosh \gamma L - \cos \gamma L] + 1[\sinh \gamma L + \sin \gamma L]\} = 0 \\ BD\{K[\sinh \gamma L - \sin \gamma L] + 1[\cosh \gamma L - \cos \gamma L]\} = 0 \end{cases}$$

$$\begin{bmatrix} \cosh(\gamma L) - \cos(\gamma L) & \sinh(\gamma L) + \sin(\gamma L) \\ \sinh(\gamma L) - \sin(\gamma L) & \cosh(\gamma L) - \cos(\gamma L) \end{bmatrix} \begin{Bmatrix} K \\ 1 \end{Bmatrix} = \underline{0}$$

This simplified boudary condition matrix lead to the definition of the constant K:

$$K = -\frac{\sinh \gamma L + \sin \gamma L}{\cosh \gamma L - \cos \gamma L}$$

Remembering that $B = D = 1$ and that $A = C = K$, it's possible to compute:

$$\begin{aligned} \Phi(x) &= A\sin(\gamma x) + B\cos(\gamma x) + C\sinh(\gamma x) + D\cosh(\gamma x) \\ &= K[\sin(\gamma x) + C\sinh(\gamma x)] + [\cos(\gamma x) + D\cosh(\gamma x)] \end{aligned}$$

7.2 Passive configuration equation of motion 3.3.5

Once the data set has been introduced and knowing that the first two bending mode are included in the model description, it's possible to compute the equation of motion generalized in equation 3.3.5.

7.2.1 Mass matrix: Eq. 3.3.4

The mass matrix results from the sum of two contributes: $[M_d]$ accounting for the free discrete *dofs* $\underline{x}_F$; $[M_m]$ for the inertia provided by the coach transverse deformation.

$$[M_d] = \begin{bmatrix}
0 & & & & & & & & & & & \\
0 & 0 & & & & & & & & & & \\
0 & 0 & 0 & & & & & & & & & \\
0 & 0 & 0 & 0 & & & & & & & & \\
0 & 0 & 0 & 0 & m_B & & & & & & & \\
0 & 0 & 0 & 0 & 0 & J_B & & & & & & \\
0 & 0 & 0 & 0 & 0 & 0 & m_B & & & & & \\
0 & 0 & 0 & 0 & 0 & 0 & 0 & J_B & & & & \\
0 & 0 & 0 & 0 & 0 & 0 & 0 & 0 & m_A & & & \\
0 & 0 & 0 & 0 & 0 & 0 & 0 & 0 & 0 & J_A & & \\
0 & 0 & 0 & 0 & 0 & 0 & 0 & 0 & 0 & 0 & 0 & \\
0 & 0 & 0 & 0 & 0 & 0 & 0 & 0 & 0 & 0 & 0 & 0
\end{bmatrix}$$

$$[M_m] = \begin{bmatrix}
0 & & & & & & & & & & & \\
0 & 0 & & & & & & & & & & \\
0 & 0 & 0 & & & & & & & & & \\
0 & 0 & 0 & 0 & & & & & & & & \\
0 & 0 & 0 & 0 & 0 & & & & & & & \\
0 & 0 & 0 & 0 & 0 & 0 & & & & & & \\
0 & 0 & 0 & 0 & 0 & 0 & 0 & & & & & \\
0 & 0 & 0 & 0 & 0 & 0 & 0 & 0 & & & & \\
0 & 0 & 0 & 0 & 0 & 0 & 0 & 0 & 0 & & & \\
0 & 0 & 0 & 0 & 0 & 0 & 0 & 0 & 0 & 0 & & \\
0 & 0 & 0 & 0 & 0 & 0 & 0 & 0 & 0 & 0 & m_{M1} & \\
0 & 0 & 0 & 0 & 0 & 0 & 0 & 0 & 0 & 0 & 0 & m_{M2}
\end{bmatrix}$$

With $m_M1 = \lambda \int_0^L \Phi_1(x)\, \Phi_1(x)\, dx$ and $m_M2 = \lambda \int_0^L \Phi_2(x)\, \Phi_2(x)\, dx$ from equation 3.1.6 computed numerically with the *trapeziodal method*, given $\Phi_i(x)$ in equation 3.1.4.

Here the resulting mass matrix, already partitioned:

$$[M] = \left[\begin{array}{cccc|cccccccc}
0 & 0 & 0 & 0 & 0 & 0 & 0 & 0 & 0 & 0 & 0 & 0 \\
0 & 0 & 0 & 0 & 0 & 0 & 0 & 0 & 0 & 0 & 0 & 0 \\
0 & 0 & 0 & 0 & 0 & 0 & 0 & 0 & 0 & 0 & 0 & 0 \\
0 & 0 & 0 & 0 & 0 & 0 & 0 & 0 & 0 & 0 & 0 & 0 \\
\hline
0 & 0 & 0 & 0 & m_B & 0 & 0 & 0 & 0 & 0 & 0 & 0 \\
0 & 0 & 0 & 0 & 0 & J_B & 0 & 0 & 0 & 0 & 0 & 0 \\
0 & 0 & 0 & 0 & 0 & 0 & m_B & 0 & 0 & 0 & 0 & 0 \\
0 & 0 & 0 & 0 & 0 & 0 & 0 & J_B & 0 & 0 & 0 & 0 \\
0 & 0 & 0 & 0 & 0 & 0 & 0 & 0 & m_A & 0 & 0 & 0 \\
0 & 0 & 0 & 0 & 0 & 0 & 0 & 0 & 0 & J_A & 0 & 0 \\
0 & 0 & 0 & 0 & 0 & 0 & 0 & 0 & 0 & 0 & m_{M1} & 0 \\
0 & 0 & 0 & 0 & 0 & 0 & 0 & 0 & 0 & 0 & 0 & m_{M2}
\end{array}\right]$$

7.2.2 Stiffness matrix: Eq. 3.3.2

The stiffness matrix results from the sum of three contributes: $[K_I]$ accounting for the primary suspension; $[K_{II}]$ accounting for the secondary suspension; $[K_m]$ accounting for the coach bending rigidity.

The primary suspension contribute is computed with the relationship of equation 3.2.3:

$$[K_I] = [\Lambda_{\Delta L_I}]^T\, [k_I]\, [\Lambda_{\Delta L_I}]$$

The matrix $[k_I] = diag\{k_I; k_I; k_I; k_I\}$ collects on its main diagonal the stiffness k_I. The *jacobian* matrix $[\Lambda_{\Delta L_I}]$ defines the suspension elongation:

$[\Lambda_{\Delta L_I}]$	z_{C11}	z_{C12}	z_{C21}	z_{C22}	z_{B1}	θ_{B1}	z_{B2}	θ_{B2}	z_A	θ_A	G_1	G_2
ΔL_{I11}	-1				1	-b						
ΔL_{I12}		-1			1	b						
ΔL_{I21}			-1				1	-b				
ΔL_{I22}				-1			1	b				

At the end the resulting matrix will be:

$$[K_I] = \begin{bmatrix}
k_I & & & & & & & & & & & \\
0 & k_I & & & & & & & & & & \\
0 & 0 & k_I & & & & & & & & & \\
0 & 0 & 0 & k_I & & & & & & & & \\
-k_I & -k_I & 0 & 0 & 2k_I & & & & & & & \\
bk_I & -bk_I & 0 & 0 & 0 & 2b^2k_I & & & & & & \\
0 & 0 & -k_I & -k_I & 0 & 0 & 2k_I & & & & & \\
0 & 0 & bk_I & -bk_I & 0 & 0 & 0 & 2b^2k_I & & & & \\
0 & 0 & 0 & 0 & 0 & 0 & 0 & 0 & 0 & & & \\
0 & 0 & 0 & 0 & 0 & 0 & 0 & 0 & 0 & 0 & & \\
0 & 0 & 0 & 0 & 0 & 0 & 0 & 0 & 0 & 0 & 0 & \\
0 & 0 & 0 & 0 & 0 & 0 & 0 & 0 & 0 & 0 & 0 & 0
\end{bmatrix}$$

The secondary suspension contribute is given by the relationship of equation 3.2.6:

$$[K_{II}] = [\Lambda_{\Delta L_{II}}]^T [k_{II}] [\Lambda_{\Delta L_{II}}]$$

The matrix $[k_{II}] = diag\{k_{II}; k_{II}\}$ collects on its main diagonal the stiffness k_{II}. The *jacobian* matrix $[\Lambda_{\Delta L_{II}}]$ defines the suspension elongation:

$[\Lambda_{\Delta L_{II}}]$	z_{C11}	z_{C12}	z_{C21}	z_{C22}	z_{B1}	θ_{B1}	z_{B2}	θ_{B2}	z_A	θ_A	G_1	G_2
ΔL_{II1}					-1				1	-a	Φ_{1F}	Φ_{2F}
ΔL_{II2}							-1		1	a	Φ_{1R}	Φ_{2R}

At the end the resulting matrix will be:

$$[K_{II}] = \begin{bmatrix}
0 & & & & & & & & & & & & \\
0 & 0 & & & & & & & & & & & \\
0 & 0 & 0 & & & & & & & & & & \\
0 & 0 & 0 & 0 & & & & & & & & & \\
0 & 0 & 0 & 0 & k_{II} & & & & & & & & \\
0 & 0 & 0 & 0 & 0 & 0 & & & & & & & \\
0 & 0 & 0 & 0 & 0 & 0 & k_{II} & & & & & & \\
0 & 0 & 0 & 0 & 0 & 0 & 0 & 0 & & & & & \\
0 & 0 & 0 & 0 & -k_{II} & 0 & -k_{II} & 0 & 2k_{II} & & & & \\
0 & 0 & 0 & 0 & ak_{II} & 0 & -ak_{II} & 0 & 0 & 2a^2k_{II} & & & \\
0 & 0 & 0 & 0 & -\Phi_{1F}k_{II} & 0 & -\Phi_{1R}k_{II} & 0 & k_{II}(\Phi_{1F}+\Phi_{1R}) & k_{II}a(\Phi_{1R}-\Phi_{1F}) & k_{II}(\Phi_{1F}^2+\Phi_{1R}^2) & & \\
0 & 0 & 0 & 0 & -\Phi_{2F}k_{II} & 0 & -\Phi_{2R}k_{II} & 0 & k_{II}(\Phi_{2F}+\Phi_{2R}) & k_{II}a(\Phi_{2R}-\Phi_{2F}) & k_{II}(\Phi_{1F}\Phi_{2F}+\Phi_{1R}\Phi_{2R}) & k_{II}(\Phi_{2F}^2+\Phi_{2R}^2) &
\end{bmatrix}$$

From a theoretical point of view, $\Phi_{iF} = \Phi_{iR} = \Phi_i$ is expected as long as the secondary suspension connection point and the beam boundary condition are symmetric. Anyway from a numerical point of view, they're not exactly the same and they are kept distinguished as provided in the data set.

The matrix $[K_m]$ is referred to the only bending mode; thus the only non null elements $k_{M1} = m_{M1}\omega_1^2$ and $k_{M2} = m_{M2}\omega_2^2$ are in the last two positions of the main diagonal:

$$[K_m] = \begin{bmatrix} 0 & & & & & & & & & & & \\ 0 & 0 & & & & & & & & & & \\ 0 & 0 & 0 & & & & & & & & & \\ 0 & 0 & 0 & 0 & & & & & & & & \\ 0 & 0 & 0 & 0 & 0 & & & & & & & \\ 0 & 0 & 0 & 0 & 0 & 0 & & & & & & \\ 0 & 0 & 0 & 0 & 0 & 0 & 0 & & & & & \\ 0 & 0 & 0 & 0 & 0 & 0 & 0 & 0 & & & & \\ 0 & 0 & 0 & 0 & 0 & 0 & 0 & 0 & 0 & & & \\ 0 & 0 & 0 & 0 & 0 & 0 & 0 & 0 & 0 & 0 & & \\ 0 & 0 & 0 & 0 & 0 & 0 & 0 & 0 & 0 & 0 & k_{M1} & \\ 0 & 0 & 0 & 0 & 0 & 0 & 0 & 0 & 0 & 0 & 0 & k_{M2} \end{bmatrix}$$

By combining the three contributes is finally possible to compute the overall system stiffness matrix, to be partitioned as follow:

$$[K] = \left[\begin{array}{cccc|cccc|cccc} k_I & 0 & 0 & 0 & -k_I & bk_I & 0 & 0 & 0 & 0 & 0 & 0 \\ 0 & k_I & 0 & 0 & -k_I & -bk_I & 0 & 0 & 0 & 0 & 0 & 0 \\ 0 & 0 & k_I & 0 & 0 & 0 & -k_I & bk_I & 0 & 0 & 0 & 0 \\ 0 & 0 & 0 & k_I & 0 & 0 & -k_I & -bk_I & 0 & 0 & 0 & 0 \\ \hline -k_I & -k_I & 0 & 0 & k_{II}+2k_I & 0 & 0 & 0 & -k_{II} & ak_{II} & -\Phi_{1F}k_{II} & -\Phi_{2F}k_{II} \\ bk_I & -bk_I & 0 & 0 & 0 & 2b^2k_I & 0 & 0 & 0 & 0 & 0 & 0 \\ 0 & 0 & -k_I & -k_I & 0 & 0 & k_{II}+2k_I & 0 & -k_{II} & -ak_{II} & -\Phi_{1R}k_{II} & -\Phi_{2R}k_{II} \\ 0 & 0 & bk_I & -bk_I & 0 & 0 & 0 & 2b^2k_I & 0 & 0 & 0 & 0 \\ 0 & 0 & 0 & 0 & -k_{II} & 0 & -k_{II} & 0 & 2k_{II} & 0 & k_{II}(\Phi_{1F}+\Phi_{1R}) & k_{II}(\Phi_{2F}+\Phi_{2R}) \\ 0 & 0 & 0 & 0 & ak_{II} & 0 & -ak_{II} & 0 & 0 & 2a^2k_{II} & k_{II}a(\Phi_{1R}-\Phi_{1F}) & k_{II}a(\Phi_{2R}-\Phi_{2F}) \\ 0 & 0 & 0 & 0 & -\Phi_{1F}k_{II} & 0 & -\Phi_{1R}k_{II} & 0 & k_{II}(\Phi_{1F}+\Phi_{1R}) & k_{II}a(\Phi_{1R}-\Phi_{1F}) & k_{II}(\Phi_{1F}^2+\Phi_{1R}^2)+k_{M1} & k_{II}(\Phi_{1F}\Phi_{2F}+\Phi_{1R}\Phi_{2R}) \\ 0 & 0 & 0 & 0 & -\Phi_{2F}k_{II} & 0 & -\Phi_{2R}k_{II} & 0 & k_{II}(\Phi_{2F}+\Phi_{2R}) & k_{II}a(\Phi_{2R}-\Phi_{2F}) & k_{II}(\Phi_{1F}\Phi_{2F}+\Phi_{1R}\Phi_{2R}) & k_{II}(\Phi_{2F}^2+\Phi_{2R}^2)+k_{M2} \end{array}\right]$$

7.2.3 Damping matrix: Eq. 3.3.3

In the passive configuration, the dampers are installed in parallel to the spring.

For this reason the *jacobian* of the elongation velocity $[\Lambda_{\Delta L_I}]$ and $[\Lambda_{\Delta L_{II}}]$ are the same of used for the stiffness matrix computation. Consequently, the three contributes $[R_I]$, $[R_{II}]$ and $[R_m]$ have the same structure of the stiffness ones, but $(c_I\ c_{II})$ replace $(k_I;\ k_{II})$.

Given $c_{M1} = \xi_1\ 2\, m_{M1}\, \omega_1^2$ and $c_{M2} = \xi_2\ 2\, m_{M2}\, \omega_2^2$, the final expression will be:

$$[R] = \left[\begin{array}{cccc|cccc|cccc} c_I & 0 & 0 & 0 & -c_I & bc_I & 0 & 0 & 0 & 0 & 0 & 0 \\ 0 & c_I & 0 & 0 & -c_I & -bc_I & 0 & 0 & 0 & 0 & 0 & 0 \\ 0 & 0 & c_I & 0 & 0 & 0 & -c_I & bc_I & 0 & 0 & 0 & 0 \\ 0 & 0 & 0 & c_I & 0 & 0 & -c_I & -bc_I & 0 & 0 & 0 & 0 \\ \hline -c_I & -c_I & 0 & 0 & c_{II}+2c_I & 0 & 0 & 0 & -c_{II} & ac_{II} & -\Phi_{1F}c_{II} & -\Phi_{2F}c_{II} \\ bc_I & -bc_I & 0 & 0 & 0 & 2b^2c_I & 0 & 0 & 0 & 0 & 0 & 0 \\ 0 & 0 & -c_I & -c_I & 0 & 0 & c_{II}+2c_I & 0 & -c_{II} & -ac_{II} & -\Phi_{1R}c_{II} & -\Phi_{2R}c_{II} \\ 0 & 0 & bc_I & -bc_I & 0 & 0 & 0 & 2b^2c_I & 0 & 0 & 0 & 0 \\ 0 & 0 & 0 & 0 & -c_{II} & 0 & -c_{II} & 0 & 2c_{II} & 0 & c_{II}(\Phi_{1F}+\Phi_{1R}) & c_{II}(\Phi_{2F}+\Phi_{2R}) \\ 0 & 0 & 0 & 0 & ac_{II} & 0 & -ac_{II} & 0 & 0 & 2a^2c_{II} & c_{II}a(\Phi_{1R}-\Phi_{1F}) & c_{II}a(\Phi_{2R}-\Phi_{2F}) \\ 0 & 0 & 0 & 0 & -\Phi_{1F}c_{II} & 0 & -\Phi_{1R}c_{II} & 0 & c_{II}(\Phi_{1F}+\Phi_{1R}) & c_{II}a(\Phi_{1R}-\Phi_{1F}) & c_{II}(\Phi_{1F}^2+\Phi_{1R}^2)+c_{M1} & c_{II}(\Phi_{1F}\Phi_{2F}+\Phi_{1R}\Phi_{2R}) \\ 0 & 0 & 0 & 0 & -\Phi_{2F}c_{II} & 0 & -\Phi_{2R}c_{II} & 0 & c_{II}(\Phi_{2F}+\Phi_{2R}) & c_{II}a(\Phi_{2R}-\Phi_{2F}) & c_{II}(\Phi_{1F}\Phi_{2F}+\Phi_{1R}\Phi_{2R}) & c_{II}(\Phi_{2F}^2+\Phi_{2R}^2)+c_{M2} \end{array}\right]$$

7.3 Controlled configuration equation of motion 3.3.16

By comparing the passive and the controlled system, it's possible to notice that the mass $[M]$ and the stiffness $[K]$ matrices are the very same of the one already discussed; on the contrary the damping matrix $[R] = [R_{II}] + [R_m]$ loses the primary suspension contribute $[R_I]$. The resulting damping matrix is:

$$[R] = \left[\begin{array}{cccc|cccc|cccc}
0 & 0 & 0 & 0 & 0 & 0 & 0 & 0 & 0 & 0 & 0 & 0 \\
0 & 0 & 0 & 0 & 0 & 0 & 0 & 0 & 0 & 0 & 0 & 0 \\
0 & 0 & 0 & 0 & 0 & 0 & 0 & 0 & 0 & 0 & 0 & 0 \\
0 & 0 & 0 & 0 & 0 & 0 & 0 & 0 & 0 & 0 & 0 & 0 \\
\hline
0 & 0 & 0 & 0 & c_{II} & 0 & 0 & 0 & -c_{II} & ac_{II} & -\Phi_{1F}c_{II} & -\Phi_{2F}c_{II} \\
0 & 0 & 0 & 0 & 0 & 0 & 0 & 0 & 0 & 0 & 0 & 0 \\
0 & 0 & 0 & 0 & 0 & 0 & c_{II} & 0 & -c_{II} & -ac_{II} & -\Phi_{1R}c_{II} & -\Phi_{2R}c_{II} \\
0 & 0 & 0 & 0 & 0 & 0 & 0 & 0 & 0 & 0 & 0 & 0 \\
0 & 0 & 0 & 0 & -c_{II} & 0 & -c_{II} & 0 & 2c_{II} & 0 & c_{II}(\Phi_{1F}+\Phi_{1R}) & c_{II}(\Phi_{2F}+\Phi_{2R}) \\
0 & 0 & 0 & 0 & ac_{II} & 0 & -ac_{II} & 0 & 0 & 2a^2c_{II} & c_{II}a(\Phi_{1R}-\Phi_{1F}) & c_{II}a(\Phi_{2R}-\Phi_{2F}) \\
0 & 0 & 0 & 0 & -\Phi_{1F}c_{II} & 0 & -\Phi_{1R}c_{II} & 0 & c_{II}(\Phi_{1F}+\Phi_{1R}) & c_{II}a(\Phi_{1R}-\Phi_{1F}) & c_{II}(\Phi_{1F}^2+\Phi_{1R}^2)+c_{M1} & c_{II}(\Phi_{1F}\Phi_{2F}+\Phi_{1R}\Phi_{2R}) \\
0 & 0 & 0 & 0 & -\Phi_{2F}c_{II} & 0 & -\Phi_{2R}c_{II} & 0 & c_{II}(\Phi_{2F}+\Phi_{2R}) & c_{II}a(\Phi_{2R}-\Phi_{2F}) & c_{II}(\Phi_{1F}\Phi_{2F}+\Phi_{1R}\Phi_{2R}) & c_{II}(\Phi_{2F}^2+\Phi_{2R}^2)+c_{M2}
\end{array}\right]$$

7.3.1 Lagrangian of primary suspension: Eq. 3.3.15

The *lagrangian* $\underline{Q}_I = \delta L/\delta \underline{q}$ has the role to spread the virtual work $\delta L = \overrightarrow{F} \times \overrightarrow{\delta s}$ over the independent variables. In matrix notion, it can be expressed as:

$$\delta L = \underline{u}_f^T \, \underline{\delta s}_I$$

The forces $(f_{I_{ij\,U}};\ f_{I_{ij\,L}})$ are collected in the vector $\underline{u}_f$; but since $f_{I_{ij\,U}} = -f_{I_{ij\,L}}$ it's possible for sake of simplicity to use the vector $\underline{u}_F$ generated by the controller, defined as:

$$\underline{u}_f = \begin{Bmatrix} f_{I_{11\,U}} \\ f_{I_{11\,L}} \\ f_{I_{12\,U}} \\ f_{I_{12\,L}} \\ f_{I_{12\,U}} \\ f_{I_{12\,L}} \\ f_{I_{21\,U}} \\ f_{I_{21\,L}} \\ f_{I_{22\,U}} \\ f_{I_{22\,L}} \end{Bmatrix} = \begin{bmatrix} 1 & 0 & 0 & 0 \\ -1 & 0 & 0 & 0 \\ 0 & 1 & 0 & 0 \\ 0 & -1 & 0 & 0 \\ 0 & 0 & 1 & 0 \\ 0 & 0 & -1 & 0 \\ 0 & 0 & 0 & 1 \\ 0 & 0 & 0 & -1 \end{bmatrix} \begin{Bmatrix} f_{I_{11}} \\ f_{I_{12}} \\ f_{I_{21}} \\ f_{I_{22}} \end{Bmatrix} = [\Lambda_{u_f F}]\, \underline{u}_F$$

The virtual displacement $\underline{\delta s}_I$ defines the forces application point displacement and can be define by means of the superimposition principle:

$$\delta s_{I_{ij\,L}} = \delta z_{Cij} \qquad\qquad \delta s_{I_{ij\,U}} = \delta z_{Bi} \pm b\delta\theta_{Bi}$$

Since $\delta s_{I_{ij}}$ is a function of the independent variables, it can be expressed in matrix notion $\underline{\delta s}_I = [\Lambda_{\Delta s_I}]\, \underline{\delta x}$ given the *jacobian* matrix $[\Lambda_{\delta s_I}]$:

$[\Lambda_{\delta s_I}]$	δz_{C11}	δz_{C12}	δz_{C21}	δz_{C22}	δz_{B1}	$\delta\theta_{B1}$	δz_{B2}	$\delta\theta_{B2}$	δz_A	$\delta\theta_A$	δG_1	δG_2
$\delta s_{I_{11\,U}}$					1	-b						
$\delta s_{I_{11\,L}}$	1											
$\delta s_{I_{12\,U}}$					1	b						
$\delta s_{I_{12\,L}}$		1										
$\delta s_{I_{21\,U}}$							1	-b				
$\delta s_{I_{21\,L}}$			1									
$\delta s_{I_{22\,U}}$							1	b				
$\delta s_{I_{22\,L}}$				1								

Thus recalling the virtual work definition, it's possible to state that:

$$\underline{Q}_I = \frac{\delta L}{\underline{\delta q}} = \frac{\underline{u}_f^T \underline{\delta s}_I}{\underline{\delta q}} \qquad \Longrightarrow \qquad \underline{Q}_I = \underline{u}_F^T \left[\Lambda_{u_{fF}}\right]^T \left[\Lambda_{\delta s_I}\right]$$

The resulting $\underline{Q}_I$ is a row vector; by transposing it is possible to get:

$$\underline{Q}_I = \left[\Lambda_{\delta s_I}\right]^T \left[\Lambda_{u_{fF}}\right] \underline{u}_F = \left[Q_I\right] \underline{u}_F$$

$$\left[Q_I\right] = \left|\begin{array}{cccc} -1 & 0 & 0 & 0 \\ 0 & -1 & 0 & 0 \\ 0 & 0 & -1 & 0 \\ 0 & 0 & 0 & -1 \\ \hline 1 & 1 & 0 & 0 \\ -b & b & 0 & 0 \\ 0 & 0 & 1 & 1 \\ 0 & 0 & -b & b \\ 0 & 0 & 0 & 0 \\ 0 & 0 & 0 & 0 \\ 0 & 0 & 0 & 0 \\ 0 & 0 & 0 & 0 \end{array}\right|$$

7.4 TF of *Nishimura* model: equation 3.4.5

The transfer function of the *Nishimura* secondary suspension model provide an idea about how the forces are transmitted depending on the excitation frequency.

In order to describe the state of this system, two independent variable (ΔL_{II}; y) are needed. The force generated can be computed as follow from the elongations definition:

$$\begin{aligned} F &= -k_{II}\Delta L_{II} - k_{II_U}\left(\Delta L_{II} - y\right) \\ &= -k_{II}\Delta L_{II} - k_{II_L}\, y - c_{II}\,\dot{y} \end{aligned}$$

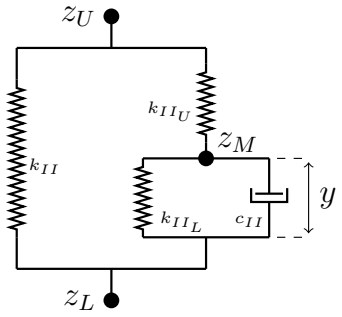

The first step for the transfer function computation is to move the force definition equation from the time to the frequency domain: this is possible by assuming an harmonic excitement $\Delta L_{II} = \Delta L_{I_0}\, e^{j\,\Omega t}$.

$$\begin{aligned} F_0 &= -(k_{II} + k_{II_U})\Delta L_{II_0} + k_{II_U} y_0 \\ &= -k_{II}\Delta L_{II_0} - (j\,\Omega c_{II} + k_{II_L}) y_0 \end{aligned}$$

The independent variable y will be an harmonic response $y_0\, e^{j\,\Omega t}$ as well since the two variables are related by the continuity equation about the node z_M defined in 3.4.4. By performing an equilibrium to the vertical forces acting on z_M is possible to get:

$$-k_{II_U}\left(\Delta L_{II} - y\right) = -k_{II_L}\, y - c_{II}\,\dot{y}$$

That in the frequency domain gives the equation relating (ΔLII; y):

$$y_0 = \frac{k_{II_U}}{(k_{II_L} + k_{II_U}) + j\,\Omega\, c_{II}}\,\Delta L_{II_0}$$

By substituting this relationship in the frequency domain generated force equation, it finally possible to get the transfer function for a given input ΔL_{II}:

$$\begin{aligned} F_0 &= -\left[(k_{II} + k_{II_U}) - \frac{k_{II_U}^2}{(k_{II_L} + k_{II_U}) + j\,\Omega\, c_{II}}\right]\,\Delta L_{II_0} \\ &= -\left[k_{II} + \frac{k_{II_U}(k_{II_L} + j\,\Omega c_{II})}{(k_{II_L} + k_{II_U}) + j\,\Omega c_{II}}\right]\Delta L_{II_0} \end{aligned}$$

The two expression are equivalent and lead to the generic equation:

$$F_0 = -\,\frac{(k_{II} + k_{II_L} + k_{II_U}) + j\,(k_{II} + k_{II_U})\,\Omega\, c_{II}}{(k_{II_L} + k_{II_U}) + j\,\Omega\, c_{II}}\,\Delta L_{II_0}$$

7.5 Passive configuration with air suspension

7.5.1 Mass matrix: Eq. 3.4.10

As long as there's no mass associated to the *Nishimura* air spring model, the mass matrix is the very same of the other configuration.

There are two contributes: one for the discrete *dofs* $[M_d]$, which is a diagonal matrix as long as the independent variables correspond to the bodies centre of mass rotations and displacements; the other for the inertia associated to the transverse vibration $[M_m]$ which has its only element in correspondence of the flexible independent variable:

$$[M_d] = \begin{bmatrix} 0 & & & & & & & & & & & \\ 0 & 0 & & & & & & & & & & \\ 0 & 0 & 0 & & & & & & & & & \\ 0 & 0 & 0 & 0 & & & & & & & & \\ 0 & 0 & 0 & 0 & m_B & & & & & & & \\ 0 & 0 & 0 & 0 & 0 & J_B & & & & & & \\ 0 & 0 & 0 & 0 & 0 & 0 & m_B & & & & & \\ 0 & 0 & 0 & 0 & 0 & 0 & 0 & J_B & & & & \\ 0 & 0 & 0 & 0 & 0 & 0 & 0 & 0 & m_A & & & \\ 0 & 0 & 0 & 0 & 0 & 0 & 0 & 0 & 0 & J_A & & \\ 0 & 0 & 0 & 0 & 0 & 0 & 0 & 0 & 0 & 0 & 0 & \\ 0 & 0 & 0 & 0 & 0 & 0 & 0 & 0 & 0 & 0 & 0 & 0 \end{bmatrix} \qquad [M_m] = \begin{bmatrix} 0 & & & & & & & & & & & \\ 0 & 0 & & & & & & & & & & \\ 0 & 0 & 0 & & & & & & & & & \\ 0 & 0 & 0 & 0 & & & & & & & & \\ 0 & 0 & 0 & 0 & 0 & & & & & & & \\ 0 & 0 & 0 & 0 & 0 & 0 & & & & & & \\ 0 & 0 & 0 & 0 & 0 & 0 & 0 & & & & & \\ 0 & 0 & 0 & 0 & 0 & 0 & 0 & 0 & & & & \\ 0 & 0 & 0 & 0 & 0 & 0 & 0 & 0 & 0 & & & \\ 0 & 0 & 0 & 0 & 0 & 0 & 0 & 0 & 0 & 0 & & \\ 0 & 0 & 0 & 0 & 0 & 0 & 0 & 0 & 0 & 0 & m_{M1} & \\ 0 & 0 & 0 & 0 & 0 & 0 & 0 & 0 & 0 & 0 & 0 & m_{M2} \end{bmatrix}$$

With $m_M1 = \lambda \int_0^L \Phi_1(x)\, \Phi_1(x)\, dx$ and $m_M2 = \lambda \int_0^L \Phi_2(x)\, \Phi_2(x)\, dx$ from equation 3.1.6 computed numerically with the *trapeziodal method*, given $\Phi_i(x)$ in equation 3.1.4.

Here the resulting mass matrix, already partitioned:

$$[M] = \left[\begin{array}{cccc|cccccccc} 0 & 0 & 0 & 0 & 0 & 0 & 0 & 0 & 0 & 0 & 0 & 0 \\ 0 & 0 & 0 & 0 & 0 & 0 & 0 & 0 & 0 & 0 & 0 & 0 \\ 0 & 0 & 0 & 0 & 0 & 0 & 0 & 0 & 0 & 0 & 0 & 0 \\ 0 & 0 & 0 & 0 & 0 & 0 & 0 & 0 & 0 & 0 & 0 & 0 \\ \hline 0 & 0 & 0 & 0 & m_B & 0 & 0 & 0 & 0 & 0 & 0 & 0 \\ 0 & 0 & 0 & 0 & 0 & J_B & 0 & 0 & 0 & 0 & 0 & 0 \\ 0 & 0 & 0 & 0 & 0 & 0 & m_B & 0 & 0 & 0 & 0 & 0 \\ 0 & 0 & 0 & 0 & 0 & 0 & 0 & J_B & 0 & 0 & 0 & 0 \\ 0 & 0 & 0 & 0 & 0 & 0 & 0 & 0 & m_A & 0 & 0 & 0 \\ 0 & 0 & 0 & 0 & 0 & 0 & 0 & 0 & 0 & J_A & 0 & 0 \\ 0 & 0 & 0 & 0 & 0 & 0 & 0 & 0 & 0 & 0 & m_{M1} & 0 \\ 0 & 0 & 0 & 0 & 0 & 0 & 0 & 0 & 0 & 0 & 0 & m_{M2} \end{array}\right]$$

7.5.2 Damping matrix: Eq 3.4.11

Because of the *Nishimura* air spring arrangment, there's no longer a linear damper connected directly in between the car body and the bogie frame. For this reason during the computation of the damping matrix it's necessary to account only for two contributes: $[R_I]$ for the primary suspension; $[R_m]$ for the damping effect of the car body vibrations.

In particular the primary suspension contribute is given by the relationship:

$$[R_I] = [\Lambda_{\Delta L_I}]^T \, [c] \, [\Lambda_{\Delta L_I}]$$

Where $[c] = diag\{c_I; c_I; c_I; c_I\}$ collects the damping values of the primary suspension; the *jacobian* $[\Lambda_{\Delta L_I}]$ provides the information about the kinematic relationship defining the suspension elongation and can be computed by means of the *superimposition* principle:

$[\Lambda_{\Delta L_I}]$	z_{C11}	z_{C12}	z_{C21}	z_{C22}	z_{B1}	θ_{B1}	z_{B2}	θ_{B2}	z_A	θ_A	G_1	G_2
ΔL_{I11}	-1				1	-b						
ΔL_{I12}		-1			1	b						
ΔL_{I21}			-1				1	-b				
ΔL_{I22}				-1			1	b				

On the contrary $[R_m]$ has its only non null value $c_{M1} = \xi_1 2 m_M \omega_1$ and $c_{M2} = \xi_2 2 m_M \omega_2$ on the main diagonal in correspondence of the bending mode independent variables:

$$[R_I] = \begin{bmatrix}
c_I & & & & & & & & & & & \\
0 & c_I & & & & & & & & & & \\
0 & 0 & c_I & & & & & & & & & \\
0 & 0 & 0 & c_I & & & & & & & & \\
-c_I & -c_I & 0 & 0 & 2c_I & & & & & & & \\
bc_I & -bc_I & 0 & 0 & 0 & 2b^2c_I & & & & & & \\
0 & 0 & -c_I & -c_I & 0 & 0 & 2c_I & & & & & \\
0 & 0 & bc_I & -bc_I & 0 & 0 & 0 & 2b^2c_I & & & & \\
0 & 0 & 0 & 0 & 0 & 0 & 0 & 0 & 0 & & & \\
0 & 0 & 0 & 0 & 0 & 0 & 0 & 0 & 0 & 0 & & \\
0 & 0 & 0 & 0 & 0 & 0 & 0 & 0 & 0 & 0 & 0 & \\
0 & 0 & 0 & 0 & 0 & 0 & 0 & 0 & 0 & 0 & 0 & 0
\end{bmatrix}$$

$$[R_m] = \begin{bmatrix}
0 & & & & & & & & & & & \\
0 & 0 & & & & & & & & & & \\
0 & 0 & 0 & & & & & & & & & \\
0 & 0 & 0 & 0 & & & & & & & & \\
0 & 0 & 0 & 0 & 0 & & & & & & & \\
0 & 0 & 0 & 0 & 0 & 0 & & & & & & \\
0 & 0 & 0 & 0 & 0 & 0 & 0 & & & & & \\
0 & 0 & 0 & 0 & 0 & 0 & 0 & 0 & & & & \\
0 & 0 & 0 & 0 & 0 & 0 & 0 & 0 & 0 & & & \\
0 & 0 & 0 & 0 & 0 & 0 & 0 & 0 & 0 & 0 & & \\
0 & 0 & 0 & 0 & 0 & 0 & 0 & 0 & 0 & 0 & c_{M1} & \\
0 & 0 & 0 & 0 & 0 & 0 & 0 & 0 & 0 & 0 & 0 & c_{M2}
\end{bmatrix}$$

The resulting damping matrix is:

$$[R] = \left[\begin{array}{cccc|cccccccc}
c_I & 0 & 0 & 0 & -c_I & bc_I & 0 & 0 & 0 & 0 & 0 & 0 \\
0 & c_I & 0 & 0 & -c_I & -bc_I & 0 & 0 & 0 & 0 & 0 & 0 \\
0 & 0 & c_I & 0 & 0 & 0 & -c_I & bc_I & 0 & 0 & 0 & 0 \\
0 & 0 & 0 & c_I & 0 & 0 & -c_I & -bc_I & 0 & 0 & 0 & 0 \\
\hline
-c_I & -c_I & 0 & 0 & 2c_I & 0 & 0 & 0 & 0 & 0 & 0 & 0 \\
bc_I & -bc_I & 0 & 0 & 0 & 2b^2c_I & 0 & 0 & 0 & 0 & 0 & 0 \\
0 & 0 & -c_I & -c_I & 0 & 0 & 2c_I & 0 & 0 & 0 & 0 & 0 \\
0 & 0 & bc_I & -bc_I & 0 & 0 & 0 & 2b^2c_I & 0 & 0 & 0 & 0 \\
0 & 0 & 0 & 0 & 0 & 0 & 0 & 0 & 0 & 0 & 0 & 0 \\
0 & 0 & 0 & 0 & 0 & 0 & 0 & 0 & 0 & 0 & 0 & 0 \\
0 & 0 & 0 & 0 & 0 & 0 & 0 & 0 & 0 & 0 & c_{M1} & 0 \\
0 & 0 & 0 & 0 & 0 & 0 & 0 & 0 & 0 & 0 & 0 & c_{M2}
\end{array}\right]$$

7.5.3 *Lagrangian* of air spring suspension: Eq 3.4.9

The *Lagrangian* of the air spring $\underline{Q_{II}}$ is obtained from the definition of the virtual work:

$$\underline{Q}_{II} = \frac{\delta L}{\delta \underline{x}} = \frac{\underline{F}_{II}^T \delta \underline{s}_{II}}{\delta \underline{x}}$$

As long as the virtual displacements is a function of the independent coordinates, it can be expressed in matrix notion $\delta \underline{s}_{II} = [\Lambda_{\delta s_{II}}]\, \delta \underline{x}$ given the *jacobian* matrix:

$[\Lambda_{\delta s_{II}}]$	δz_{C11}	δz_{C12}	δz_{C21}	δz_{C22}	δz_{B1}	$\delta\theta_{B1}$	δz_{B2}	$\delta\theta_{B2}$	δz_A	$\delta\theta_A$	δG_1	δG_2
δs_{II1_U}									1	-a	Φ_{1R}	Φ_{2R}
δs_{II1_L}					1							
δs_{II2_U}									1	a	Φ_{1F}	Φ_{2F}
δs_{II2_L}							1					

For sake of simplicity, since $F_{II_{i\,U}} = -F_{II_{i\,L}}$ the vector collecting the secondary suspension forces $\underline{F}_{II} = \{F_{II_{1\,U}};\ F_{II_{1\,L}};\ F_{II_{2\,U}};\ F_{II_{2\,l}}\}$ can be reorganized as follow:

$$\underline{F}_{II} \;=\; \begin{Bmatrix} f_{II_{1\,U}} \\ f_{II_{1\,L}} \\ f_{II_{2\,U}} \\ f_{II_{2\,L}} \end{Bmatrix} \;=\; \begin{bmatrix} 1 & 0 \\ -1 & 0 \\ 0 & 1 \\ 0 & -1 \end{bmatrix} \begin{Bmatrix} f_{II_{1\,U}} \\ f_{II_{2\,U}} \end{Bmatrix} \;=\; [\Lambda_{Ff}]\, \underline{f}_{II}$$

Where $f_{II_{iU}} = -k_{II\,U}\, \Delta L_{II_{i\,U}}$. Again the elongation is a function of the independent variables, thus it can be expressed in matrix notion $\underline{\Delta L}_{II_U} = [\Lambda^x_{\Delta L_{II\,N}}]\, \underline{x} \,+\, [\Lambda^y_{\Delta L_{II\,N}}]\, \underline{y}$ by means of the superimposition principle given the *jacobian* matrix:

	$[\Lambda^x_{\Delta L_{II\,N}}]$												$[\Lambda^y_{\Delta L_{II\,N}}]$	
	z_{C11}	z_{C12}	z_{C21}	z_{C22}	z_{B1}	θ_{B1}	z_{B2}	θ_{B2}	z_A	θ_A	G_1	G_2	y_1	y_2
$\Delta L_{II_{1U}}$					-1				1	-a	Φ_{1R}	Φ_{2R}	-1	
$\Delta L_{II_{2U}}$							-1		1	a	Φ_{1F}	Φ_{2F}		-1

The resulting *lagrangian* can be computed from equation 3.4.9:

$$\begin{aligned} \underline{Q}_{II}^T &= \underline{F}_{II}^T\, [\Lambda_{\delta s_{II}}] \;=\; -k_{II\,U}\, \left(\underline{f}_{II}^T\, [\Lambda_{Ff}]^T\right)\, [\Lambda_{\delta s_{II}}] \\ &=\; -k_{II\,U}\, \left(\underline{x}^T\, [\Lambda^x_{\Delta L_{II\,N}}]\, [\Lambda_{Ff}]^T \,+\, \underline{y}^T\, [\Lambda^y_{\Delta L_{II\,N}}]\, [\Lambda_{Ff}]^T\right)\, [\Lambda_{\delta s_{II}}] \end{aligned}$$

That after the transposition result in the expression:

$$\underline{Q}_{II} = -k_{II\,U}\, \left([\Lambda_{\delta s_{II}}]^T\, [\Lambda_{Ff}]\, [\Lambda^x_{\Delta L_{II\,N}}]\, \underline{x} \,+\, [\Lambda_{\delta s_{II}}]^T\, [\Lambda_{Ff}]\, [\Lambda^y_{\Delta L_{II\,N}}]\, \underline{y}\right) = [Q^x_{II}]\underline{x} \,+\, [Q^y_{II}]\underline{y}$$

With the proper matrix multiplication, it's possible to define the *lagrangia* matrices as follow:

$$[Q^x_{II}] = -k_{II_U} \left|\begin{array}{cccc|cccc|cccc} 0&0&0&0&0&0&0&0&0&0&0&0\\ 0&0&0&0&0&0&0&0&0&0&0&0\\ 0&0&0&0&0&0&0&0&0&0&0&0\\ 0&0&0&0&0&0&0&0&0&0&0&0\\ \hline 0&0&0&0&1&0&0&0&-1&\text{a}&-\Phi_{1R}&-\Phi_{2R}\\ 0&0&0&0&0&0&0&0&0&0&0&0\\ 0&0&0&0&0&0&1&0&-1&\text{-a}&-\Phi_{1F}&-\Phi_{1R}\\ 0&0&0&0&0&0&0&0&0&0&0&0\\ 0&0&0&0&\text{-1}&0&\text{-1}&0&2&0&\Phi_{1F}+\Phi_{1R}&\Phi_{2F}+\Phi_{2R}\\ 0&0&0&0&\text{a}&0&\text{-a}&0&0&2a^2&a(\Phi_{1F}-\Phi_{1R})&a(\Phi_{2F}-\Phi_{2R})\\ 0&0&0&0&-\Phi_{1R}&0&Phi_{1F}&0&\Phi_{1F}+\Phi_{1R}&a(\Phi_{1F}-\Phi_{1R})&\Phi^2_{1F}+\Phi^2_{1R}&\Phi_{1R}\Phi_{2R}+\Phi_{1F}\Phi_{2F}\\ 0&0&0&0&-\Phi_{2R}&0&Phi_{2F}&0&\Phi_{2F}+\Phi_{2R}&a(\Phi_{2F}-\Phi_{2R})&\Phi_{1R}\Phi_{2R}+\Phi_{1F}\Phi_{2F}&\Phi^2_{2F}+\Phi^2_{2R} \end{array}\right|$$

$$[Q^y_{II}]^T = -k_{II_U} \left|\begin{array}{cccc|cccccccc} 0&0&0&0&0&0&1&0&\text{-1}&\text{-a}&-\Phi_{1F}&-\Phi_{2F}\\ 0&0&0&0&1&0&0&0&\text{-1}&\text{a}&-\Phi_{1R}&-\Phi_{2R} \end{array}\right|$$

7.5.4 Stiffness matrix: Eq 3.4.12

Once the contribute of the secondary suspension *lagrangian* $[Q^x_{II}]$ has been computed, it's possible to assembly the stiffness matrix $[K]$, made of four contributes: $[K_I]$ accounting for the primary suspension; $[K_{II}]$ for the main spring of the secondary suspension; $[K_m]$ accounting for the bending rigidity of the car body; $[Q^x_{II}]$ as explained in the rearrangement of the equation of motion.

For what concern $[K_I]$ and $[K_{II}]$, the usual relationships hold:

$$[K_I] = [\Lambda_{\Delta L_I}]^T [k_I] [\Lambda_{\Delta L_I}] \qquad [K_{II}] = [\Lambda_{\Delta L_{II}}]^T [k_{II}] [\Lambda_{\Delta L_{II}}]$$

Given $[k_I] = diag\{k_I;\ k_I;\ k_I;\ k_I\}$, $[k_{II}] = diag\{k_{II};\ k_{II}\}$ and recalling the *jacobian* matrices already introduced:

$[\Lambda_{\Delta L_I}]$	z_{C11}	z_{C12}	z_{C21}	z_{C22}	z_{B1}	θ_{B1}	z_{B2}	θ_{B2}	z_A	θ_A	G_1	G_2
ΔL_{I11}	-1				1	-b						
ΔL_{I12}		-1			1	b						
ΔL_{I21}			-1				1	-b				
ΔL_{I22}				-1			1	b				

$[\Lambda_{\Delta L_{II}}]$	z_{C11}	z_{C12}	z_{C21}	z_{C22}	z_{B1}	θ_{B1}	z_{B2}	θ_{B2}	z_A	θ_A	G_1	G_2
ΔL_{II1}					-1				1	-a	Φ_{1F}	Φ_{2F}
ΔL_{II2}							-1		1	a	Φ_{1R}	Φ_{2R}

While $[K_m]$ contains on its main diagonal the modal stiffness $k_{M1} = m_M\omega_1^2$ and $k_{M2} = m_M\omega_2^2$, in correspondance of the *dofs* $(G_1;\ G_2)$.

Their final expression as usual is:

$$[R_I] = \begin{bmatrix} k_I & & & & & & & & & & & \\ 0 & k_I & & & & & & & & & & \\ 0 & 0 & k_I & & & & & & & & & \\ 0 & 0 & 0 & k_I & & & & & & & & \\ -k_I & -k_I & 0 & 0 & 2k_I & & & & & & & \\ bk_I & -bk_I & 0 & 0 & 0 & 2b^2k_I & & & & & & \\ 0 & 0 & -k_I & -k_I & 0 & 0 & 2k_I & & & & & \\ 0 & 0 & bk_I & -bk_I & 0 & 0 & 0 & 2b^2k_I & & & & \\ 0 & 0 & 0 & 0 & 0 & 0 & 0 & 0 & 0 & & & \\ 0 & 0 & 0 & 0 & 0 & 0 & 0 & 0 & 0 & 0 & & \\ 0 & 0 & 0 & 0 & 0 & 0 & 0 & 0 & 0 & 0 & 0 & \\ 0 & 0 & 0 & 0 & 0 & 0 & 0 & 0 & 0 & 0 & 0 & 0 \end{bmatrix} \quad [R_m] = \begin{bmatrix} 0 & & & & & & & & & & & \\ 0 & 0 & & & & & & & & & & \\ 0 & 0 & 0 & & & & & & & & & \\ 0 & 0 & 0 & 0 & & & & & & & & \\ 0 & 0 & 0 & 0 & 0 & & & & & & & \\ 0 & 0 & 0 & 0 & 0 & 0 & & & & & & \\ 0 & 0 & 0 & 0 & 0 & 0 & 0 & & & & & \\ 0 & 0 & 0 & 0 & 0 & 0 & 0 & 0 & & & & \\ 0 & 0 & 0 & 0 & 0 & 0 & 0 & 0 & 0 & & & \\ 0 & 0 & 0 & 0 & 0 & 0 & 0 & 0 & 0 & 0 & & \\ 0 & 0 & 0 & 0 & 0 & 0 & 0 & 0 & 0 & 0 & k_{M1} & \\ 0 & 0 & 0 & 0 & 0 & 0 & 0 & 0 & 0 & 0 & 0 & k_{M2} \end{bmatrix}$$

$$[K_{II}] = \begin{bmatrix} 0 & & & & & & & & & & & \\ 0 & 0 & & & & & & & & & & \\ 0 & 0 & 0 & & & & & & & & & \\ 0 & 0 & 0 & 0 & & & & & & & & \\ 0 & 0 & 0 & 0 & k_{II} & & & & & & & \\ 0 & 0 & 0 & 0 & 0 & 0 & & & & & & \\ 0 & 0 & 0 & 0 & 0 & 0 & k_{II} & & & & & \\ 0 & 0 & 0 & 0 & 0 & 0 & 0 & 0 & & & & \\ 0 & 0 & 0 & 0 & -k_{II} & 0 & -k_{II} & 0 & 2k_{II} & & & \\ 0 & 0 & 0 & 0 & ak_{II} & 0 & -ak_{II} & 0 & 0 & 2a^2k_{II} & & \\ 0 & 0 & 0 & 0 & -\Phi_{1F}k_{II} & 0 & -\Phi_{1R}k_{II} & 0 & k_{II}(\Phi_{1F}+\Phi_{1R}) & k_{II}a(\Phi_{1R}-\Phi_{1F}) & k_{II}(\Phi_{1F}^2+\Phi_{1R}^2) & \\ 0 & 0 & 0 & 0 & -\Phi_{2F}k_{II} & 0 & -\Phi_{2R}k_{II} & 0 & k_{II}(\Phi_{2F}+\Phi_{2R}) & k_{II}a(\Phi_{2R}-\Phi_{2F}) & k_{II}(\Phi_{1F}\Phi_{2F}+\Phi_{1R}\Phi_{2R}) & k_{II}(\Phi_{2F}^2+\Phi_{2R}^2) \end{bmatrix}$$

According to the equation 3.4.12, is at the end possible to get the combination:

$$[K_I] + [K_{II}] + [K_m] - [Q_{II}^x]$$

References

[1] **SM Savaresi, C Poussot-Vassal, C Spelta, O Sename, L Dugard**. *Semi active suspension control design for vehicles*. Elsevier, 2010.

[2] **RM Goodall, W Korum**. *Active controls in ground transportation - A review of the state of the art and future potentials*. Vehicle system dymanics 12, 1983, 225-257.

[3] **B Fu, RL Giossi, R Persson, S Stichel, S Bruni, R Goodall**. *Active suspension in railway vehicles: a literature survey*. Railway Engineering Science, Springer, March 2020, 3-35.

[4] **HE Tseng, D Hrovat**. *State of the art survey: active and semi active suspension control*. Vehicle System Dynamics: International Journal of Vehicle Mechanics and Mobility, 2015, 1-29.

[5] **S Bruni, R Goodall, TX Mei, H Tsunashima**. *Control and monitoring for railway vehicle dynamics*. Vehicle System Dynamincs, Vol.45, August 2007, 743-779.

[6] **R Goodall**. *Active railway suspension: implementation status and technological trends*. Vehicle System Dynamincs, Vol.28, 1997, 87-117.

[7] **RM Goodall, S Bruni, TX Mei**. *Concepts and prospects for actively controlled railway gear*. Vehicle System Dynamincs, Vol.44, 2006, 60-70.

[8] **L Bala Murugan, J Jancirani**. *An investigation on semi active suspension damper and control strategies for vehicle ride comfort and road holding*. Journal of Systems and Control Engineering, Institution of Mechanical Engineers, 2012, 1119-1129.

[9] **A Orväs, S Stichel, R Persson**. *Ride comfort improvements in high speed train with active secondary suspension*. Journal of Mechanical System, Transportation and Logistic, 2010, 206-215.

[10] **J Park, Y Shin, H Hur, W You**. *A practical approach to active lateral suspension for railway vehicles*. Meas Control, 2019, 1195-1209.

[11] **Y Maruyama, K Ishihara, T Matsui, S Koizumi**. *Development of an active suspension system for railway vehicle*. Proceeding of IECON '94 - 20th annual conference of IEEE industrial electronics, 2002, 2011-2016.

[12] **EM Elbeheiry, AC Karnopp, ME Elaraby, AM Abdelaaouf**. *Advanced ground vehicle suspension system: a classified bibliography*. Vehicle System Dynamics: International Journal of Vehicle Mechanics and Mobility, 2007.

[13] **RN Yerrawar, RR Arakerimath**. *Development of methodology for semi active suspension system using MR damper*. Materials today: Proceedings, 2017, 9295-9303.

[14] **WF Milliken**. *Active suspension*. SAE Technical Paper, 1988.

[15] **DE Simon, M Ahmadian, HR Robertshaw, P Kachroo, MEF Kasarda, D Leo**. *An investigation of effectiveness of SkyHook suspension for controlling roll dynamics of Sport Utility Vehicles using magneto rheological dampers*. Disseration submitted to the Faculty of the Virginia Plytechnic Institute, 2001.

[16] **HC Sohn, KS Hong, JK Hendrick**. *Semi active control of the MacPherson suspension system: hardware in the loop simulations*. Proceeding of the 2000 IEEE, International Conference on Control Applications, 2000.

[17] **HC Sohn, KT Hong, KS Hong, WS Yoo**. *An adaptive control for semi active suspension system*. Jounal of Vehicle Design, Vol.34, 2004.

[18] **Y Sugahara, T Takigami, A Kazato**. *Suppressing vertical vibration in railway vehicles through air spring damping control*. Journal of System Design adn Dynamics, Vol.1, 2007, 212-223.

[19] **TY Liang, ZD Wang, MX Tang, WL Zhang**. *Study on semi active secondary suspension of railway vehicle*. International Conference on Transportation, Mechanical and Electrical Engineering, 2011, 1269-1272.

[20] **JS Tang**. *Passive and semi active airspring suspension for rail passenger vehicles - theory and practive*. Proceedingof the Institution of Mechanical Engineering, Part F: Journal of Rail and Rapid Transit, 1996, 103-117.

[21] **Y Sugahara, T Takigami, M Sampei**. *Suppressing vertical vibration in railway vehicles through primary suspension damping force control*. Journal of System Design and Dynamics, Vol.1, 2007, 224-235.

[22] **Y Sugahara, A Kazato, T Takigami, R Koganei**. *Suppression of vertical vibration in railway vehicle by controlling the damping force of primary and secondary suspension*. QR of RTRI, Vol.49, 2008, 7-18.

[23] **Y Sugahara, A Kazato, R Koganel, M Sampei, S Nakaura**. *Suppression of vertical bending and rigid body mode vibration in railway vehicle car body by primary and secondary suspension control: results of simulations and running tests using Shinkansen vehicle*. Journal of rail and rapid transit, 2009, 517-531.

[24] **Y Sugahara, N Watanabe, T Takigami, R Koganei**. *Vertical vibration suppression system for railway vehicles based on primary suspension damping control: system development and vehicle running test results*. QR of RTRI, Vol.52, 2011, 13-19.

[25] **Y Sugahara, T Kojima**. *Suppression of vertical vibration in railway vehicle carbodies through conrol of damping force in primary suspension: presentation of tresults with running tests with meter-gauge can on a secondary line*. WIT Transactions on the built environment, Vol.181, 2019, 329-336.

[26] **D Karnopp, MJ Crosby, RA Harwood**. *Vibration control using semi-active force generators*. Journal of engineering for industry, 1974, 619-626.

[27] **SM Savaresi, E Siliani, S Bittanti**. *Semi active suspensions: an optimal control strategy for a quarter car model*. IFAC Advavces in Automotive Control, 2004, 553-558.

[28] **SM Savaresi, E Siliani, S Bittanti**. *Acceleration driven damper: an optimal control algorithm for comfort oriented semiactive suspension*. Journal of Dynamics Systems, Measurement and Control, Vol.127, 2005, 218-229.

[29] **M Nagai, Y Sawada**. *Active suspension for flexible structure control of high speed ground vehicles*. IFAG 10th Triennal World Congress, 1987, 198-202.

[30] **R Peresson, B Fu, RL Giossi, S Bruni, E Di Gialleonardo, B Fu, B Liu, L Baeza, X Liu, R Goodall**. *Innovative running gear solutions for new dependable, sustainable, intelligent and comfortable rail vehicles*. European project: Run2Rail, 2019.

[31] **L Mazzola, M Berg**. *Secondary suspension of railway vehicles - air spring modelling: performance and critial issues*. Journal of rail and rapid transit, 2014, 225-241.

[32] **S Matsumiya, S Nishioka, S Nishimura, M Suzuki**. *On the diaphragm air spring "Sumride"*. Sumitomo search, 1969, 2: 86-92.